Alma Mater Studiorum – Università di Bologna

DOTTORATO DI RICERCA

Ciclo XXI

Settore scientifico disciplinare di afferenza: CHIM/12

TITOLO TESI

Application of FTIR Microscopy To Cultural Heritage Materials

Presentata da: **JOSEPH Edith Michelle Maryse**

Coordinatore Dottorato **Relatore**

Prof. G. Longoni **Prof. R. Mazzeo**

Esame finale anno 2009

*“*Dans *la vie, rien n’est à craindre, tout est à comprendre”*

Marie Curie

Contents

I FTIR MICROSCOPY FOR CULTURAL HERITAGE

I.1 Introduction

Multidisciplinary area where scientists and conservator-restorers as well as art historians and archaeologists are involved, research in conservation has been developed from the early 1950s, giving a significant contribution to the conservation-restoration of cultural heritage. In fact, only through a profound knowledge about the nature and conditions of constituent materials, suitable decisions on the conservation and restoration measures can be adopted and preservation practices enhanced. Ancient artworks can be considered as complex heterogeneous systems where numerous interactions between the different components as well as degradation and ageing phenomena take place (Figure 1). The study of these multi-layers structures is complicated by the difficulties to physically separate the different layers due to their thickness (1-200 µm). Moreover, a single layer is often composed of a mixture of various compounds, such as pigment and binding medium for paintings, which are not distributed homogeneously. In order to have a deepened understanding of these phenomena, advanced analytical techniques are therefore required at a molecular level to characterize the nature of the compounds but also to obtain chemical and physical information about ongoing changes.

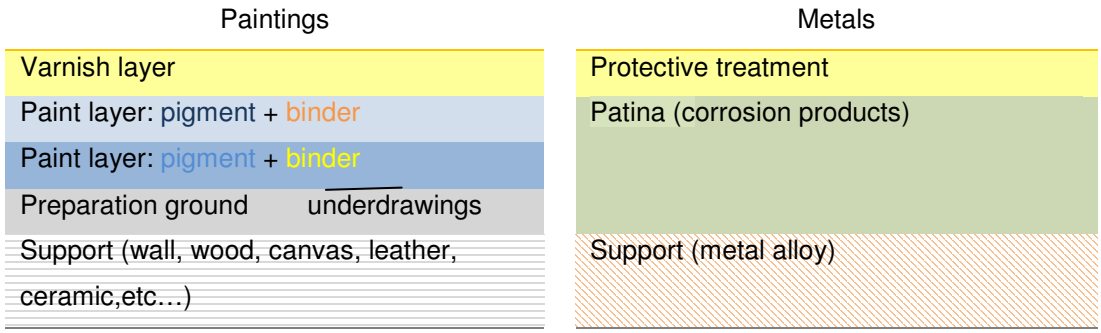

Figure 1 – Schematic view of the structure of cultural heritage artefacts.

In art conservation laboratories, infrared (IR) spectroscopy is the most widely applied method for the investigation of cultural heritage materials as many of their inorganic and organic constituents show characteristic absorptions in the mid-IR range 4000–600 cm^{-1} (Derrick, Stulik et al. 1999; Casadio and Toniolo 2001; Bitossi, Giorgi et al. 2005). From the early beginning of IR spectroscopy, its use has been mentioned for the examination of paintings and artifacts

(Gettens 1952; Olin 1966). Later in the 1970s, the transition from dispersive IR to Fourier transform Infrared (FTIR) instruments has really improved resolution and detection limits, and the possibilities offered by this technique have been presented for resolving conservation issues (Low and Baer 1977). Afterward, the beginning of the 1980s has witnessed the introduction of micro-sampling accessories for FTIR spectroscopy and, in particular, the development of FTIR microscopy which became an essential tool in the micro-destructive analysis of small samples (Messerschmidt and Harthcock 1988; Humecki 1995; Katon 1996).

A FTIR microscope consists of a FTIR spectrometer combined with an optical microscope, which incorporates all-reflecting optics and aspherical surfaces adapted to the infrared radiation for minimizing optical aberrations (Figure 2).

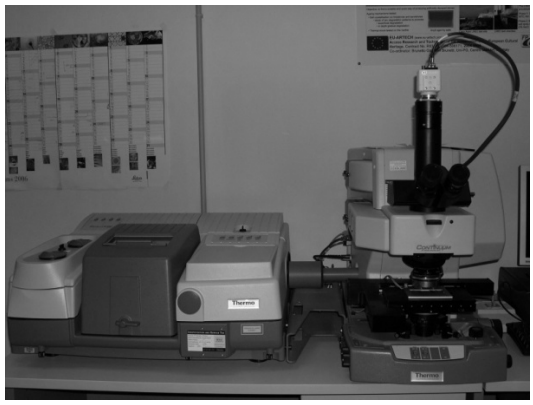

Figure 2 – FTIR microscopy.

The conventional infrared light source (typically a Globar silicon bar heated to 1500 K), which emits radiation from 1.5 µm up to a few tens of microns, is directly directed to the microscope instead of the spectrometer's sample chamber, without any modification to the interferometer. The user interface for data acquisition and processing is also the same as for conventional FTIR spectroscopy. The microscope is designed for observation in transmission and in reflection using typical magnification of 6x, 15x and 32x with numerical aperture ranging from 0,3 to 0,7. A system of dichroic mirrors allows visible light and IR radiation to pass through the same optical system, permitting to first

observe the region of interest and then record IR spectra at the same point without moving the stage of the microscope (Figure 3).

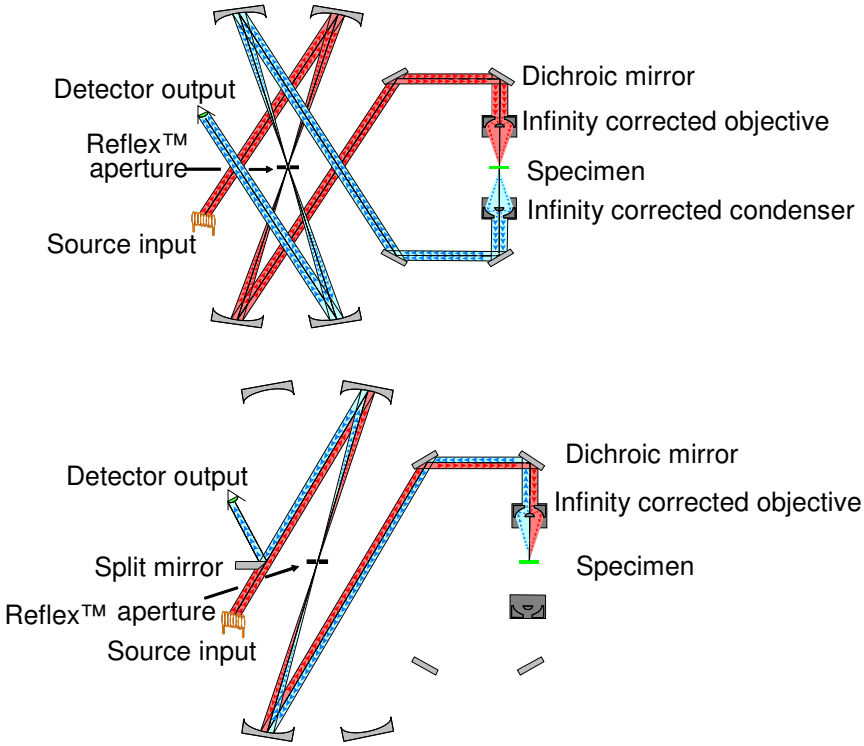

Figure 3 – Infrared radiation pathway in transmission (up) and reflection (down) modes for a FTIR microscope with a single-element detector.

The radiation can be focused on small areas, reducing the amount of material necessary for the analysis and allowing different regions of a heterogeneous sample, which cannot be physically separated, to be isolated. Using a single-element mercury-cadmium-telluride (MCT) detector, the investigated area is selected through adjustable rectangular apertures from 150 x 150 μm^2 to 10 x 10 μm^2 and the aperture image can be either illuminated onto the sample or observed on the computer screen delimited by a red line (Figure 4). In the case of multi-channel detector, the entire field of view (FOV) of the optical signal is recorded and no aperture is required. Typical IR sensitive focal plane array (FPA) detectors include 64 x 64, 128 x 128 and 256 x 256 elements (pixels) arranged in a regular pattern.

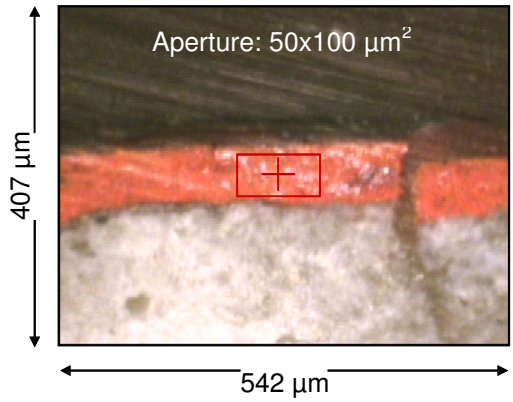

Figure 4 – Selection of the area to be analysed through adjustable aperture.

Several papers have been reported on the application of FTIR microscopy to the field of conservation and the analysis of cultural heritage materials such as pigments, binding media, varnishes, dyes, protective treatments, degradation products and others (Van't Hul-Ehrnreich 1970; Baker, Von Endt et al. 1988; Baker and Von Endt 1988; Turner and Watkinson 1993; Gillard, Hardman et al. 1994; Derrick 1995; Pilc and White 1995; Langley and Burnstock 1999; Paluszkiewicz and Dominik 2002; Sato and Sasaki 2005).

The interpretation of FTIR results can be facilitated by online reference libraries which are accessible from numerous web sources (Vahur, Virro et al. 2005):

- CAMEO -Conservation Art and Material Encyclopedia Online, *http://cameo.mfa.org/index.asp*,
- IRUG - infrared users group, *http://www.irug.org/ed2k/search.asp*,
- UT testing centre, *http://ut.ee/katsekoda/IR_Spectra/*,
- e-VISART - e-vibrational spectroscopic databases, *http://ehu.es/udps/database/database1.html*,
- NIST chemistry webBook, *http://webbook.nist.gov/chemistry/name-ser.html*,
- SDBS - Spectral Database for Organic Compounds, *http://riodb01.ibase.aist.go.jp/sdbs/cgi-bin/cre_index.cgi?lang=eng*,
- Mid/Far IR Catalogue of Minerals and Gems, *http://www.geocities.com/ostroum/catalogue.htm*.

In these databases, the reference spectra available should carefully be used since they mostly represent individual standards, which can with difficulties be compared with samples taken from ancient artefacts and composed of complex mixtures. Moreover, these reference spectra are often recorded on fresh-prepared samples and therefore they cannot be directly compared to those obtained from real samples due to the ageing processes encountered in aged artefacts, where present compounds are modified and/or degradation products are formed.

I.2 Sampling criteria

Optimization of instrumentation has permitted to gather a larger amount of information from samples at the level of micrometers. However, the most importance step for the analysis remains the correct collection and preparation of samples. When dealing with cultural heritage artefacts, by definition unique and rare, the number of samples should be reduced to the minimum. Obtaining a representative set of samples, related to the problem encountered, may also present some difficulties due to the presence of an inhomogeneous matrix. Therefore, with the help of non-destructive techniques, some background information can be obtained and sampling undoubtedly facilitated. Indeed, the number and the location of the samples can be defined according to the first results obtained during in situ analyses. X-radiography, X-Ray Fluorescence (XRF) or multispectral imaging represent the non-invasive methods mainly employed for such survey investigation on art objects.

X-radiography permits to obtain contrasted images in gray scale according to the X-rays absorption degree of the different elements present (Graham and Eddie 1985). For easel paintings, for instance, retouching, superposed compositions or past interventions on the support can be documented with this technique (Padfield, Saunders et al. 2002). On the other hand, the internal structure of sculptures or ceramics is also easily observed (O'Connor and Brooks 2007).

Based on the different X-rays energies emitted by a sample after excitation, XRF is an important tool to perform single-spot elemental analysis. For

example, this technique allows the identification of numerous inorganic compounds employed as painting materials (Moioli and Seccaroni 2000; Ferrero, Roldán et al. 2002; Desnica and Schreiner 2006). Besides, the alloy composition and the nature of corrosion patinas can be also determined for metal artworks (Cesareo, Ridolfi et al. 2006; Karydas 2007; Bonizzoni, Galli et al. 2008) as well as the different components used in the manufacture of ceramics and glasses (Röhrs and Stege 2004; Nakai, Yamada et al. 2005; Uhlir, Griesser et al. 2008). However, the information is simultaneously obtained from the top paint layers and should be carefully interpreted due to the penetration depth of X-rays and the resulting difficulties to distinguish between the different layers underneath the surface.

Using diverse regions of the electromagnetic radiation from near-infrared (1100 nm) to ultraviolet (320 nm), multispectral imaging is a versatile method to obtain information about the state of conservation and execution technique of an art object (Teule 1999; Balas and Pelecoudas 2000; Mazzeo and Joseph 2005; Fischer and Kakoulli 2006). This digital portable system is particularly used for the study of paintings as it combines different imaging techniques: VIS reflection, infrared (IR) reflection, false-color IR, fluorescence and ultraviolet (UV) reflection. It is thus possible to characterise and locate underdrawings (IR reflection), get a very first appreciation of pigments' composition present on the outermost paint layers (false-color IR mode), document the presence of lacunas and past restoration interventions (IR reflection, fluorescence and UV reflection).

Non-destructive techniques supply complementary information on the composition and state of conservation and, if available, they should be performed previously to any sampling as they are helpful for taking appropriate decisions on the amount, number and location of samples. It is worth saying that non-destructive approaches alone are insufficient to fully characterise and evaluate the state of conservation of an art object. So far, samples are required not only for a deepened chemical analysis but also for detailed stratigraphic characterisation of the different layers. In theory, samples should be taken from the most representative area, but, due to the minimum invasiveness requested, they are generally collected from pre-existing cracks, lacunas or edges. However, carefully paying attention to the conditions in which they have been

collected, these samples can give interesting information which can be validated by further analyses.

I.3 Sample preparation methods

As mentioned above, the accuracy of the investigation depends not only from a representative sampling but also from an adequate preparation of the sample for the analysis. With the FTIR microscopy and its related accessories, the amount of sample necessary is reduced to less than 1 µg.

For the analysis of a multilayered structure, one method is the removal of some particles under stereomicroscope. The difficulties encountered to physically divide different layers, together with the unhomogeneities presented within each layer make this method complicated. Nevertheless, it can be very useful in case of dispersed particles collected during the sampling. Nowadays, the standard method includes an entire fragment and its preparation as cross section with an embedding resin. In particular, polyester resins are commonly used due to their proprieties adequate with most samples: colorless, room temperature curing and easy sectioning. After embedding and transversal sectioning, the cross sections are grinded and polished to reach a planar surface, where the whole stratigraphy is visible.

The most frequent methods used to analyze a sample, both as particle and fragment, by infrared microspectroscopy are discussed below.

I.3.1 Transmission measurements

With the IR radiation passing through the sample, infrared transmission (T) is the standard method used for qualitative analysis and more specifically for quantitative analysis (Figure 5).

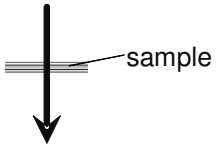

Figure 5 – Schematic view of transmission analysis.

It can be simply correlated with the absorption (A), which is proportional to both the concentration of the sample (c) and its thickness (l), as described by the Lambert Beer's law (Griffiths and De Haseth 1986) in the equation 1 where the extinction coefficient ε ($l.mol^{-1}.cm^{-1}$) is a characteristic property of the absorbing material.

$$A=\varepsilon cl = -\log T \quad (1)$$

Transmission measurements benefit also for a high energy throughput and a resulting high sensibility, which explain the large collections of IR transmission spectra produced in the past and their use as reference for comparison with other infrared methods. Working with apertures implicates to pay attention to diffraction effects, which result in radiation bending and occur when the radiation passes trough slit on the same order of dimension of its wavelength. In FTIR microscopy, the spatial resolution related to the aperture's dimension can therefore not be lower than the theoretical diffraction limit of about 10 µm without obtaining extra information from outside the analysed area. In practice, some difficulties are encountered for obtaining a good signal-to-noise ratio (S/N) with aperture of 10x 10 µm and it's better to work with aperture of 20 x 20 µm to have enough energy to perform spectra.

I.3.1.a *NaCl windows*

Many IR transparent materials can be used as IR window materials: they are selected on the basis of their frequency range of use and chemical compatibility. Among them, the low-cost sodium chloride (NaCl) is one of the most commonly employed, covering the entire mid-IR region. However, some precautions should be taken as NaCl windows are moisture sensitive and they should therefore be kept in a dessicated cabinet. They can also be easily scratched and need a regular polishing to maintain their transparency. Barium fluoride (BaF_2) windows are also largely used for their transparency and low water solubility. Samples can be placed directly onto the window, or after flattening if they are too thick using a roller blade or a micro-compression cell. The preparation is preferably carried out and completed under a

stereomicroscope. Solids materials, such as films, powders, particles or fibres can be analysed with this method (Martoglio, Bouffard et al. 1990; Gillard, Hardman et al. 1994).

I.3.1.b *Diamond anvil cell*

A micro-compression cell with two diamond windows can be also used. The hardness and inertness of diamond allow the analysis of a large variety of samples, including rubbery or reactive ones, without any contamination. In some cases, a part from the need to be flattened, the sample can be taken back for further analyses. The IR spectrum of diamond presents absorption bands between 2500 and 1800 cm^{-1}, a spectral region where few compounds absorb. The acquisition of a background spectrum, collected from a free zone of the diamond window will remove this interference. The diamond anvil cell is a simple device which can be placed directly on the stage of a FTIR microscope and, thus, has been widely used for the analysis of painting or archeological materials (Bruni, Cariati et al. 1999). Recently, diamond anvil cell has also been proposed for the study of multilayered samples (van der Weerd, Heeren et al. 2004; Cotte, Susini et al. 2008). After careful positioning on a diamond window followed by compression, the sample stratigraphy can be preserved with only an expansion of each individual layers.

I.3.1.c *Thin sections*

Transmission measurements can be also performed on thin sections obtained after polishing or microtoming of an embedded cross section. In order to have high-quality spectra, their thickness should be below 15 µm. On one hand, thin sections generally prepared by polishing for petrographic studies cannot be used with FTIR spectroscopy since these sections are sticked on a glass slide with glue, which have both strong absorbance bands in mid-IR region. Some soluble adhesives are available but they require for their removal the use of solvents, which are incompatible with the need of avoiding any interaction with the unknown sample. On the other hand, microtomes are very complex instruments which require knowledge and precision. In fact, even if this

procedure is has been proposed as a standard method in the literature (Derrick, Stulik et al. 1999; Zieba-Palus 1999), in presence of materials with different hardness, the section can be easily deformed with particle loss and curling. Moreover, a contamination from the embedding resin can occur in the spectra due to its smearing during microtoming. Some alternatives using IR transparent salts, such as silver chloride (AgCl) or potassium bromide (KBr), have been also proposed (Pilc and White 1995; Langley and Burnstock 1999) but present some inconvenient (darkening or accelerated corrosion for AgCl) which necessitate a rapid examination of the samples. Recently, Van der Weerd has illustrated an elegant option which foresees the polishing of a sample embedded in KBr on both sides until a thin slide remains (van der Weerd, Heeren et al. 2004). This delicate method has the advantage of avoiding interferences in the spectra but results in the nearly completely loss of the sample originally embedded.

I.3.2 Reflection measurements

At any interface between two materials, an incident radiation is split into reflected and transmitted beams in different proportions according to the refractive index ratio of the two materials in question, as described by the Fresnel's equations (Griffiths and De Haseth 1986) in figure 6.

$$R = \frac{\left[\left(\frac{n_1 \cos\theta_i - n_2\sqrt{1-\left(\frac{n_1}{n_2}\sin\theta_i\right)^2}}{n_1 \cos\theta_i + n_2\sqrt{1-\left(\frac{n_1}{n_2}\sin\theta_i\right)^2}}\right)^2 + \left(\frac{n_1\sqrt{1-\left(\frac{n_1}{n_2}\sin\theta_i\right)^2} - n_2\cos\theta_i}{n1\sqrt{1-\left(\frac{n_1}{n_2}\sin\theta_i\right)^2} + n_2\cos\theta_i}\right)^2\right]}{2}$$

$$T = 1 - R$$

Figure 6 – Reflection (R) and transmission (T) coefficients for unpolarised incidence light in terms of the incidence angle (Θ_i) and the refractive indexes of the first (n_1) and second (n_2) mediums.

Based on this principle, in parallel to transmission measurements, reflection techniques have been widely developed due to the non-destructivity of this type of analysis towards the sample analysed. In fact, reflection measurements can

also be directly performed on the surface of an object without any sampling and thus have been easily applied on a large variety of materials. If the object is small enough, it can be placed directly on the microscope stage otherwise a side port reflectance accessory can be used. As for transmission mode, diffraction effects occur also in reflection mode and the theoretical spatial resolution limit is 10 µm, even if the apertures are usually set to 20 µm in order to obtain good quality spectra.

I.3.2.a *Specular reflection measurements*

Specular reflection is a mirror-like reflection where the incident and reflection angles of the IR radiation are equal (Figure 7).

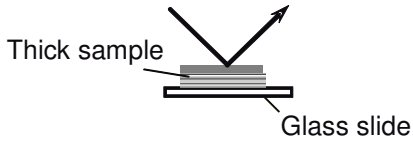

Figure 7 – Schematic view of specular reflection analysis.

In order to obtain high-quality spectra, the surface of the sample should be very shiny and therefore its reflectance optimised by polishing (van Loon, Keune et al. 2005). Generally, the reflectance spectra are further converted into absorbance spectra with a Kramers-Kronig transformation correcting *Reststrahlen* bands, frequency shifts or changes in relative intensity, which may arise. However, in real cases where surface are not totally reflecting, the resultant spectrum may also present contributions from diffuse reflection, refraction or scattering and the transformation will not work. With this method, either object's surface or embedded cross sections can be analysed (Baker, Van Der Reyden et al. 1989; Majolino, Migliardo et al. 1996; Bruni, Cariati et al. 1999). For these latter, the surface quality can be improved using adequate mechanical polishing methods or advanced techniques such as ion milling system or focused ion beam. The first method comprises a dry polishing on Micro-mesh® tissues with the help of a polishing holder, which exerts constant and minimal pressure on the cross section and permits to obtain high surface quality (van Loon, Keune et al. 2005). The second one requires costly systems, which really enhance the surface quality of cross sections, as demonstrated

elsewhere (Lins, Giannuzzi et al. 2002; Boon and Asahina 2006). However, they may also not been appropriate with the presence of organic substances as they used beams of argon or gallium ions which may damage organic compounds present on the surface and therefore need further accurate investigations.

I.3.2.b *Reflection-absorption measurements*

Reflection-absorption measurements are defined when the IR radiation passes through a thin film and is reflected back by a metal surface set under the sample (Dannenberg, Forbes et al. 1960), as illustrated in figure 8.

Figure 8 – Schematic view of reflection-absorption analysis.

The thin layer, which should not excess 15 µm of thickness, is crossed twice by the incident radiation and the high-quality spectra obtained are comparable to those registered in transmission mode. Nevertheless, Reflection-Absorption Spectrometry can be applied in some restricted cases such as the study of protective coatings on metal artworks or the characterisation of varnish layers on gilded art objects (Mohamed, Rateb et al. 2004). It is also a simple method, which can be proposed in alternative to transmission measurements. In fact, samples (films, powders, particles or fibres...) can be easily prepared by flattening in the same way as for the analysis with NaCl windows (van Zelst, Von Endt et al. 1988; Cardamone 1989; Kharbade and Saxena 1991).

I.3.2.c *Attenuated total reflection measurements*

Attenuated total reflection (ATR) is based on the principle of total reflection. At the interface between two materials with different refractive index, the incident radiation is in part reflected and in part refracted. Total reflection is observed

when the incident radiation passes from a high refractive index material to another with lower refractive index with a particular incidence angle, called critical angle, for which the reflection coefficient of the Fresnel's law is $R_s=R_p=1$. In particular, internal reflection occurs at incidence angles greater than this critical angle. However, in such cases, an evanescent wave is created at the surface of the high refractive index material or internal reflection element (IRE) and can penetrate another optically less dense placed in contact. In ATR measurements, the IR radiation reflected by IREs, commonly called crystals, is therefore attenuated from a little fraction absorbed by a sample inserted in closed contact with these IREs (Figure 9).

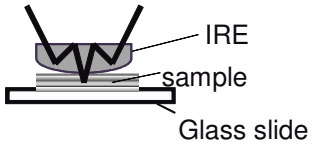

Figure 9 – Schematic view of attenuated total reflection analysis.

Different materials have been used for the fabrication of internal reflection elements. Having the highest refractive index (4.0), germanium is the most commonly used but it is relatively soft and may easily be scratched. Alternatively, the use of silicon, which is a harder material with a refractive index of 3.41, has become important. Diamond is also an excellent option since this material is transparent in the visible light and its absorption bands occurring around 2000 cm^{-1} can be easily removed with the collection of a background. The use of ATR has been successfully reported for a large variety of samples due to the fact that the spectra obtained in this mode are similar to those recorded in transmission mode. Nevertheless, some distortions of relative intensity shifts are visible in ATR spectra since the evanescent wave's penetration depth (d_p) depends of the refractive index of both IRE and material analysed but is also function of wavelength, as presented by the equation 2 below where λ is the wavelength of incidence radiation, n_1 the refractive index of IRE, n_2 the refractive index of sample and θ the incidence angle of radiation on the interface (Reffner and Martoglio 1995).

$$dp = \frac{\lambda}{2\pi n_1 \sqrt{\sin^2 \theta - (n_2/n_1)^2}}$$

2

Especially, absorption bands at lower wavenumbers are enhanced and those present at higher wavenumbers are less intense or absent. Furthermore, the sample's refractive index is function of wavelength and frequency shifts are also observed, principally at lower wavenumbers (Belali, Vigoureux et al. 1995). Some ATR correction algorithms are proposed in most commercially available FTIR software but are not efficient in case of analysis of mixtures, as samples from cultural artefacts can be. Therefore, the simplest way to compare ATR and transmission spectra is to create a reference library of known compounds, whose spectra can be afterwards compared with unknown samples. An important advantage is that, as previously reported by different authors (Reffner and Martoglio 1995; Lewis and Sommer 1999), the ATR configuration allows to investigate smaller area due to the magnification factor of the IRE. For example with an aperture of 100 µm x 100 µm and an IRE of Germanium (refractive index = 4), the actual investigated area is 25 x 25 μm^2. Employing a bigger aperture for a comparable analysed area than in specular reflection mode, the diffraction limit is therefore reduced, with a S/N ratio also increased. ATR spectroscopy has been successfully applied to different artistic materials either on fragments (particles, fibres...) or embedded cross sections (Derrick 1991; Casellato, Vigato et al. 2000; Khanjian and Stulik 2003; Nevin 2005; Shashoua and Bonde Johansen 2005; Ryhl-Svendsen 2007).

I.4 Molecular mapping/imaging

FTIR chemical maps/images or functional group maps/images can be obtained plotting the intensities of characteristic absorption bands against their spatial position on a selected sample area (Treado and Morris 1993; Krishnan, Powell et al. 1995). Collecting a large number of spectra, the sample's surface can systematically be studied in both transmission and reflection mode. First, it is possible to achieve a line scan recording spectra at regular intervals across its

entire structure either moving the sample stage manually or using a software control (Derrick, Stulik et al. 1992). Then, with the help of a motorised stage, molecular mapping or imaging can also be performed on large areas (Harthcock and Atkin 1988a). Each map or image represents spatial position (x, y) and absorption (blue-red colour scale) at a specific wavelength. Overlapping all the maps/images corresponding to each wavelength, the data set can be represented in four dimensions as a hypercube in the infrared frequency domain (Figure 10).

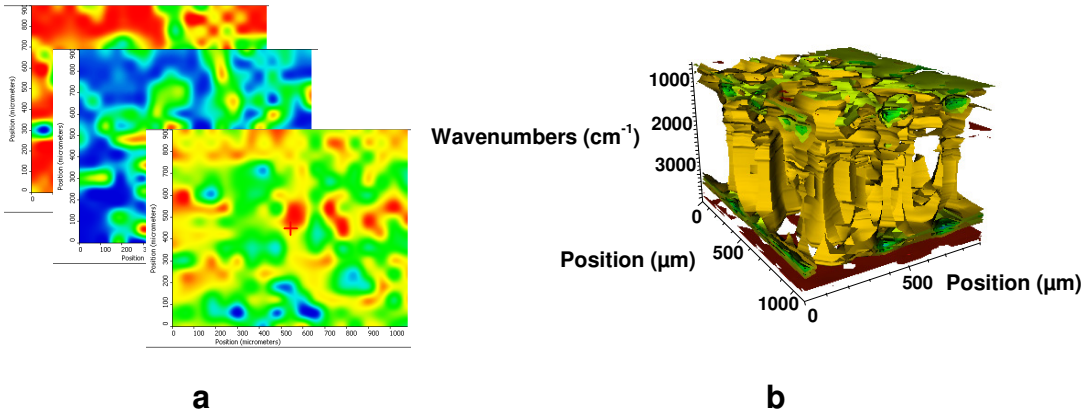

Figure 10 – Single 2d maps obtained for different wavelengths (a) assembled together to obtain the hypercube (b).

FTIR mapping is a single-point sequential data collection in which the investigated area is selected through adjustable apertures (Figure 11a). The effective resolution is related to the aperture dimensions and cannot be lower that the diffraction limit of 10 µm. However, choosing a stage step size lower than the aperture dimensions, the spatial resolution can be also increased as stated by different authors (Harthcock and Atkin 1988b; Krishnan, Powell et al. 1995; Bhargava, Wall et al. 2000). Moreover, higher spatial resolution can be also obtained using ATR mode (Lewis and Sommer 2000) or coupling the FTIR microscope with a synchrotron source (Reffner, Martoglio et al. 1995b; Dumas and Miller 2003).

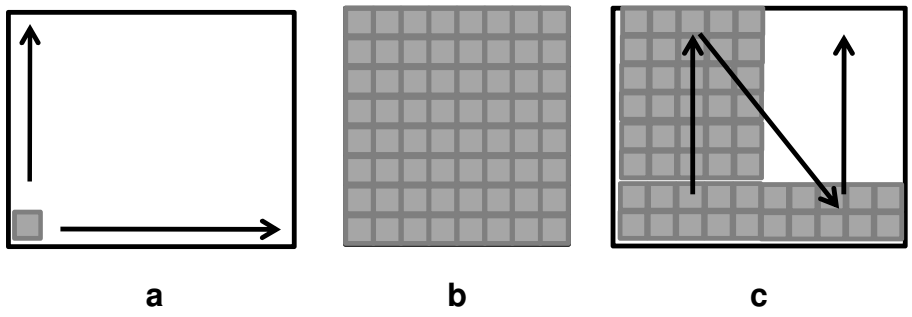

Figure 11 – Schematic representation of the acquisition mode for a) mapping,b) imaging and c) raster scanning.

With no aperture and a focal plane array detector, FTIR imaging is a simultaneous and therefore faster data collection which is obviously useful in the study of dynamic processes where chemical changes appeared rapidly (Ebizuka, Wakaki et al. 1995; Lewis, Treado et al. 1995; Burka and Curbelo 2000), as shown in figure 11b. In this system, the spatial resolution is related to the pixel dimension of about 6 µm, but unfortunately this means also a poor S/N ratio. It is worth saying that, in the case of small and rare cultural heritage samples, the requested time for scanning analysis (~ 1-3 hours for mapping, 5-10 minutes for imaging) does not enter into consideration. Both mapping and imaging systems permit obtaining molecular information, which can be further combined with other imaging techniques such as optical microscopy, SEM-EDX or Raman spectroscopy.

Recently, linear array detectors have been developed combining several mercury cadmium telluride (MCT) detectors together and thus reducing the time of analysis by the number of detectors without loss of spectral quality (figure 11c). The spatial resolution is here determined by the pixel dimension of about 25 µm but can also be lowered to about 6 µm using optical zooms or ATR configuration. These detectors may represent a good compromise between mapping and imaging systems (Levin and Bhargava 2005; Bhargava and Levin 2007). However, possible overlapping between absorbance bands from different compounds with similar chemical features (functional groups) may result in inaccurate images. Mathematical manipulations can enhanced the FTIR map/images providing a possible separation of these features and is also useful to individuate components, which may have not previously been detected due to the large amount of data collected (Ward, Reffner et al. 1994; Huffman

and Brown 2007). In fact, chemometric methods, such as principal component analysis (PCA) or factor analysis (FA), make use of the whole spectrum and extract images that represent the respective component's distribution or variation factors. These aspects and the different FTIR imaging techniques will be evaluated in part III of this thesis.

I.5 Scope of the thesis

This research is aimed at evaluating and validating the use of different FTIR microscopic analytical methods applied to the study of three different art conservation issues: the characterisation of the artistic execution technique, the studies on degradation phenomena and the performance evaluation of protective treatments. Chapter II-1 includes the development of an integrated approach for the characterisation of the execution technique adopted for the realisation of an artwork. In fact, FTIR spectroscopy permits to obtain molecular information which is complementary to those obtained with other analytical techniques and hence allows a complete picture of material's constitution and execution technique to be achieved. As already mentioned, extended libraries of FTIR spectra are available on fresh materials and their comparison with aged samples is difficult to be performed. The investigation on the ageing processes encountered in old artefacts is however essential for their right conservation-preservation. As example for paintings, the characterisation of the degradation products formed during ageing represents therefore one of the most important issues in conservation research, to which purpose FTIR microscopy has been used as described in chapter II-2. Constant effort is also needed to develop novel methods on conservation-restoration in order to better fit conservative problems. In the evaluation of innovative protective treatments, FTIR microscopy can be combined with further elemental analyses to characterise and estimate the performances and stability of newly developed treatments as presented in chapter II-3. In a second part, recent developments in FTIR spectroscopy are underlined. In particular in chapter III-1, an innovative embedding system is reported focusing on the characterisation and localisation of organic substances in cross sections. Furthermore, chapter III-2 points up the new opportunities offered by a conventional diamond ATR accessory coupled

with a focal plane array detector to obtain chemical images of multi-layered paint cross sections. Finally, the latest FTIR techniques available are illustrated in a comparative study. The recent introduction of linear plane array detector and synchrotron source permit reducing the spatial resolution limit, as highlighted in chapter III-3.

I.6 Publications

This thesis has produced the following publications, which are listed according to the chapter they refer to:

Chapter II-1

Mazzeo, R., E. Joseph, V. Minguzzi, G. C. Grillini, P. Baraldi, D.Prandstraller (2006). "Scientific investigations of the Tokhung-Ri tomb mural paintings of the Koguryo era, Democratic People's Republic of Korea." Journal of Raman Spectroscopy **37**(10): 1086-1097. DOI: 10.1002/jrs.1592.

Mazzeo, R., E. Joseph, S. Prati, V.Minguzzi, G.C. Grillini, P. Baraldi, D. Prandstraller (2007). Scientific examination of mural paintings of the Koguryo Tombs. Mural paintings of the Silk Road. Cultural Exchanges Between East and West. T. National Research Institute for Cultural Properties. London, Archetype Publications Ltd.**:** 163-172. ISBN: 9781904982227.

Chapter II-2

Mazzeo, R., S. Prati, M. Quaranta, E. Joseph, E. Kendix, M. Galeotti (2008). Attenuated total reflection micro FTIR characterisation of pigment–binder interaction in reconstructed paint films." Analytical and Bioanalytical Chemistry **392**(1): 65-76. DOI: 10.1007/s00216-008-2126-5.

Chapter II-3

Joseph, E., P. Letardi, R. Mazzeo, S. Prati, M. Vandini (2007). Innovative Treatments for the Protection of Outdoor Bronze Monuments. Metal 07, triennialmeeting of ICOM-CC Metal Working Group, Amsterdam, September 17-21. B.Ankersmit, C. Degrigny, I. Joosten and R. van Langh. Amsterdam, Netherlands Institute of Conservation**:** 71-77.

Mazzeo, R., S. Bittner, G. Farron, R. Fontinha, D. Job, E. Joseph, P. Letardi, M.Mach, S. Prati, M. Salta, A. Simon (2007). Development and Evaluation of New Treatments for Outdoor Bronze Monuments. Conservation Science 2007. J. Townsend. London, Archetype publications: 40-48. ISBN: 9781904982340.

Di Francesco, C., M. Ragazzino, B. Ferriani, M. Matteini, M. Realini, C. Conti, R. Mazzeo, E. Joseph, S. Prati (2007). Esperienze innovative e conferme nei

trattamenti a base di ossalati solubili su superfici lapidee e leghe metalliche: intervento e monitoraggio nel cantiere del portale di Santa Maria delle Grazie a Milano. Scienze e beni culturali XXIII convegno 2007. Il consolidamento degli apparati architettonici e decorativi. Marghera, ARCADIA RICERCHE srl**:** 245-256. ISBN 978-88-95409-11-5.

Chapter III-1

Mazzeo, R., E. Joseph, S. Prati, A. Millemaggi (2007). "Attenuated Total Reflection-Fourier transform infrared microspectroscopic mapping for the characterisation of paint cross-sections." Analytica Chimica Acta **599**(1): 107-117. DOI:10.1016/j.aca.2007.07.076.

Other publications:

Mazzeo, R. and E. Joseph (2004). Micro-destructive analytical investigation for conservation and restoration. Monumenti in bronzo all'aperto. Esperienze di conservazione a confronto. P. Letardi, I. Trentin and G. Guida. Firenze, Nardini Editore**:** 53-58. ISBN 88-404-4090-9.

Mazzeo, R., E. Joseph, V. Minguzzi, G. Gautier, S. Prati, M. Tao, L. M. van Valen (2004). Scientific investigation on traditional manufacturing technique used in Yuan Dynasty mural paintings. Conservation of Ancient Sites on the Silk Road, proccedings of the 2nd International Conference on the Conservation of Grotto Sites, June 28 - July 3, Mogao Grottoes, Dunhuang. Los Angeles, Getty Conservation Institute**:** in press.

Mazzeo, R. and E. Joseph (2006). Applicazione di imaging multispettrale allo studio e conservazione di graffiti e dipinti murali siti nell'edificio delle ex-carceri, Palazzo Steri (Pa). Lo stato dell'arte 3: III congresso nazionale IGIIC, Palermo, Palazzo Steri, 22-24 settembre 2005: volume degli atti. Firenze, Nardini Editore: 18-23. ISBN 88-404-4144-1.

Mazzeo, R. and E. Joseph (2005). The use of FTIR micro-ATR spectroscopy and FTIR mapping for the surface characterisation of bronze corrosion products. Art'05, 8th International Conference on Non-Destructive Investigation and Microanalysis for the Diagnostics and Conservation of Cultural and Environmental Heritage, Lecce.

Joseph, E. (2006). FTIR micro spectroscopy applied to the analysis of painted surface. Young chemists' workshop on chemistry for the conservation of cultural heritage: present and future perspective, CERC3. Perugia, Italy, 20-22 March. Online abtract, http://www.eu-artech.org/index.php?option=com_content&task=view&id=59.

Mazzeo, R., E. Joseph, V. Minguzzi, F. Modugno, S. Prati (2006). Indagini scientifiche sui dipinti murali della dinastia Yuan (1279-1368 d. C.) situati nel sito archeologico di Yao Wang Shan, Cina. Diagnosi, conservazione e restauro di dipinti murali dell'estremo Oriente: quando oriente e occidente s'incontrano e si confrontano. R. Mazzeo. Ravenna, Longo Editore**:** 65-79. ISBN 8880635050.

Mazzeo, R., S. Prati, E. Joseph (2006). Falsificazione di bronzi archeologici in estremo oriente Vero e falso nelle opere d'arte e nei materiali storici: il ruolo dell'archeometria. Atti della giornata nazionale dei Lincei, November 8 2006. Roma, Accademia Nazionale dei Lincei**:** 141-160. ISBN 0394-0705.

Mazzeo, R. and E. Joseph (2007). "Attenuated total reflectance microspectroscopy mapping for the characterisation of bronze corrosion products." European Journal of Mineralogy **19**(3): 363-371. DOI: 10.1127/0935-1221/2007/0019-1733.

Mazzeo, R., E. Joseph, et al. (2007). Indagini di imaging multispettrale e analisi microFTIR per la caratterizzazione dei materiali originali e di restauro del globo celeste di V. Coronelli. Restaurare il cielo. Il restauro del globo celeste faentino di VincenzoCoronelli. N. Scianna. Bologna, CLUEB**:** 48-61. ISBN 978-88-491-3006-5.

Kendix, E., G. Moscardi, R. Mazzeo, P. Baraldi, S. Prati, E. Joseph, S. Capelli (2008). "Far infrared and Raman spectroscopy analysis of inorganic pigments." Journal of Raman Spectroscopy **39**(8): 1104-1112. DOI: 10.1002/jrs.1956.

Kendix, E., S. Prati, et al. (2008). "Far infrared spectroscopy of pigments in art." Meddelelser om konservering **2**: 3-10.

Kendix, E., S. Prati, et al. (2008). "ATR and transmission Analysis of pigments by means of far infrared spectroscopy." Analytical and Bioanalytical Chemistry: accepted for publication. DOI: 10.1007/s00216-009-2691-2.

II SCIENCE FOR CONSERVATION ISSUES

II.1 EXECUTION TECHNIQUE: Setting-up of an integrated analytical methodology, the Koguryo mural paintings.

One of the most important applications of FTIR microscopy is the identification of the artwork's constitutent materials and the characterisation of the adopted execution technique and state of conservation. FTIR microscopy by itself cannot solve all the conservation issues and therefore a research methodology, which involves the use of complementary analytical techniques, should be adopted. Here below are presented, as example of how such a methodology can be set up, the scientific investigations conducted for the first time on the North Korean Koguryo mural paintings, UNESCO world cultural heritage.

II.1.1 Introduction

Very few publications are available on materials and techniques used by far East Asian artists to paint mural decorations and this lack of knowledge may affect very much the planning and execution of the conservation-restoration interventions to be adopted (Chen, Sinkai et al. 1997; Kang, Yi et al. 2001; Moon, Hong et al. 2002; Yi, Yu et al. 2003; Mazzeo, Baraldi et al. 2004; Mazzeo, Cam et al. 2004). However in the last decade, the interest of conservation science in studying painting materials and techniques used in Far East Asian art has grown thanks to the availability and use of integrated analytical approach (Mazzeo 2006). In the framework of the UNESCO workshops on the Conservation and Preservation of the Koguryo mural paintings organized in Pyongyang in 2004 and 2005, scientific investigations have been carried out on the Tokhung-Ri, Yaksu-ri, Susan-ri and Jinpa-ri tombs of the Koguryo Dynasty (37 B.C. – 668 A.D.), which are located in the sub-urban Pyongyang, Democratic People's Republic Korea.

Built in 408 A.D., the Tokhung-ri tomb belongs to a minister Jing and is built in stone masonry covered by a turf mound. It consists of two chambers, containing paintings and Chinese ideograms, interconnected by a short passage (Figure 12). After its re-discovery in 1976, the soil, which filled the tomb after a precedent plunder, was removed and the paintings cleaned with water and

soap. Actually the tomb is in a critical state of conservation due to salt deposits, paint layers detachments and condensation caused by a double-glass barrier built up in 1994 (Luján Lunsford 2004).

Figure 12 – Detail of knights from the Tokhung-ri tomb's mural paintings.

From the same period, the Yaksu-ri tomb is semi-buried in a sloping hill. It has a similar structure as the Tokhung-ri tomb and its paintings represent an important example of the early stage of the Koguryo murals in which both the genre scenes and the Four Directional Animals are depicted on the same wall (Lena 2004). The tomb was discovered in 1958 during an archaeological excavation. Glass barriers have been mounted in 2001 after micro-organisms proliferation has been observed on the paint surfaces. Discovered in 1971, the third tomb (Susan-ri), attributed to the general Goheul, dates back to the second half of the 5th century A.D.. It consists in one chamber at the end of a corridor, with elegant feminine painted figures in a similar iconography as for the late 7th century tomb of Takamatsu in Japan[10]. From the second half of the 6th century, the last tomb (Jinpa-ri N.1) has the same structure as Susan-ri tomb and its walls are decorated with the Four Directional Animals, flying clouds and a honeysuckle pattern.

A representative sampling from all four tombs was performed in close collaboration with mural painting conservator-restorers after careful examination of the painted surfaces. In this research, FTIR microscopy has been associated to optical and polarizing microscopy, environmental scanning electron microscopy coupled with energy-dispersive X-ray analysis (ESEM-EDX), X-ray diffraction (XRD), thermal analyses (thermogravimetry - TG, differential

thermogravimetry - DTG and differential thermal analyses - DTA), Pyrolysis Gas Chromatography Mass Spectrometry (Py-GC-MS) as well as Raman spectroscopy, with the aim to characterise together the material constitution, the state of conservation and the execution technique.

II.1.2 Experimental methods

II.1.2.a *Sampling*

Sixteen samples were collected from the different tombs and submitted to complementary analyses (Table 1). Due to their micro-scale size, an attempt to optimise the analytical sequence of different techniques, according to their non-destructive and micro-destructive nature respect to the sample (Matteini and moles 2003), is here proposed and could represent a general scheme to be followed for the study of paint samples collected as powder or fragment form (Figure 13).

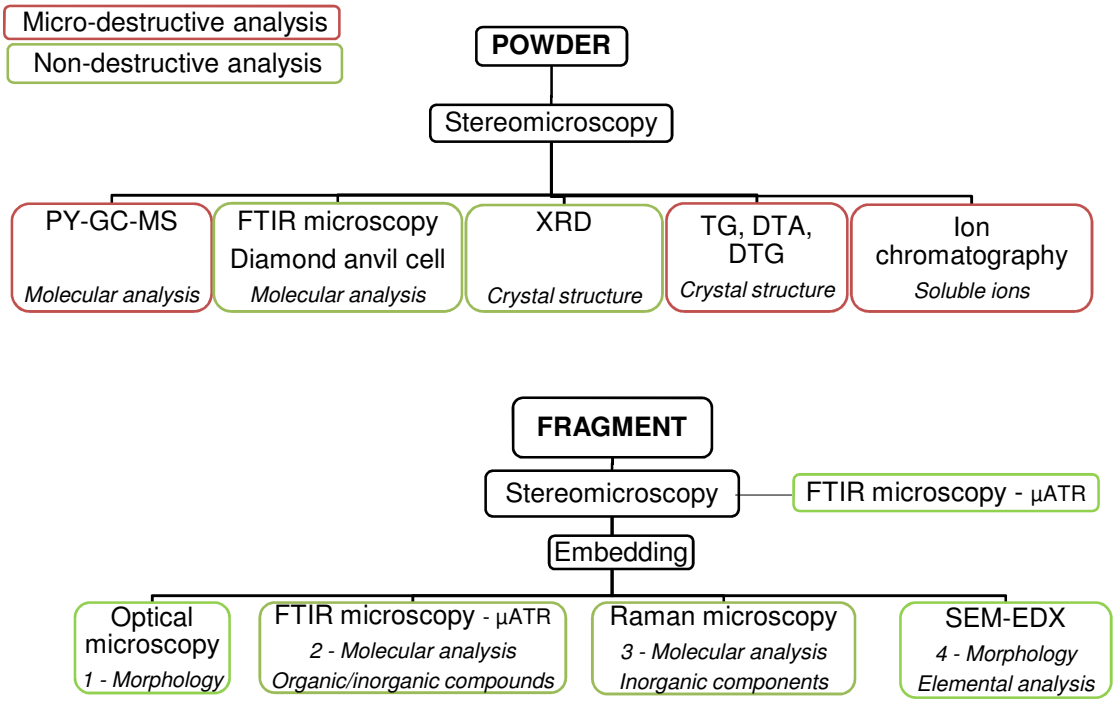

Figure 13 – Scheme of the analytical sequence adopted with paint samples in powder or fragment form with preferential order indicated.

Tomb	Sample	Colour	Type of analysis									
			stereomicroscope	OM	PLM	SEM-EDX	EP-SEM-EDX	XRD, microXRD	TG, DTG, DTA	FTIR, microFTIR	microRaman	PY-GC-MS
Tokhung-ri	TT1	Dark red	x	x		x				x	x	x
	TT2	Yellow	x	x		x				x	x	x
	TT3	Green	x	x		x				x	x	x
	TT4	Black/red	x	x	x	x				x	x	x
	TT5	Yellow	x	x		x				x	x	
	TT6	White deposit	x							x		
	TT7	Brown	x	x	x	x		x	x			
	TT8	Black	x	x			x					x
	TT9	Red	x	x	x		x					x
Yaksu-ri	YT1	Red (dark)	x	x			x			x		x
	YT2	Yellow	x	x			x			x		x
	YT3	Black	x	x			x			x		x
	YR1-05	Blue(blue dragon)	x	x			x					
Susan-ri	ST1	Green/blue	x	x			x			x		x
	ST2	Red	x	x		x		x				
Jinpa-ri N.1	JT1	Red	x	x		x		x				

Table 1 – List of analysed samples

II.1.2.b *Techniques*

All samples, except TT6 and ST2 as powder, have been embedded in a polyester resin (Struers Serifix), cross-sectioned and polished with conventional methods using silicon carbide card with successive grid from 120, 400, 800, to 1000.

II.1.2.b.1 *Optical and polarising microscopy*

First step after the preparation of cross sections, this technique allow their stratigraphic characterisation under both visible and ultraviolet light: numbers of

layers, colour of paint layers, presence of pigments' mixtures, presence of organic substances, repaints... In particular, the UV light observation is typically used as a first tool to qualitatively detect and locate the presence of organic materials (binding media, varnishes, etc.) thanks to the fluorescence effects generated by such materials when submitted to a UV radiation source (Matteini and moles 2003). An optical microscope Olympus BX51M has been used for the dark field observation and photomicrographs recorded with a scanner digital camera Olympus DP70. For samples TT4, TT7 and TT9, petrographic thin sections have been prepared and observed under polarised light in order to obtain mineralogical, structural and textural data.

II.1.2.b.2 *Scanning electron Microscopy*

Such technique should be ideally performed last due to the carbon or gold sputtering necessary on non-metallic cross sections in order to increase their low conductivity, enhance secondary electron emission and prevent charge accumulation and thermal damage. In fact, in the case of further analyses to be performed afterwards, the cross section will be polished again and the stratigraphy can be therefore slightly modified. The elemental composition has been determined using a Philips XL 20 scanning electron microscope (SEM) with an energy dispersive X-ray (EDX) analyser at an acceleration voltage of 25-30 keV, lifetime>50sec, CPS ≈2000 and working distance 34mm. EDX-4 software equipped with a ZAF correction procedure for bulk specimens has been used for semi-quantitative analyses of X-ray intensities. A Zeiss EVO 50 EP extended pressure scanning electron microscope (EP-SEM) equipped with an INCA EDX detector has been also used for samples TT8, TT9, ST1 and all four samples from Yaksu-ri tomb. In this case, no sputter coating is needed and the cross sections can be directly analysed without any additional preparation. The analyses have been performed with INCA energy software, variable pressure mode at a 70 Pa internal chamber pressure, using an acceleration voltage of 20-25 keV, lifetime 400 sec, CPS≈ 12500 and working distance 8 mm.

II.1.2.b.3 *X-Ray diffraction*

On sample TT7, non-destructive XRD analyses have been performed. A Philips PW 1710 diffractometer has been used for semi-quantitative mineralogical analyses, using CuKα radiation, 40kV/30mA, divergence and detector slits of 1°, 0.02° 2Θ step size, and time for step of 1 s. A Micro-area X-Ray Diffractometer equipped with a micro photo camera to focus the X-ray beam has been also employed at the National Research Institute of Cultural Heritage – Conservation Science Division (Daejon, Republic of Korea). In collaboration with Hong Jong Ouk and Han Min Su, micro areas (max 50 x 50 µm) of samples ST2 (powder) and JT1 (cross section) have been directly analysed without any particular preparation.

II.1.2.b.4 *Thermal analyses*

Micro-destructive thermogravimetric (TG), differential thermogravimetric (DTG) and differential thermal (DTA) analyses have been also carried out on sample TT7 to identify and quantify the carbonate content, using a Setaram TAG 24 apparatus with heating rate 20°C/min, CO_2 atmosphere and heating range from 20° to 1000°C. Such analyses should always be inserted at the end of the analytical procedure, apart from the fact that large quantity of sample can be available.

II.1.2.b.5 *Micro-FTIR spectroscopy (µFTIR)*

As many of inorganic compounds and organic substances show characteristic absorptions in the mid-IR range 4000–600 cm^{-1}, FTIR microscopy represents one of the first analytical techniques applied to cultural artefacts. A Nicolet Continuµm FTIR microscope has been used in reflection mode with a micro slide-on ATR (Si crystal) device or in transmission mode with a diamond anvil cell on some particles. The FTIR microscope is equipped with a MCT (Mercury Cadmium Telluride) detector cooled by liquid nitrogen and a 15x Thermo-Electron Infinity Reflachromat objective with a tube factor of 10x. Single-point ATR measurements have been performed directly on the external and internal

surfaces of a fragment before its embedding or, later on its cross section. Transmission measurements have been recorded from single particles selected under a stereomicroscope and pressed with a diamond anvil cell. Spectra from 4000 to 650 cm^{-1} (ATR/diamond cell) have been registered with a FTIR Thermo Nicolet Avatar 370, at a resolution of 4 cm^{-1} and a mirror velocity of 1.8988 $cm.s^{-1}$. A total of 64 scans have been recorded and the resulting interferogram averaged. Acquisition and post-run processing have been carried out using Nicolet "Omnic" software.

II.1.2.b.6 *Micro-Raman spectroscopy (µRaman)*

As some inorganic compounds do not absorb in the mid-infrared region, µRaman measurements have been also performed directly on the fragment's surface or its cross section directing the laser light through a 50x objective of an Olympus microscope. The Raman analyses have been carried out with a Jobin Yvon-Horiba Labram and a laser at 632.8 nm, at a power ranging from 0.5 to 5 mW (slit: 5 cm^{-1}) according with the thermal stability of the compounds to be investigated, and a CCD (330x1100 pixels) detector cooled by the Peltier effect at 200°K. A Jasco 2000 spectrometer combined with an Olympus microscope, cooled with liquid nitrogen, has been also used with a laser at 488 nm and a power range lower than 1 mW. The spectra have been generally recorded between 1100 and 100 cm^{-1}. The possible presence of organic substances has been studied at high wavenumbers, whereas the inorganic compounds, in particular oxides and sulphides, have been investigated at lower wavenumbers. For each paint fragment or layer, an average of 30 particles has been analysed, with a variable collection time according to the magnitude of the scattering signal.

II.1.2.b.7 *Pyrolysis Gas Chromatography Mass Spectrometry (Py-GC-MS)*

Being a micro-destructive technique, Py-GC-MS should be performed at the end of the whole analytical procedure, exception made if the sample quantity is sufficient to conduct analyses in parallel on similar fragments. Pyrolysis

experiments have been performed using an integrated system consisting of a CDS Pyroprobe 1000 heated filament pyrolyser (Chemical Data System, Oxford, PA, USA) and a Varian 3400 gas-chromatograph coupled to a Saturn II ion-trap mass spectrometer (Varian Analytical Instruments, Walnut Creek, CA, USA). A DB-5MS J&W capillary column (30m x 0,25 mm i.d.; 0.25 µ film thickness) has been programmed from 50 °C to 300 °C at 5°C.min^{-1}, keeping the initial temperature 2 min. The samples (< 1 mg) have been pyrolysed in duplicate without treatment through a quartz sample holder at 700 °C for 10 s. Methylating conditions have been used adding 5 µl of an aqueous solution of 25% of tetramethylammonium hydroxide (TMAH) to the sample before pyrolysis; in this way methylation of carboxylic and hydroxyl groups has been achieved. The Py-GC interface has been kept at 250 °C and the injection port at 250 °C with a split injection mode (1:50 split ratio). Helium gas has been used at a flow rate of 1.5 ml.min^{-1}. Mass spectra (1 scan.sec^{-1}) were recorded under electron impact at 70 eV from 40 to 450 m/z.

II.1.3 Results

II.1.3.a *Stone substrate and preparation layer*

The characterization of the stone substrate was carried out only on sample TT7 collected from the Tokhung-ri tomb. The greyish stone seems constituted of a granite rock with a granular texture characterised by a partial pseudo-parallel orientation, so that an exfoliation with preferential detachments is produced within the stone structure. Non destructive analyses, such as optical microscopy on thin section and XRD, have revealed the presence of different minerals: polycrystalline quartz, potassium feldspar, plagioclase, mica (mainly biotite with traces of muscovite) associated with apatite, zircon and opaque minerals (probably sulphides and/or iron oxy-hydroxide). Hence, the stone substrate can be classified as a quartz monzonite with an iso-oriented structure (Figure 14). Visual examination of stone substrates from the other tombs seems to show a similar classification.

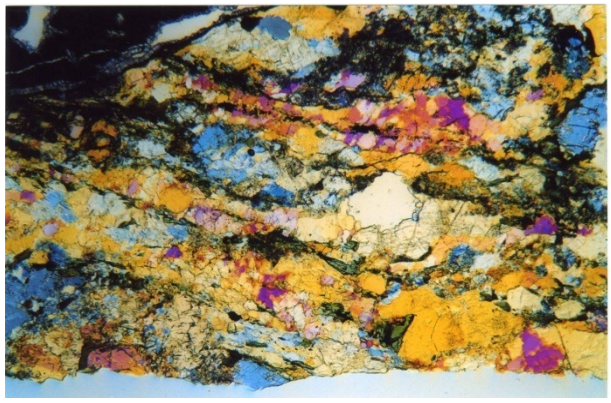

Figure 14 - PLM microphotograph of sample TT7 in thin section.

µFTIR analysis has been first performed and indicated the presence of calcite at 2512, 1795, 1431, 877, 712 cm^{-1} with magnesite ($MgCO_3$) at 745 cm^{-1} and silicates at 1013 cm^{-1} (Figure 15). Afterwards, SEM-EDX and, in parallel, TG and DTA analyses have confirmed that calcite was present with quartz and clay mineral components as well as calcite rich in magnesium or dolomite $CaMg(CO_3)_2$.

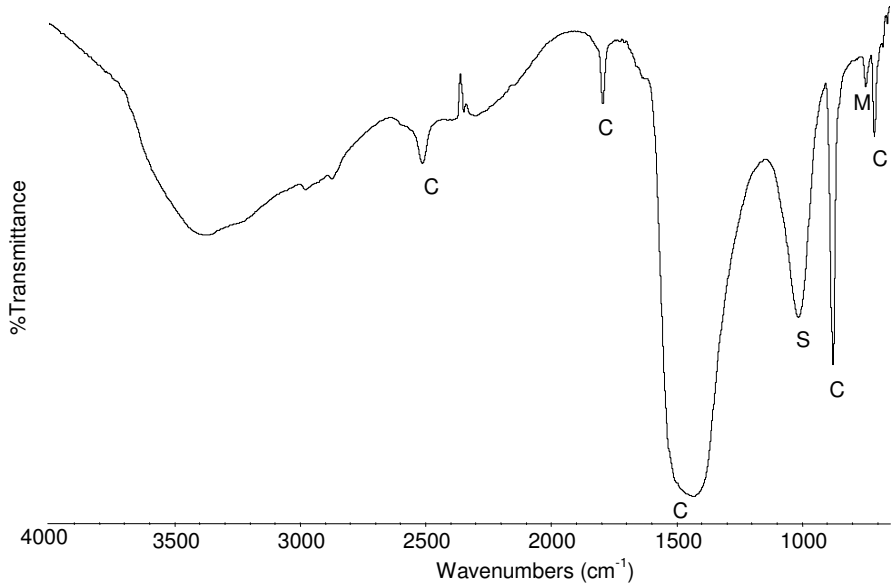

Figure 15 - µFTIR transmittance spectrum (4000-650 cm^{-1}) of the preparation layer from sample TT3 (C, calcite; S, silicates; M, magnesite).

All preparation layers resulted to be constituted of the same compounds. In Tokhung-ri samples, some traces of a translucent material has been investigated with µFTIR (Figure 16) and resulted to be constituted of a siloxane

material, as showed from the strong absorption bands present in the 1130-1000 cm^{-1} region (Si-O-Si stretching), at 2159 cm^{-1} (Si-H stretching) and 1245 cm^{-1} (Si-Ethyl deformation) (Smith 1974). This scarce material is randomly present within the preparation layers and therefore cannot represent the residue of a siloxane based protective coating or consolidant applied during past interventions without being constantly distributed within the cross-section and in particular on the outermost external surface. More probably it may result from antifoaming agents, which are commonly added to detergents and whose presence is linked to the soap used to clean the murals in 1976.

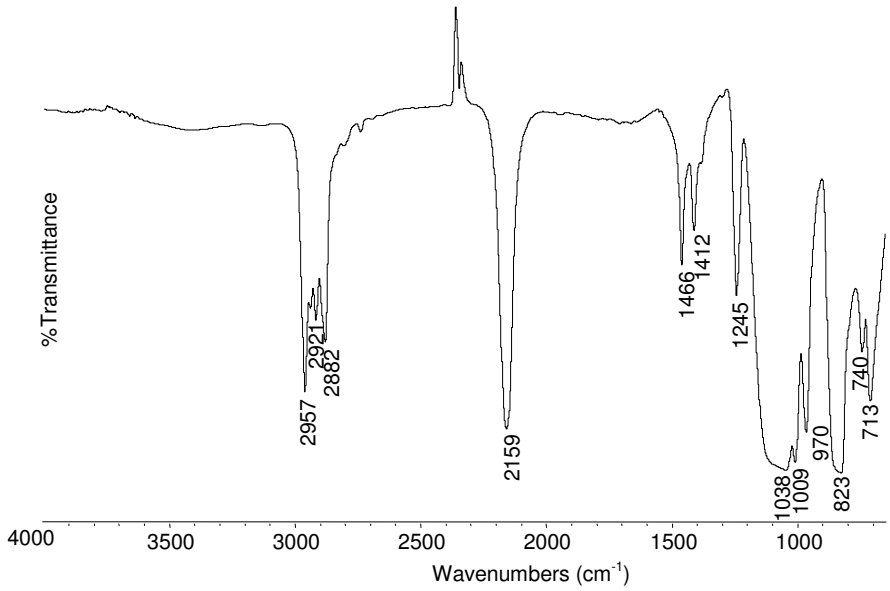

Figure 16 - µFTIR transmittance spectrum (4000-650 cm^{-1}) of the translucent material identified as siloxane.

Regarding the Yaksu-ri tomb, SEM observations showed a sub-division of the preparation layer into two or three sub-layers, indicating the overlapping of different lime wash applications (Figure 17).

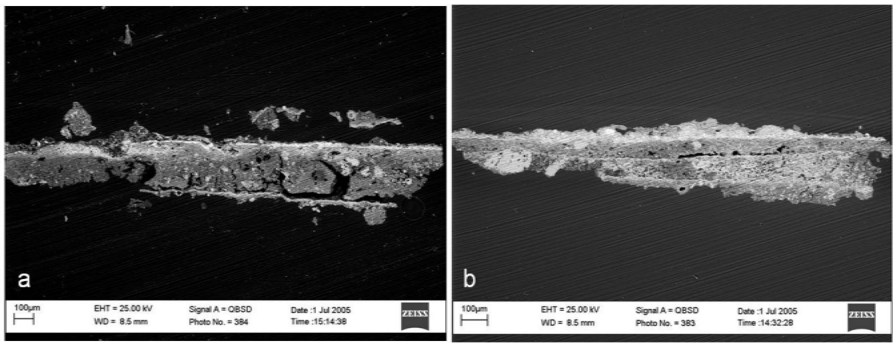

Figure 17 - Back scattered electron images of (a) sample YT1 and (b) sample YT2.

II.1.3.b *Paint layers*

The red, yellow, green and black tonalities of Koguryo mural paintings have been analysed and the results are summarised in table 2. The limited mineral pigments have all been applied in single layer, except sample TT4 showing a double layer structure with a carbon black layer (belonging to an inscription) superimposed to a red paint layer. Iron oxide red (hematite, Fe_2O_3) pigment has been used for all red colours. In particular, this pigment have been finely ground in Yaksu-ri (sample YT1) and Jinpa-ri murals (sample JT1) or added with black magnetite (Fe_3O_4) in Tokhung-ri (samples TT1 and TT9) to obtain a darker tonality (Figure 18). The use of magnetite has been also reported in literature for Far East Asian art (Rokuro and Mitsuharu 1931; Shuye 1987).

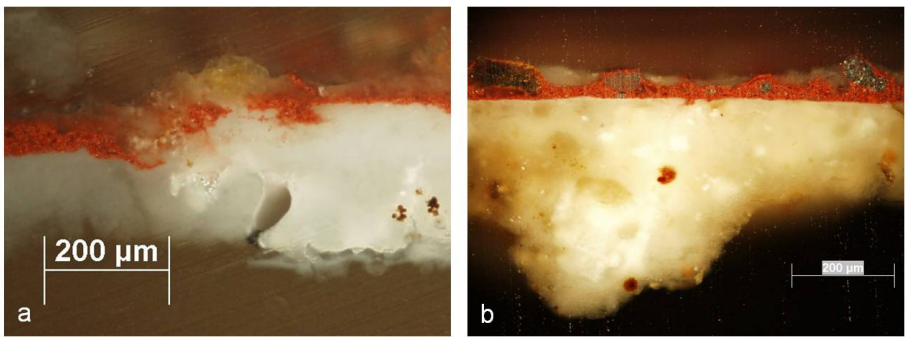

Figure 18 – Cross section (100 x original magnification) of sample a) YT1 and b) TT1.

On Susan-ri murals on a light red area, micro area XRD analyses have shown the presence of vermillion (HgS) with traces of iron red oxide (Figure 19). Even if this pigment has been widely employed on mural paintings, its use for fresco

technique is not recommended due to its tendency to darken when exposed to a basic environment. The limited quantity of sample has not allowed ascertaining the presence of an eventual binding medium and further investigations should be foreseen.

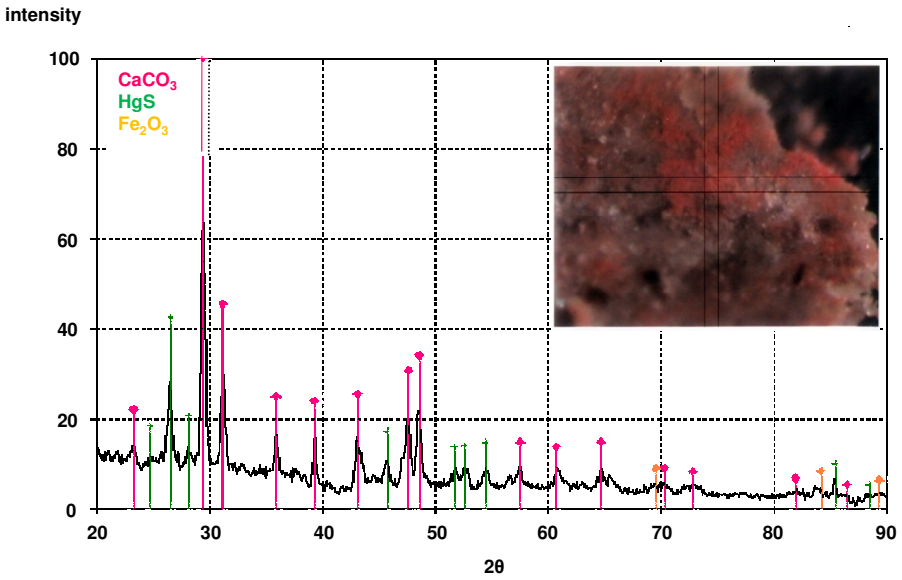

Figure 19 – micro area XRD spectrum (50 x 50 µm) on sample ST2 with rays indicated for calcite $CaCO_3$ (pink), vermilion HgS (green) and iron red oxide Fe_2O_3 (yellow).

In samples TT2, TT5 and YT2, the yellow colours have been obtained with iron oxide yellow (goethite). Regarding the green colours, optical microscopy, µFTIR and SEM-EDX have been performed following the analytical sequence suggested above and allowed the identification of green earth pigment (3557, 1081, 801, 750 and 683 cm^{-1}), used pure (sample TT3) or mixed with carbon black in a calcium matrix (sample TT8). On the surface of sample TT3, a thin organic layer has been also identified by µFTIR compression cell as microcrystalline wax (Figure 20).

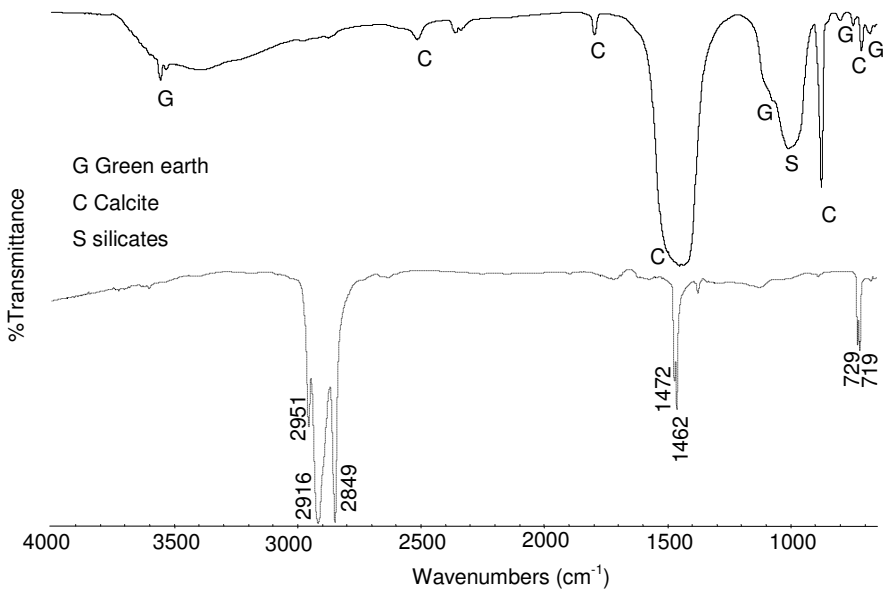

Figure 20 – µFTIR transmittance spectra (4000-650 cm^{-1}) of the green paint layer and of the external organic layer (dashed line) from sample TT3.

On this other part, the sample ST1 has been also collected from a green area but resulted to be constituted of a black layer (probably carbon) superimposed to a yellow ochre (Fe and Si in abundance), as showed by optical microscopy and EP-SEM (Figure 21).

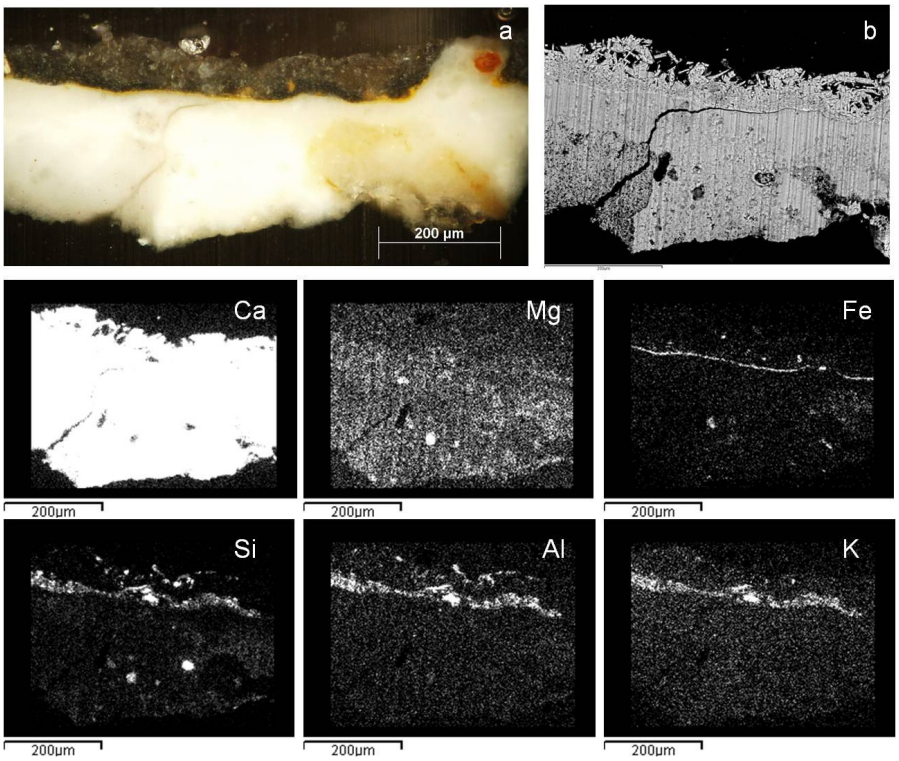

Figure 21 – Sample ST1: a) cross section microphotograph (200x original magnification), b) Back scattered electron image of the area submitted to EDX mapping, EDX mapping of Ca, Mg, Fe, Si, Al and K elements.

The only blue sample has been collected from the figure "*blue dragon*" of the Yaksu-ri tomb. It represents one of the few blue painted areas which have been mentioned by archaeologists. However, no chemical element imputable to blue pigments such as smalt, azurite or lapis lazuli has been detected with SEM-EDX analysis. On the contrary, it has been found the same composition (Ca and C with traces of Mg and Si) as for the black layer of samples ST1 and YT3. In fact, some carbon-based pigments present an intrinsic bluish tone (Winter 1983): charcoal black, ivory or bone black, lamp or carbon black. Probably, this latter may have been used for the blue dragon due to the absence in SEM-EDX analyses of both opaque and elongated particles for charcoal black as well as P element for bone and ivory black.

Either µFTIR, µRaman or EDX analyses have showed the presence of calcite in preparation layers and besides as binding material in all paint layers. Moreover during optical microscopy observations, no discontinuity between the preparation and paint layers has been observed as well as any fluorescence of

eventual organic binding media. Pyrolysis Gas Chromatography Mass Spectrometry has further confirmed these results.

II.1.3.c *Concretions and deposits*

A thin layer of re-crystallized calcite is also located in the outermost paint surfaces of many samples. Under PLM observations, this calcite shows an ultra fine cryptocrystalline structure of primary genesis, which differs from the one (a spatic subhedral microcrystalline structure of secondary genesis) found for the calcite in preparation and paint layers (Figure 22).

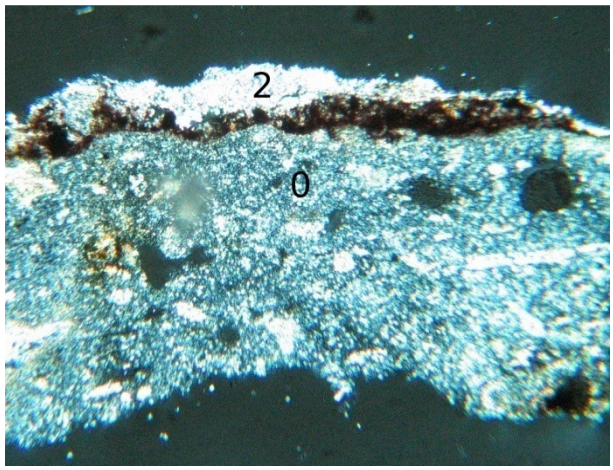

Figure 22 – PLM of sample TT9 (100x original magnification) with recristallised calcite (layer 2) and preparation layer (layer 0).

Re-crystallized calcite with similar structure and characteristics has also been identified on the mural paintings from the Catacombs of Villa Torlonia (Rome, Italy). The high level of relative humidity (RH) and carbon dioxide (CO_2) present within these tombs are assumed to play an important role in its formation. First, the calcite may be solubilised by the water enriched in CO_2 (RH 90-95%) as described with the equation 3:

$$CaCO_3 + CO_2 + H_2O \longleftrightarrow Ca(HCO_3)_2 \qquad 3$$

Then, the newly formed calcium bicarbonate $Ca(HCO_3)_2$ can re-crystallize into calcium carbonate $CaCO_3$, if not leached by more water. Linked to this

formation mechanism, a hard white deposit TT6 has been collected on the murals of the Tokhung-ri tomb and resulted to be constituted of $Mg(HCO_3)(OH)\cdot 2H_2O$, nesquehonite. This mineral is generally found as concretions from mines of magnesite rocks and therefore should be related with the particular composition of the preparation layer where both magnesite and dolomite have been detected.

II.1.4 Conclusions

The proposed sequence of analytical techniques has been optimized in function of the limited quantity of sample available and this methodology has permitted to identify the painting materials and characterise the adopted execution technique and state of conservation. The scientific results have contributed to accurately select the most appropriate conservation-restoration interventions actually in progress. Some features typical of a fresco technique have been confirmed: pigments suitable with a basic environment, presence of calcite both in preparation and paint layers, absence of discontinuity within the stratigraphy and furthermore no evidence of organic binding media. In the fresco technique, dry pigments are ground with water and brushed onto a wet lime plaster, which then reacts with CO_2 to form a pigmented calcium carbonate layer. At present, these mural paintings could represent the first example of a fresco technique used in Far East Asia, whether it has been intentionally achieved or not by North Korean painters. An exception is the red sample with vermilion pigment found in Susan-ri tomb and for which further investigations, such as historical literature survey or visual examination with raking light, are necessary as the majority of the wall paintings studied so far (Mazzeo, Baraldi et al. 2004; Mazzeo 2006) have been painted with secco techniques. Especially, it would be interesting to perform similar investigations on the Koguryo mural paintings located in China.

II.1.5 Acknowledgements

The National Bureau for Cultural Property Conservation of the Democratic People's Republic of Korea is thanked for providing samples of the Koguryo mural paintings. Thanks are also extended to Ms. Junhi Han (project coordinator, UNESCO, Division of Cultural Heritage) and Mr. Rodolfo Lujan Lunsford (mural painting conservator-restorer). Mr. Hong Jong Ouk and Mr. Han Min Su (National Research Institute of Cultural Heritage, Conservation Science Division, Daejon, Korea) are thanked for their collaboration in performing the analyses of samples ST2 and JT1.

II.2 DEGRADATION PHENOMENA: metals carboxylates formation during the ageing of paintings

A part for the characterisation of the execution technique, FTIR microscopy is also widely applied for the study of degradation phenomena. In particular in this chapter, the interaction between pigments and binding media during ageing is presented. In fact, degradation processes may result in the production of metal soaps on the paintings surface which modifies their visible appearance and state of conservation. In order to characterize the nature of metal soaps found on paintings, several naturally aged oil and egg yolk tempera paint reconstructions made with different pigments have been submitted to ATR-FTIR microspectroscopy. Standard metal palmitates have also been synthesised and analysed by FTIR microscopy, to help identifying the metal soaps formed. For red lead and litharge paints, it has been observed that the production of lead soaps seems to be associated with the formation of lead carbonate. Moreover, the formation rate of lead carboxylates seemed to differ according to the pigment's nature and a larger amount of carboxylates has been found for red lead and litharge respect to lead white, Naples yellow and lead tin yellow. On both oil and egg tempera paints, the formation of metal soaps has also been confirmed on zinc, manganese, cadmium and copper paints. Particularly, ATR mapping performed on azurite paints has showed the contemporary presence of copper carboxylates and malachite in their degraded areas. Furthermore, the key role played by manganese in the production of metals soaps for sienna and umber has been for the first time observed.

II.2.1 Introduction

On paintings, the ageing processes have important consequences on both the visible appearance and the state of conservation. In fact, the formation of metal soaps results in the increased transparency of the paintings due to the gradual loss of the pigment hiding power as well as protrusions or efflorescence also called blooming effect.

Environmental humidity also plays a crucial role in the hydrolysis of triglycerides leading to the formation of more hydrophilic and soluble compounds, such as metal soaps (O'Neill and Brett 1969; Bell 1970; Plater, De Silva et al. 2003; Robinet and Corbeil 2003; Keune and Boon 2004; Keune 2005). These latter can aggregate and are sometimes present as surface protrusions which may expand and break up the paint layer (Keune, Noble et al. 2002; Higgitt, Spring et al. 2003), as shown in figure 23. A part from paintings, metal carboxylates have also been detected on the surfaces of metal objects due to interactions between the metal substrate and either gilding, surface treatments based on drying oil or other organic substrates such as leather (Robinet and Corbeil 2003; Mazzeo and Joseph 2007).

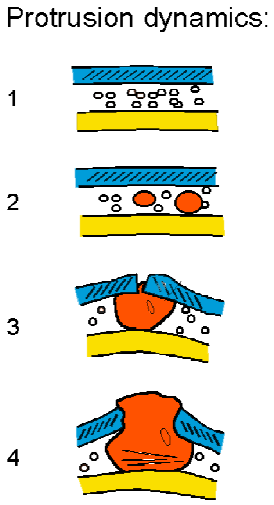

Figure 23 - Scheme of the formation of lead soap aggregates based on the mechanisms presented by Boon et al.: 1) intact paint, 2) early stage with small lead soap aggregates, 3) mature stage with aggregate expansion, 4) protusion with remineralisation. (Boon, van der Weerd et al. 2002; Keune 2005).

In painted artworks, several studies have been published on the interaction between metal ions, present as driers or pigments, and organic binding media, especially drying oils. Among the different analytical techniques used, FTIR spectroscopy has been focused on the role played by pigments on the long-term changes in the oil binding medium (van der Weerd, van Loon et al. 2005). A triglyceride hydrolysis process has been identified with the shifting and broadening of the carbonyl band in presence of pigments such as lead and zinc white. In order to define the degradation processes, the reduced intensity of the ester asymmetric stretching and the contemporary formation of metal carboxylates have been used as markers. Gas chromatography has also

underlined their implication in the analytical detection of linseed oil (Colombini, Modugno et al. 1999; Gimeno-Adelantado, Mateo-Castro et al. 2001) and the catalytic effect induced by different pigments on the hydrolysis of the triglycerides (Chiavari, Fabbri et al. 2005). Moreover, the production of short chain fatty acids, such as acetic and oxalic acids, aldehydes and diacids has been demonstrated (Mills 1966). While several papers have already been published on the formation of lead, copper and zinc carboxylates (O'Neill and Brett 1969; Bell 1970; Keune, Noble et al. 2002; Higgitt, Spring et al. 2003; Plater, De Silva et al. 2003; Robinet and Corbeil 2003; Keune and Boon 2004; Keune 2005; Cotte, Checroun et al. 2007), research on other types of metal carboxylates has been so far neglected. Therefore, this chapter presents the analytical results achieved for the chemical characterization of the interactions between pigments and binding media. Attenuated total reflectance (ATR) microspectroscopy measurements have been performed non-destructively on the surface of 10 years naturally aged oil and egg tempera paint samples. These reconstructions have accurately been prepared following ancient recipes to provide conservation scientists and conservator-restorers with reference materials and standards for instrumental analysis and visual examinations (Aldrovandi, Altamura et al. 1996). In order to facilitate the identification of metal carboxylates, metal palmitates have been synthesised and their specific ATR-FTIR spectra recorded.

II.2.2 Experimental methods

II.2.2.a *Synthesis of metal palmitates*

For each metal ion, the different metal carboxylates obtained from the relative fatty acids show differences in the spectral range 1000–1300 cm^{-1} according to the number of CH_2 present in the alkyl lateral chain. On paintings, however, the simultaneous formation of different metal carboxylates during ageing processes does not allow their differentiation. Nevertheless different metal ions give rise to different metal carboxylates, which can be distinguished based on the position

of the COO^- band (Robinet and Corbeil 2003). Thus only lead, cobalt, zinc, cadmium and manganese palmitates have been synthesised.

Lead palmitate has been prepared according to a method reported elsewhere (Plater, De Silva et al. 2003). 30 mL of a 0.02 M solution of lead nitrate $Pb(NO_3)_2$ in H_2O:EtOH:MeOH (5:5:2 in v/v) has been mixed with 12.5 mL of a 0.02 M solution of palmitic acid in MeOH and the mixture has been left for 10 min in an ultrasonic bath. The precipitate has been filtered, washed with EtOH and then vacuum-dried. According to the literature (Kambe 1961), cobalt palmitate has been prepared by dropwise addition of 2.5 mL of a 0.4 M solution of cobalt acetate $Co(CH_3COO)_2 \cdot 4H_2O$ in EtOH to 6 mL of a 0.3 M solution of palmitic acid in H_2O and stirring for 2h. The blue precipitate has been then filtered and vacuum-dried.

The preparation method of zinc, manganese and cadmium palmitates has been adapted from the synthesis of cobalt palmitate. Cadmium and zinc palmitates have been prepared by dropwise addition of 3 mL of a 0.3 M water solution of cadmium acetate $Cd(CH_3COO)_2 \cdot 2H_2O$ and zinc acetate $Zn(CH_3COO)_2 \cdot 2H_2O$ respectively to 12 mL of a 0.2 M solution of palmitic acid in EtOH. Both solutions have been left at 50 °C for 3h and the respective precipitates have then been filtered and vacuum-dried. Manganese(II) and (III) palmitates have been prepared by dropwise addition of 3 mL of a 0.4 M water solution of Mn^{II} acetate $Mn(CH_3COO)_2$ and Mn^{III} acetate $Mn(CH_3COO)_3 \cdot 3H_2O$ respectively to 12 mL of a 0.25 M solution of palmitic acid in EtOH. For Mn^{II}, the formation of the precipitate has been immediate whereas for Mn^{III} the carboxylate has been obtained after 1h at 50°C. Both precipitates have then been filtered and vacuum-dried. The copper palmitate has kindly been provided by The Canadian Conservation Institute (Robinet and Corbeil 2003).

II.2.2.b *Standard paint samples*

In 1996, some oil and egg tempera paint reconstructions have been prepared by conservator-restorers of the Opificio delle Pietre Dure in Florence following the Cennino Cennini's paint recipes (Thompson Jr 1954). They consisted of mixtures of pigments with different binding media applied on a wood support prepared with a rabbit glue water solution (1:16) saturated with gypsum (Table

2). Afterwards, these paint reconstructions have been stored in a closed metal cupboard at ambient environmental conditions (Aldrovandi, Altamura et al. 1996). For the oil paint standards, stand linseed oil has been used and for the egg tempera paint standards, the recipe is based on 1/4 egg white, 1/4 vinegar and 2/4 yolk mixed together. Films made of stand linseed oil and egg tempera have been also prepared as reference materials.

Colour	Name	Chemical Formula[1]	Oil paint	Egg tempera paint
Blue	Azurite	$Cu_3(CO_3)_2(OH)_2$	x	x
	Indigo	$C_{16}H_{10}N_2O_2$	x	
	Lapis lazuli	$(Na,Ca)_4(AlSiO_4)_3(SO_4,S,Cl)$	x	x
	Cobalt blue	$CoAl_2O_4$	x	x
	Prussian blue	$Fe_7(CN)_{18}$	x	
	Artificial ultramarine	$Na_{8\text{-}10}Al_6Si_6O_{24}S_{2\text{-}4}$	x	x
	Cerulean blue	$CoO{\cdot}SnO_2$	x	
Red	Cadmium red	CdS, CdSe	x	
	Red lead	Pb_3O_4	x	x
	Kermes	$C_{18}H_{12}O_9$	x	
	Madder	$C_{14}H_8O_4 + C_{14}H_8O_5$	x	
	Burnt sienna	$Fe_2O_3 + MnO_2 + Al_2O_3{\cdot}SiO_2{\cdot}nH_2O$	x	
	Bole	$Al_2O_3{\cdot}SiO_2 + Fe_2O_3$	x	x
	Red ochre	Fe_2O_3, silicate s	x	
	Burnt umber	$Fe_2O_3 + MnO_2$ + silicates	x	x
	Raw umber	$MnO_2 + Fe(OH)_3$ + silicates	x	x
Yellow	Naples yellow	$Pb_3(Sb_3O_4)_2$	x	x
	Litharge	PbO	x	x
	Cadmium yellow	CdS	x	x
	Orpiment	As_2S_3	x	x
	Lead tin yellow	Pb_2SnO_4 or $PbSn_2SiO_7$	x	x
	Realgar	As_4S_4	x	x
	Raw sienna	$FeO(OH) + MnO_2 + Al_2O_3{\cdot}SiO_2{\cdot}nH_2O$	x	x
	Yellow ochre	$Fe_2O_3{\cdot}H_2O$, silicates	x	x
	Mars yellow	$Fe(OH)_3 + Al(OH)_3 + CaSO_4{\cdot}nH_2O$	x	x
	Indian yellow	$C_{19}H_{16}MgO_{11}{\cdot}6H_2O$	x	x
Green	Malachite	$Cu_2(CO_3)(OH)_2$	x	x
	Green earth	Glauconite + celadonite ($Fe^{(II)}$, Mg, K aluminosilicates)	x	
	Cobalt green	CoO + ZnO	x	x
	Chrome oxide	Cr_2O_3	x	x
	Viridian	$Cr_2O_3{\cdot}2H_2O$	x	x
	Veronese green	$Cu_3(AsO_4)_2{\cdot}4H_2O$	x	
White	Lead white	$2PbCO_3{\cdot}Pb(OH)_2$	x	x
	Zinc white	ZnO	x	x
	Titanium white	TiO_2	x	x
	chalk	$CaCO_3$	x	x
Black	Ivory black	$Ca_3(PO_4)_2 + CaCO_3$ + carbon	x	
	Vine black	amorphous carbon	x	
	Lamp black	amorphous carbon, traces of Na and K salts	x	
Gray	Bone black + Lead white	$Ca_3(PO_4)_2 + CaCO_3 + C + 2PbCO_3{\cdot}Pb(OH)_2$	x	
	Vine black + Lead white	amorphous carbon + $2PbCO_3{\cdot}Pb(OH)_2$	x	
	Lamp black + Lead white	amorphous carbon + $2PbCO_3{\cdot}Pb(OH)_2$	x	

Table 2 - List of pigments employed in the paint film reconstructions.

[1] *As reported on the specification sheets of the different pigments purchased from the Zecchi company.*

II.2.2.c *Micro-ATR FTIR spectroscopy*

Both synthesised carboxylates and paint reconstructions have directly been placed onto the FTIR microscope XYZ motorized stage for the non-destructive ATR measurements (Figure 24).

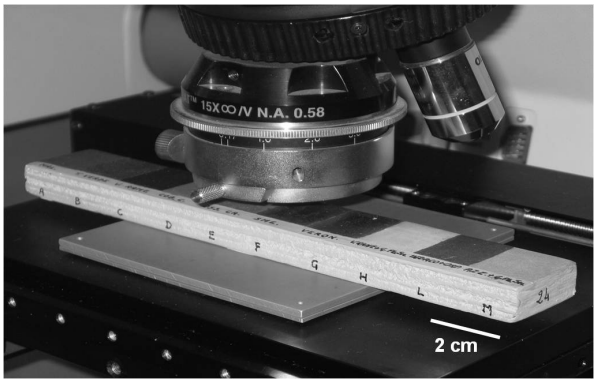

Figure 24 - A paint reconstruction positioned on the FTIR microscope motorized stage ready for analysis by the slide-on ATR objective.

A Thermo-Nicolet Nexus 5700 spectrometer has been used coupled to a Nicolet Continuum IR microscope fitted with an MCT detector cooled by liquid nitrogen and a 15x Thermo-Electron Infinity Reflachromat objective with a tube factor of 10x. ATR spectra have been acquired in the range 4000–650 cm^{-1}, at a spectral resolution of 4 cm^{-1}. A total of 64 scans have been recorded and the resulting interferogram averaged. For each sample, a minimum of three single-point ATR measurements has been performed using a slide-on ATR objective with a silicon crystal. ATR mapping has also been performed on a selected area (350 x 400 μm^2) of the azurite paint reconstruction in order to obtain information on the spatial distribution of the chemical compounds present. For each of them, the integrated absorbance of a characteristic spectral band has been used to plot their distribution as false-colour images. In order to maintain the spatial resolution, we have chosen a step size of 20 µm with an aperture of 150 µm x 150 µm, relative to an investigated area of ~ 44 x 44 μm^2 in ATR mode.

II.2.3 Results

II.2.3.a *Metal palmitates characterization*

The synthesised metal palmitates (Pb, Zn, Cu, Cd, Mn^{II} and Mn^{III}) have been characterized by FTIR microscopy with ATR measurements performed directly on some powder place onto the microscope stage (Figure 25).

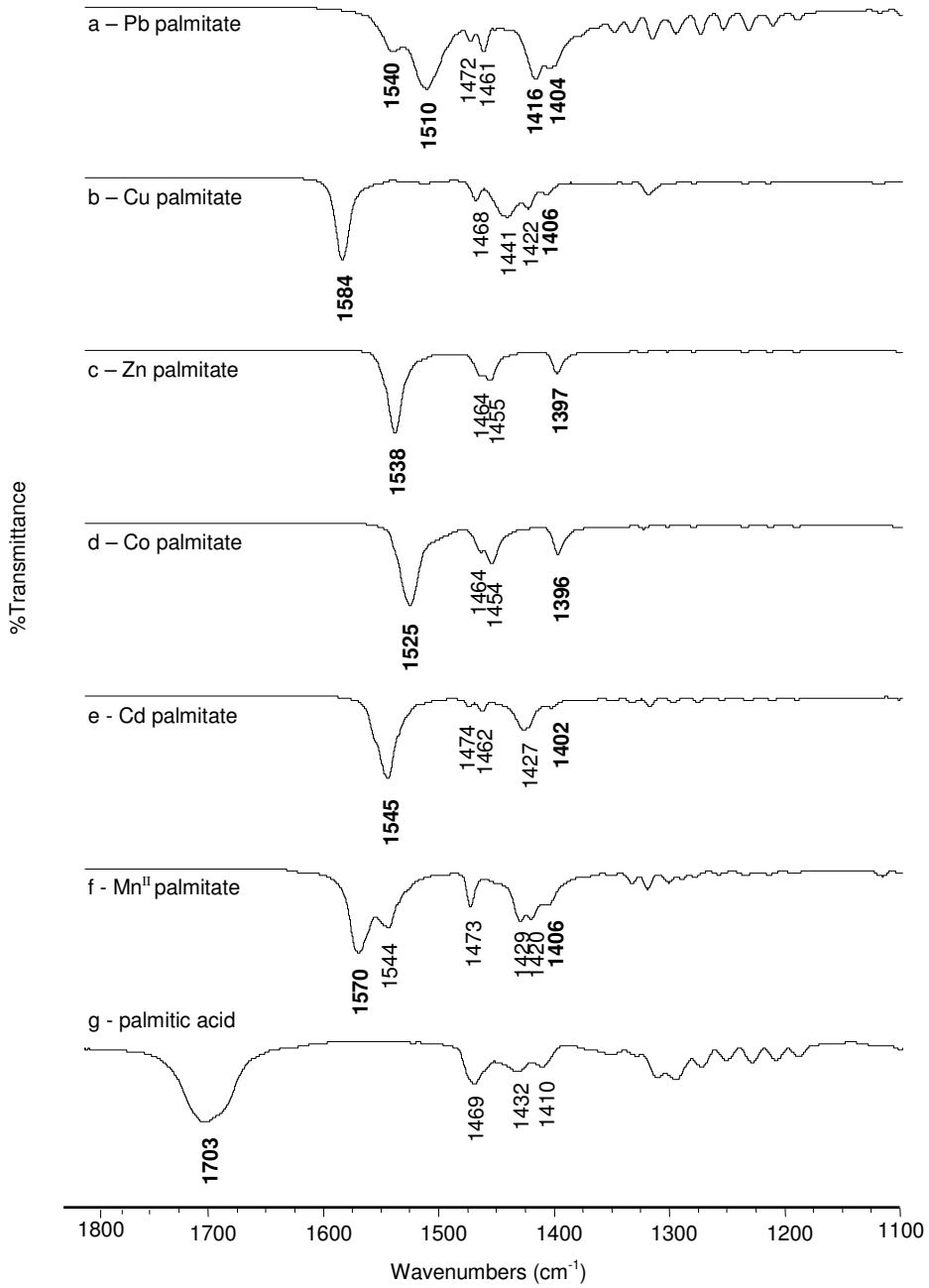

Figure 25 - µFTIR-ATR spectra (1800-1100 cm^{-1}) of a) lead palmitate, b) copper palmitate, c) zinc palmitate, d) cobalt palmitate, e) cadmium palmitate, f) Mn(II) palmitate and g) palmitic acid. The characteristic absorption bands are highlighted in bold.

All spectra present asymmetric and symmetric COO^- stretching bands in the spectral range of 1600-1400 cm^{-1}. The spectrum of lead palmitate presents an intense band at 1510 cm^{-1} and a second band at 1540 cm^{-1}. Zinc, cobalt, copper and cadmium palmitates are characterized by an asymmetric COO^- stretching band at 1538, 1525, 1584 and 1545 cm^{-1} respectively. Mn^{II} and Mn^{III} palmitates have similar spectral features and their spectra present a strong band at 1570 cm^{-1} and a weaker band at 1544 cm^{-1}. The absence of the C=O asymmetric stretching band at 1703 cm^{-1} in all spectra confirms that the precipitates are free of excess palmitic acid. These spectra will be used as references for the identification of eventual metal carboxylates formed on the surface of the paint reconstructions.

II.2.3.b *FTIR studies of aged oil and egg films*

ATR spectra have been measured on stand linseed oil and egg tempera films naturally aged for 10 years (Figure 26, table 3).

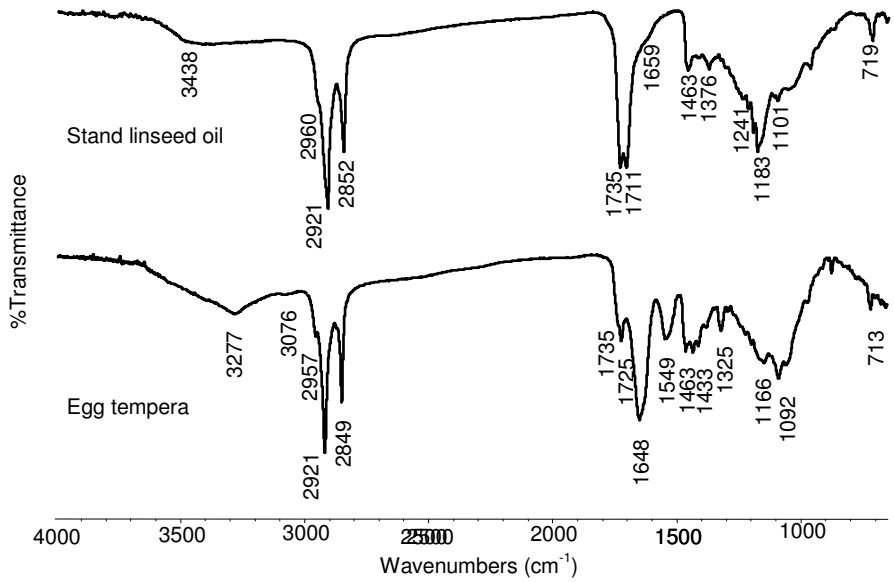

Figure 26 - µFTIR-ATR spectra (4000-650 cm^{-1}) of 10 years naturally aged films of a) stand linseed oil and b) egg tempera.

Linseed oil (cm^{-1})	Egg tempera (cm^{-1})	Assignment
3438 w		O-H stretching
	3277 m	N-H stretching
	3076 w	amide II overtone
2960 sh	2957 w	$\nu_{AS}CH_3$ stretching
2921 vs	2921 vs	$\nu_{AS}CH_2$ stretching
2873 sh	2875 w	$\nu_{S}CH_3$ stretching
2852 s	2849 s	$\nu_{S}CH_2$ stretching
1735 s	1735 sh	C=O (ester) stretching
1711 s	1725 s	C=O (acid) stretching
	1648 s	amide I (C=O) stretching
1659 sh		C=C stretching
	1549 s	amide II (N-H) bending
1463 m	1463 m	CH_3 asymmetric bending
	1433 m	CH_2 scissoring
1376 m	1380 w	CH_3 umbrella mode
1241 w		C-O-C (ester) stretching
1183 m	1166 m	C-O-C (ester) stretching
1101 w		C-O-C (ester) stretching
719 w	713 w	CH_2 rocking

Table 3 – FTIR-ATR characteristic absorptions bands of 10 years old linseed oil and egg tempera films. vs (very strong), s (strong), m (medium), w (weak), sh (shoulder).

These provide a reference for the evaluation of the interaction between pigments and binders. During ageing processes (polymerization) of oil, the double bonds present in the triglycerides undergo oxidation. In fact, a broad band at 3435 cm^{-1}, which can be attributed to alcohol stretching and hydroperoxides functions, is observed in the spectrum of stand linseed oil (O'Neil 1963). Moreover, a broadening of the C=O ester asymmetric stretching band at about 1735 cm^{-1} is also noticed. This phenomena can be explained by the triglycerides hydrolysis and thus formation of free fatty acids, associated with other degradation products such as aldehydes, ketones, anhydrides, lactones (van der Weerd, van Loon et al. 2005). In particular, the free fatty acids can be distinguished by the presence of an additional absorption band at 1711 cm^{-1}. Regarding the ageing of egg tempera paints, changes mainly affect the triglycerides moieties and are still unknown for the proteinaceous components. Also in this case, the degree of unsaturation, even if lower than in siccative oil, is reduced. In the FTIR spectrum, the intensity decreasing of the C=O ester asymmetric stretching band is observed together with the contemporary

apparition of C=O acid stretching, indicating a partial hydrolysis of the triglycerides and formation of free fatty acids (Meilunas, Bentsen et al. 1990). In the egg tempera spectrum, two strong absorption bands at around 1650 cm^{-1} (amide I, C=O stretching) and 1550 cm^{-1} (amide II, N–H bending) are also visible and are typical protein bands assigned to the amide functions of the peptide groups.

II.2.3.c *Analysis of oil and egg paint standards*

II.2.3.c.1 *Oil paint reconstructions*

In table 4, the results achieved on oil paint reconstructions are summarised.
First, metal carboxylates have not been detected for paint reconstructions involving dyes (indigo, kermes, madder and Indian yellow), chrome oxide, viridian, green earth, lapis lazuli, artificial ultramarine, chalk, titanium white, Mars yellow, realgar, orpiment and carbon blacks (vine, lamp and ivory blacks). In fact, saponification can only occur between Lewis base and Lewis acid (nucleophile and electrophile respectively). In particular, the spectral bands corresponding to the oily binder remain similar to those of the aged linseed oil reference spectrum. On the other hand, in presence of iron-based pigments, such as Prussian blue, bole, yellow and red ochre, the C=O acid asymmetric stretching has a greater intensity than the C=O ester band. A similar feature is observed also for the cobalt blue and cerulean blue. The fact that these pigments may contribute to the ester hydrolysis with iron or cobalt acting as eventual catalysts needs certainly further investigations (Figure 27).

Pigments	Metal involved	Carboxylates formation	Hydrolytic effects	Similar to pure linseed oil
Indigo				x
Kermes				x
Madder				x
Vine black				x
Lamp black				x
Orpiment	As			x
Realgar	As			x
Chalk	Ca			x
Ivory black	Ca			x
Cadmium red	Cd			x
Cadmium yellow	Cd	x		
Cobalt blue	Co		x	x
Cerulean blue	Co Sn		x	x
Chrome oxide	Cr			x
Viridian	Cr			x
Azurite	Cu	x		
Malachite	Cu	x		
Veronese green	Cu	x		
Prussian blue	Fe		x	x
Red ochre	Fe		x	x
Yellow ochre	Fe		x	x
Bole	Fe Al		x	x
Mars yellow	Fe Al Ca			x
Green earth	Fe K Mg Al			x
Indian yellow	Mg			x
Burnt sienna	Mn Fe	x		
Burnt umber	Mn Fe Al	x		
Raw umber	Mn Fe Al	x		
Raw sienna	Mn Fe Al	x		
Lapis lazuli	Na Al			x
Artificial ultramarine	Na Al			x
Red lead	Pb	x		
Litharge	Pb	x		
Lead white	Pb	x		
Vine black + lead white	Pb	x		
Lamp black + lead white	Pb	x		
Naples yellow	Pb Sb	x		
Lead tin yellow	Pb Sn	x		
Ivory black + lead white	Pb, Ca	x		
Titanium white	Ti			x
Zinc white	Zn	x		
Cobalt green	Zn, Co	x		

Table 4 - Summary of metal carboxylates' occurrence on oil paint reconstructions.

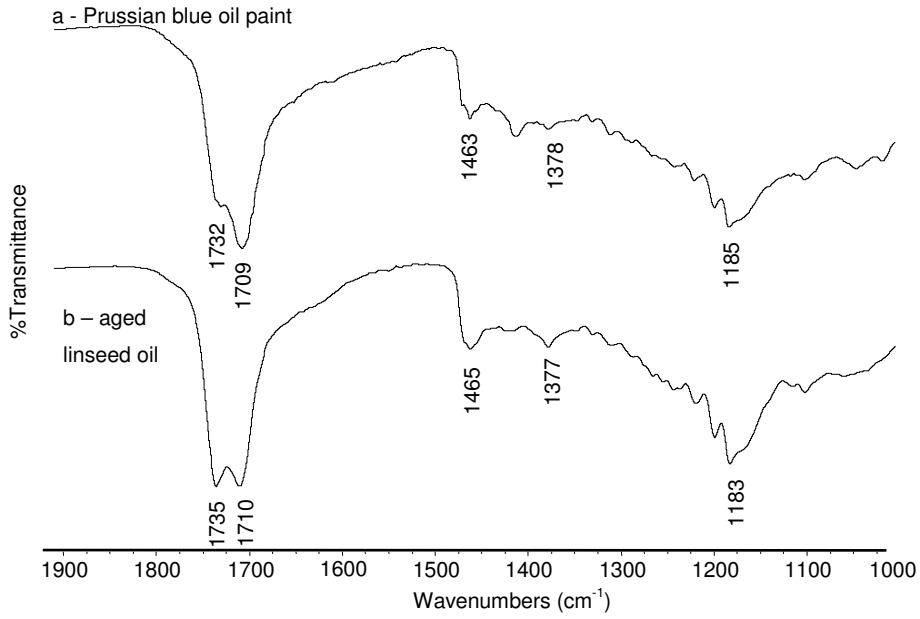

Figure 27 - µFTIR-ATR spectra (1900-1000 cm^{-1}) of 10 years naturally aged films of a) Prussian blue paint and b) stand linseed oil.

Regarding the lead-based pigments, the presence of lead carboxylates is confirmed in all paint reconstructions, even on grey paint prepared with a mixture of lead white with carbon-based pigments, but different situations are observed (Figure 28). It seems that their formation is greater in the case of litharge and red pigments than for lead white (Figures 28a-c). Moreover, the C=O free acid asymmetric stretching at 1708-1719 cm^{-1} is not resolved from the ester band for litharge, red lead and grey paint reconstructions (Figure 28f) while is appeared as a distinguished band for lead white, lead tin yellow (Figure 28d) and Naples yellow (Figure 28e). This may suggest that the conversion into metal carboxylates of the free fatty acids do not occur at the same rate for the different lead-based pigments.

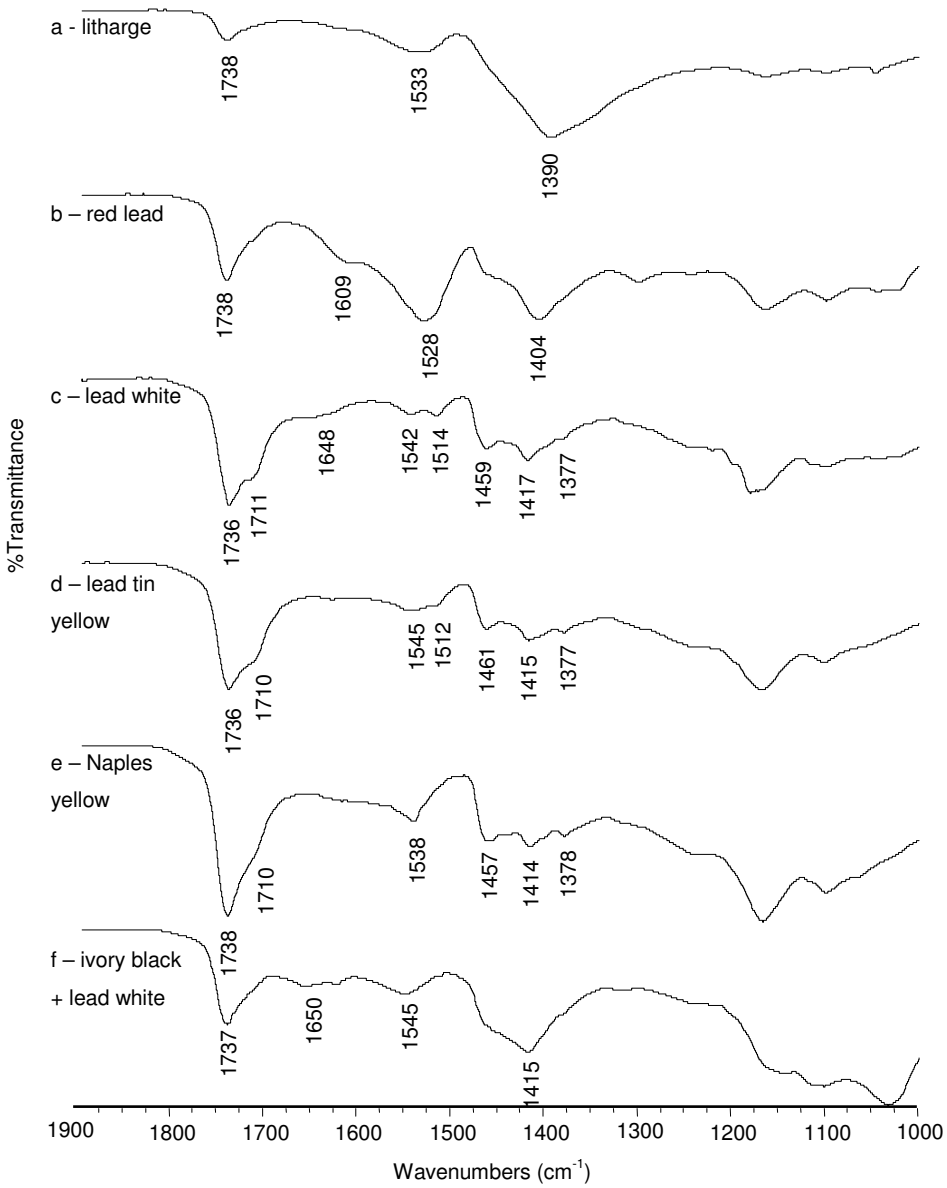

Figure 28 - µFTIR-ATR spectra (1900-1000 cm^{-1}) of 10 years naturally aged of a) litharge, b) red lead, c) lead white, d) lead tin yellow, e) Naples yellow and f) grey (ivory black + lead white) oil paints.

Also in the spectra of zinc white and cobalt green paints, the free fatty acid band cannot be resolved from the C=O ester stretching (Figure 29). Both spectra present a broad band at about 1590 cm^{-1}, which may be attributed to zinc carboxylates, as zinc oxide has been used for both paints. However, this band does not correspond to the 1540 cm^{-1} band present in the zinc palmitate reference spectrum and therefore a mixture of carboxylates with different molecular weight, may be hypothesised. In the literature, is reported the case of ionomers neutralized by zinc oxide, which forms zinc carboxylates (Ishioka,

Shimizu et al. 2000). Nevertheless, the different absorption bands have not been fully assigned even if they should be related to different coordination states of the carboxylic acids around the zinc atom.

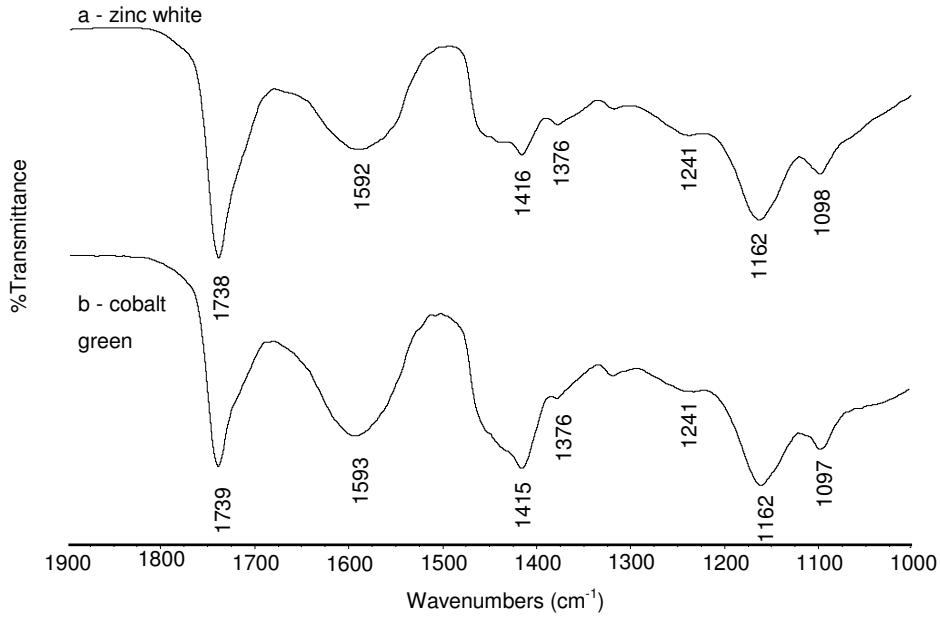

Figure 29 - µFTIR-ATR spectra (1900-1000 cm^{-1}) of 10 years naturally aged of a) zinc white and b) cobalt green oil paints.

Regarding the manganese-based pigments, the formation of manganese carboxylates has been identified for the first time with two spectral bands at 1567 and 1545 cm^{-1} (Figure 30). In fact, the interaction between an oil binding medium and manganese pigments has never been studied before. Even if iron is also present in these pigments, the production of metal carboxylates is more likely to be attributed to manganese as no carboxylates have been detected for the pigments with only iron, as described above.

Cadmium carboxylates have been only detected on cadmium yellow (CdS, cadmium sulphide) paint with the presence of band at 1537 cm^{-1} and not on cadmium red paint (Cd_2SSe, cadmium sulphide selenide) (Figure 31). The possible inhibitor effect of Se needs further studies.

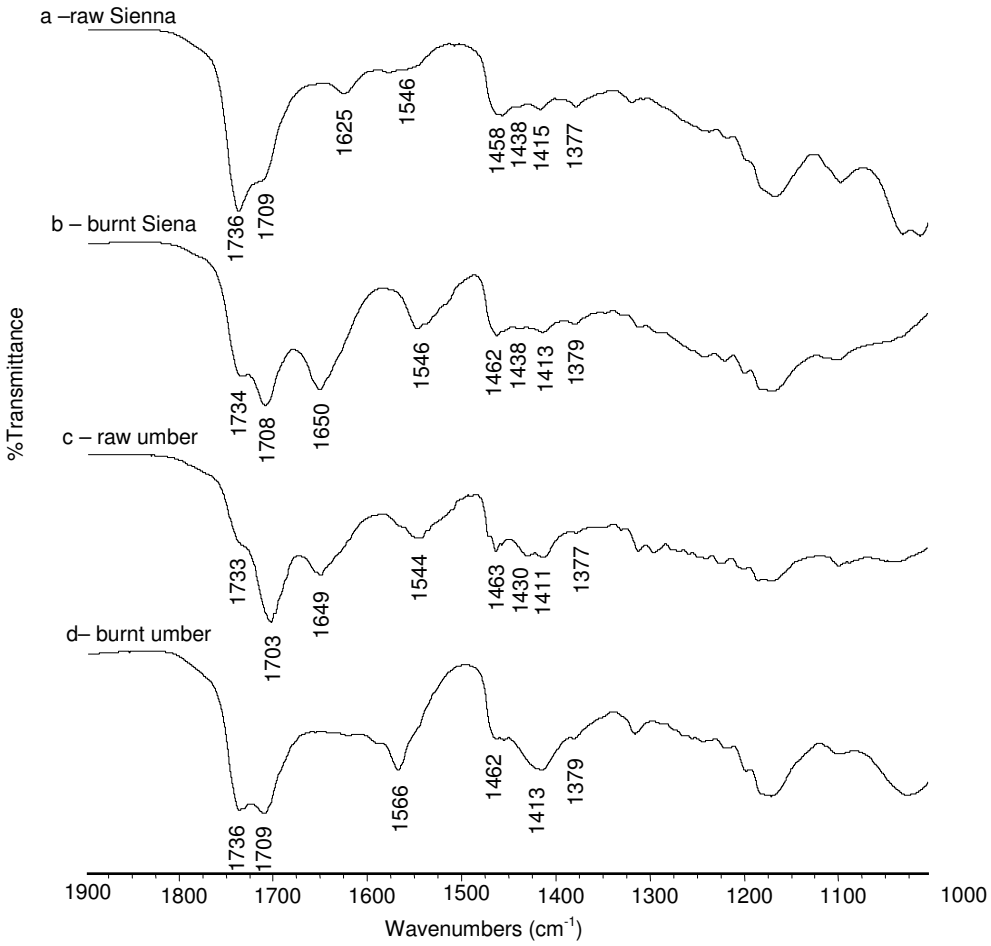

Figure 30 - µFTIR-ATR spectra (1900-1000 cm^{-1}) of 10 years naturally aged of a) raw Siena, b) burnt Siena, c) Raw umber and d) burnt umber oil paints.

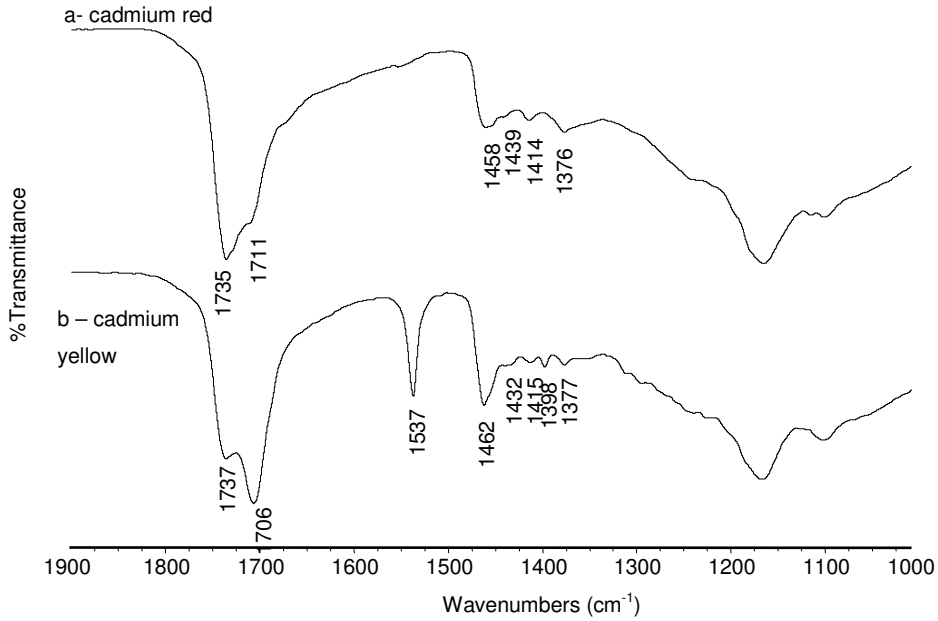

Figure 31 - µFTIR-ATR spectra (1900-1000 cm^{-1}) of 10 years naturally aged of a) cadmium red and b) cadmium yellow oil paints.

In the spectra of copper-based pigments (malachite, azurite), copper carboxylates are also formed, as indicating by the presence of an absorption band at 1585 cm^{-1}, analogous to the synthesised copper palmitate COO^- stretching band (Figure 32). In concomitance with their formation, on some green areas of the azurite paint reconstruction, azurite has been pseudomorphically replaced by malachite (Gettens and West Fitzhung 1997). An increasing moisture and carbon dioxide concentration of the surrounding environment may be responsible of this conversion, according to the following equation 4.

$$2\ Cu_3(CO_3)_2(OH)_2 + H_2O \leftrightarrow 3\ Cu_2CO_3(OH)_2 + CO_2$$

4

ATR mapping has been performed to better investigate this phenomenon (Figure 33). The integrated O-H bending absorbance band at 946 cm^{-1}, 1046 cm^{-1} has been used for plotting the distribution of azurite and malachite respectively whereas the copper carboxylates have been localized using the COO^- stretching band at 1585 cm^{-1}. The formation of the hydrophilic copper carboxylates seems greater than in the case of the malachite paint reconstruction and could be correlated with the conversion of azurite into malachite. This particular aspect is still under investigation and will be subjected to further research.

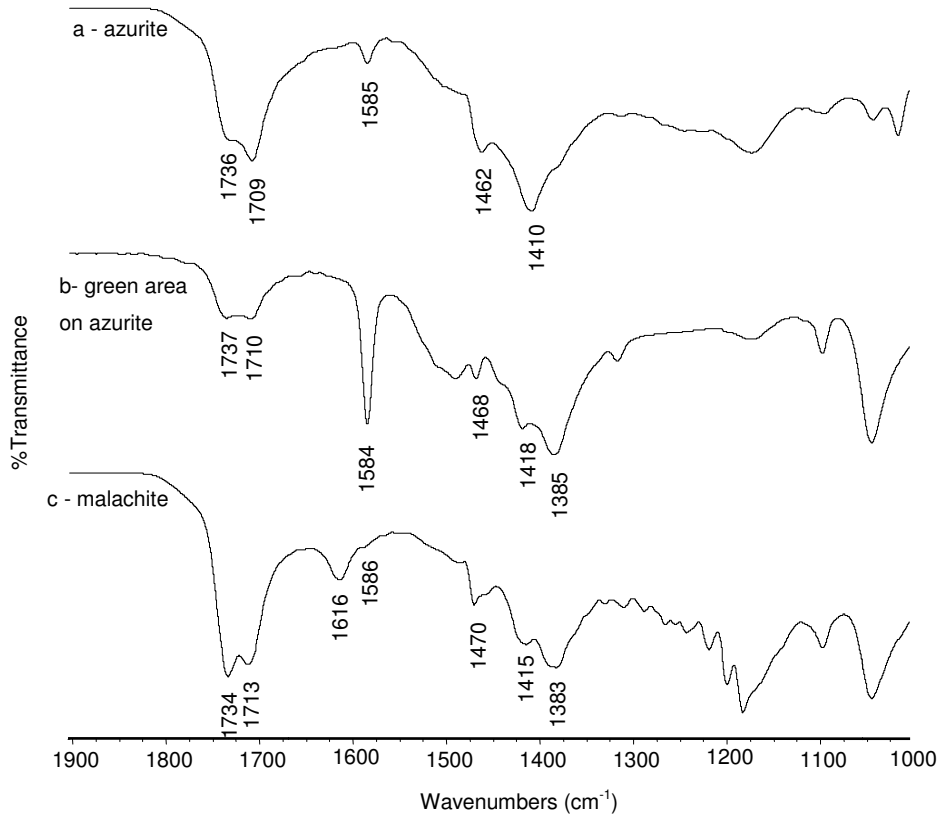

Figure 32 - µFTIR-ATR spectra (1900-1000 cm^{-1}) of 10 years naturally aged of a) azurite, b) green coloured area on azurite and c) malachite oil paints.

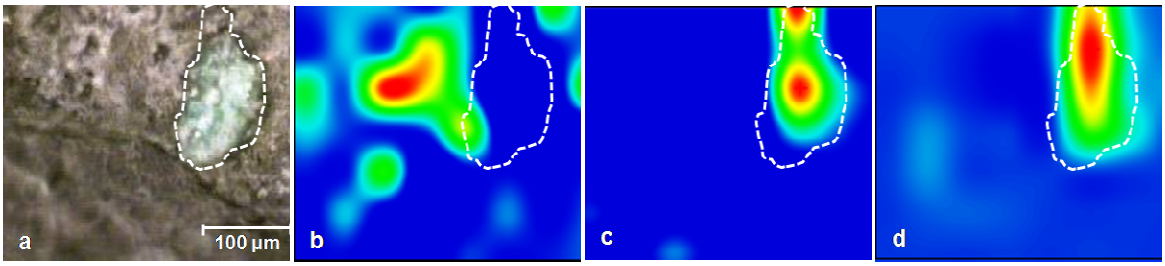

Figure 33 – ATR mapping results performed on a sected area of the azurite oil paint: a) optical image of the analysed area with the green area individuated by a dotted line. FTIR false colour distribution plots representing the integrated absorbance of b) the azurite band at 946 cm^{-1}, c) the malachite band at 1046 cm^{-1} and d) the copper carboxylates band at 1585 cm^{-1}.

II.2.3.c.2 *Egg tempera paint reconstructions*

In table 5, the results achieved on egg tempera paint reconstructions are summarised. The identification of metal carboxylates with egg tempera as binding medium should be carefully ascertained as their characteristic bands are in the same spectral range of amide II band (1545 cm^{-1}). However, their

possible presence can be hypothesised on a basis of a simple observation. In fact, in aged egg tempera films, the amide I band has a higher intensity than the amide II band and their intensity ratio is therefore higher than 1. A contribution to the amide II band from the metal carboxylates can be thus deduced when this relative intensity is inversed.

Pigments	Metal involved	Presence of carboxylates	Absence of carboxylates
Orpiment	As		x
Realgar	As		x
Chalk	Ca		x
Cadmium yellow	Cd	x	
Cobalt blue	Co		x
Chrome oxide	Cr		x
Viridian	Cr		x
Azurite	Cu	x	
Malachite	Cu	x	
Yellow ochre	Fe		x
Bole	Fe Al		x
Mars yellow	Fe Al Ca		x
Indian yellow	Mg		x
Burnt umber	Mn Fe Mn Al	x	
Raw umber	Mn Fe Mn Al	x	
Raw sienna	Mn Fe Mn Al	x	
Lapis lazuli	Na Al		x
Artificial ultramarine	Na Al		x
Red lead	Pb	x	x
Litharge	Pb	x	
Lead white	Pb	x	
Naples yellow	Pb Sb	x	
Lead tin yellow	Pb Sn	x	
Titanium white	Ti		x
Zinc white	Zn	x	
Cobalt green	Zn Co	x	

Table 5 - Summary of metal carboxylates' occurrence on egg tempera paint reconstructions.

In our case, the presence of metal carboxylates has been found on lead white, zinc white, azurite, malachite, cobalt green (Figure 34). In particular for the copper-based pigments, a resolved absorption band at 1585 cm^{-1} assignable to copper palmitate has been observed. The ATR spectrum of cobalt green paint also shows a peak at 1537 cm^{-1} assignable to Zn palmitate.

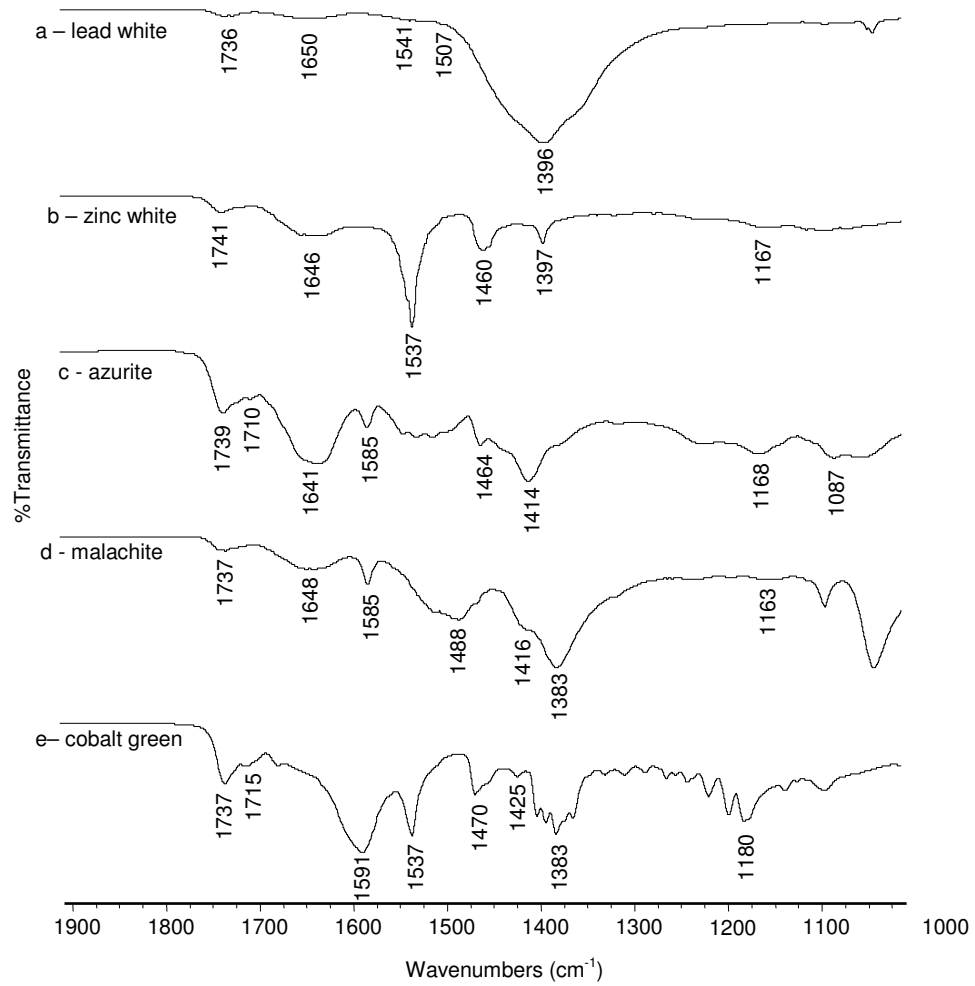

Figure 34 - µFTIR-ATR spectra (1900-1000 cm^{-1}) of 10 years naturally aged of a) lead white, b) zinc white, c) azurite, d) malachite and e) cobalt green egg tempera paints.

Cadmium, Naples and lead tin yellows show a ratio amide I/amide II lower than 1 and also distinctive bands at 1538 cm^{-1} and 1515 cm^{-1}, assignable to Cd and Pb carboxylates respectively (Figure 35a-c). The formation of metal carboxylates is also observed for raw and burnt umber with a sharp band at 1570 cm^{-1} assignable to Mn carboxylates (Figure 35e-d).

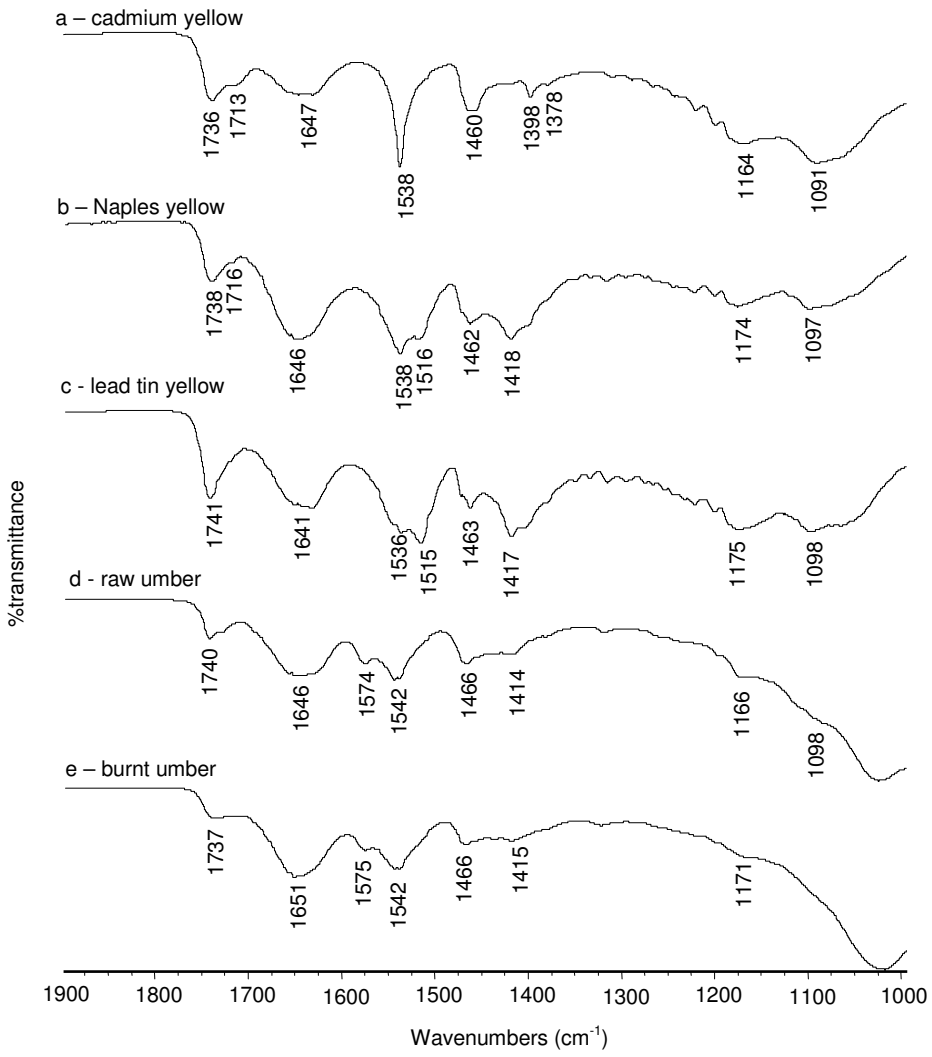

Figure 35 - µFTIR-ATR spectra (1900-1000 cm^{-1}) of 10 years naturally aged of a) cadmium yellow, b) Naples yellow, c) lead tin yellow, d) raw umber and e) burnt umber egg tempera paints.

Particularly on litharge and red lead paints, the formation of lead carboxylates (1514 cm^{-1}) is associated with lead carbonate (1400, 1044, 843 and 682 cm^{-1}) commonly present in lead white, as showed in figure 36. This may be the result of remineralisation phenomena, which have also been observed on the litharge and red lead oil paint reconstructions (figure 28a-b). In the literature, the presence of lead carbonate has been already reported in lead soaps aggregates and has been attributed to a remineralisation processes (van der Weerd, Boon et al. 2002; Higgitt, Spring et al. 2003; Keune 2005). In fact, it is known that organic components, such as acetic acid and some other acids, react with lead to produce lead acetate and lead hydroxide that, in the presence of atmospheric carbon dioxide, form lead carbonate (Oddy 1975). Moreover

litharge and red lead dissolve at different rates within oil and after 80 days, the lead concentration is ~13% for litharge and 1.7% for red lead (Shaeffer 1933). This could explain the higher conversion of litharge to lead carbonate than for red lead.

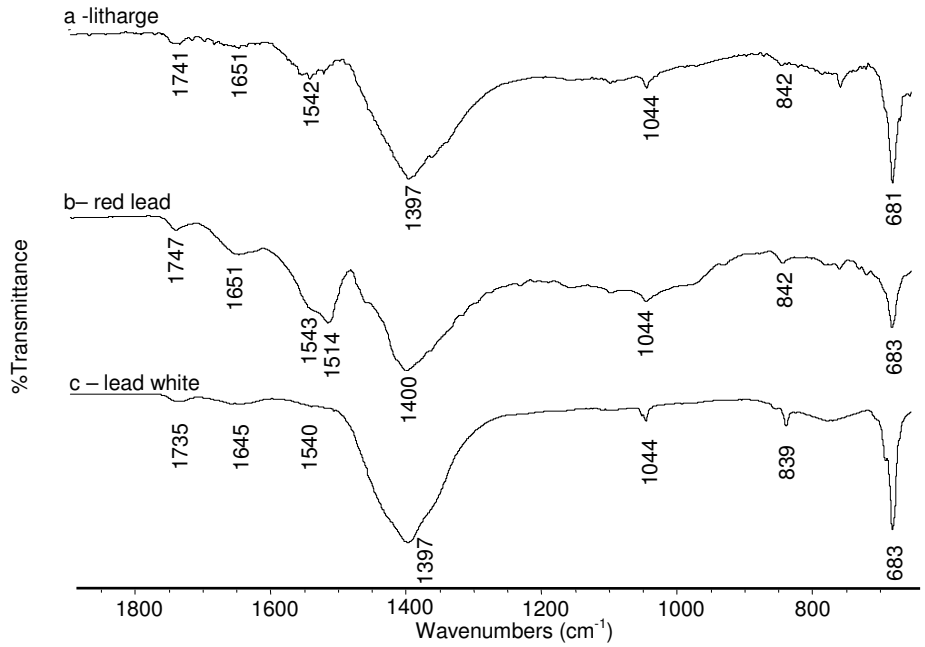

Figure 36 - µFTIR-ATR spectra (1900-650 cm^{-1}) of 10 years naturally aged of a) litharge, b) red lead, and c) lead white egg tempera paints.

II.2.4 Conclusions

In this study, micro FTIR-ATR analyses have been carried out for the characterisation of metal carboxylates resulting from the interaction between pigments and binding media. To this purpose, 10 years naturally aged oil and egg tempera paint reconstructions have been used as reference materials together with synthesised metal palmitates to help the identification of metal soaps produced. Particular attention has been given to manganese and cadmium palmitates, for which no data is reported in the scientific literature. Regarding the lead-based pigments, a larger amount of carboxylates seems to be produced by red lead and litharge compared to lead white, Naples yellow and lead tin yellow. On both pigments dispersed either in oil or egg tempera, the

ageing process is also associated with the formation of lead carbonate. Regarding the pigments with zinc, manganese and copper, the production of metal carboxylates has been detected on both aged oil and egg tempera paints. In particular for copper, the degradation phenomenon appears to be related to the conversion of azurite into pseudomorph malachite and may possibly interfere in the formation mechanism. Another important feature, which will be further investigated, is the eventual key role played by iron or cobalt during the hydrolysis of triglycerides. In fact, for nearly all spectra collected from pigments based on iron or cobalt (yellow and red ochres, bole, Prussian blue, cobalt blue, cerulean blue), no metal soaps have been identified although a C=O acid stretching band more intense than in the reference siccative oil is present. On the other hand, manganese seems to be important in the production of metals soaps and these latter have been observed for the first time on sienna and umber paints. Also for egg tempera paint reconstructions, the formation of copper, lead, manganese, cadmium and zinc carboxylates has been identified despite the overlapping of amide II band in the same spectral region.

II.2.5 Acknowledgements

Dr. A. Aldrovandi (Scientific laboratory - Opificio delle Pietre Dure, Florence, It) is thanked for providing the oil and egg tempera paint reconstructions.

II.3 EVALUATION OF RESTORATION MATERIAL'S PERFORMANCE: Evaluation of protective treatments and monitoring of corrosion behaviour within the EU-ARTECH project.

FTIR-ATR microscopy offers new analytical possibilities for monitoring the formation and localisation of corrosion products as it makes possible to perform measurements on the same surface areas at different time periods. In this chapter, innovative treatments are tested and compared with those traditionally applied for the protection of outdoor bronze monuments. In terms of consolidation and protection, the effectiveness of treatments applied on outdoor bronze monuments intrinsically depends on their patina composition and corrosion behaviour. Therefore, new conservation methods cannot be envisaged without a previous definition of the object's environmental context and patina characterisation.

A change in conservation approaches is here proposed, which takes into account the co-existence of corrosion products with different stability. This may result in the selection and adoption of treatments addressing specific corrosion features. Benzotriazole (corrosion inhibitor) and Incralac® (protective coating) have been compared with new treatments based on organo-silanes, artificial cuprite patinas, copper oxalate bio-patinas and limewater. Both artificially patinated and naturally aged bronze samples exposed to urban and marine environments have been treated with the different protective agents under study. Monitoring of their behaviour under artificial or marine natural ageing has been performed over an 18-month period in order to evaluate their long-term corrosion resistance by different analytical techniques (FTIR, SEM, EIS and colorimetric measurements).

II.3.1 Introduction

The deterioration of outdoor bronze artefacts is the result of complex interactions with the surrounding environment, leading to a wide variety of corrosion products. Electrochemical processes, chemical reactions with pollutants and physical phenomenon of deposit accumulation may lead to irreversible changes for the object in terms of appearance and structure until its

eventual loss (Leygraf and Graedel 2000). First, a well-adhered reddish-brown patina layer, composed mainly of cuprite (Cu_2O), is formed by oxidation. Later, in the presence of moisture and corrosive gases (sulphur dioxide, carbon dioxide, nitrogen oxides, etc.), different greenish patinas can be produced, depending on particular atmospheric conditions. Antlerite ($Cu_3SO_4(OH)_4$), brochantite ($Cu_4SO_4(OH)_6$) and posnjakite ($Cu_4SO_4(OH)_6 \cdot H_2O$) are the most frequent compounds in heavily polluted urban environments. Alternatively chloride-rich environments lead to the formation of atacamite and/or paratacamite ($Cu_2Cl(OH)_3$), sometimes appearing as 'pitting' corrosion features (Graedel 1987; Marabelli and Mazzeo 1993; Kratschmer, Odnevall Wallinder et al. 2002; Mazzeo 2005).

The most common approach so far adopted is to apply organic coatings which are traditionally used in industry but without adaptation of materials and methods to specific inhomogeneous and corroded surfaces. Traditional coatings which are still popular for the protection and corrosion inhibition of metal artefacts include: a) waxes (wax R21, TeCe Wachs 3534F), b) acrylic resins (Incralac®), c) corrosion inhibitors (benzotriazole). Typically, wax coatings are applied directly on the metal surface or on a previous layer of acrylic resin. In this latter system, known as the 'double coating system' widely used in Europe, the wax topcoat acts as a sacrificial layer (Marabelli and Napolitano 1991; Brostoff 2003; Letardi 2004). Their easy-of-use make the use largely diffuse even if it represents some disadvantages such as surface's darkening, frequent maintenance and incomplete reversibility (Johnson 1984; Moffett 1996). Also with the use of Incralac regular maintenance is needed and other problems have been noted such as the shiny aspect assumed by the treated surface and, in some cases, the brittleness of the film and its difficult removal over time (Brostoff 2003). Regarding benzotriazole, it is a well known toxic and human carcinogen. Moreover, even if the films of copper-benzotriazole seem to inhibit the moisture passage, they are inefficient against the copper ions which can continue to form corrosion products below the coating (Brostoff 2003).

However it is known that the effectiveness of protective treatments applied on metal artefacts intrinsically depends on the nature and chemical stability of the different corrosion products present. Nevertheless, at present, their application occurs in a non-selective way with no regards to the object's patina composition

and corrosion behaviour. There is a pressing need, as expressed by art conservators, to develop novel conservation methods which also foresee a preliminary characterisation of the constituent materials and their interaction with the environment. This may result in the selection and adoption of specific types of treatment addressing specific corrosion features and behaviour present on the corroded surfaces. Instead of applying organic coatings without any further consideration, research should be undertaken to develop innovative protective systems that can chemically and specifically modify existing corrosion products to create more stable and less soluble compounds, while still retaining the surface's physical appearance. Some criteria should be taken into account in the design of these improved protective treatments: effectiveness, durability, innocuousness for persons and environment. Regarding the reversibility, there is a very controversial point, since the original surface cannot be retrievable once corrosion processes occur. On the contrary, it is well accepted in the conservation field that coatings are only in little part removable, whereas, whenever possible, it is preferable they do not alter the original appearance of the object. Such novel approach has been evaluated within the EU-ARTECH (Access Research and Technology for the conservation of the European Cultural Heritage) project on bronze standards. Different approaches have been selected: the use of organo-silane materials; the formation of artificial copper oxalate induced by fungi; the use of limewater as corrosion inhibitor. The formation of an artificial cuprite layer will not be presented in this thesis.

II.3.1.a *Organo-silanes*

A preliminary examination of different organo-silane materials has been performed both on 80 years naturally aged copper plates and on part of the sceptre of the equestrian bronze statue of Bartolomeo Colleoni, located in Venice. Silanes of new generation (Pilz and Römich 1998; Pilz and Vogel 1999; Zucchi, Grassi et al. 2004), which are usually applied to protect stone monuments, have been selected for their ability to produce, after hydrolysis and alcohol/water condensation, chemical bonds with copper hydroxysulphates and/or hydroxychlorides (Figure 37). In order to compare their performance, electron impedance spectroscopy (EIS) measurements have been carried out to

evaluate their corrosion resistance and colour measurements for the eventual chromatic alterations. On the treated samples exposed seven months to the industrial/marine environment of Venice, two of the tested silanes have showed corrosion resistance comparable to those treated with the acrylic resin (Incralac®) (Joseph, Letardi et al. 2007). The fluoroalkylsilanes Dynasylan F8263 and Dynasylan Sivo Clear K1/K2 have therefore been selected as materials to be submitted to further tests exposed in this chapter.

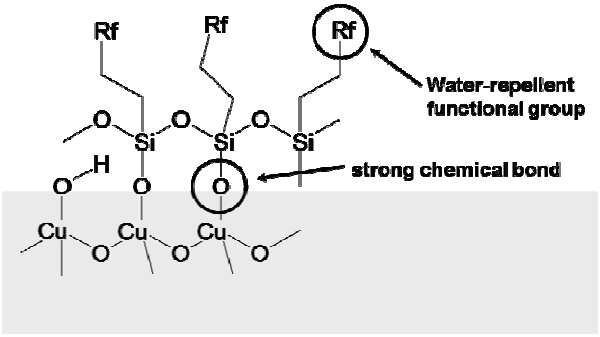

Figure 37 - Scheme of the possible chemical interaction of silanes with copper corrosion products.

II.3.1.b *Artificial copper oxalates by fungi*

In the literature, some species of fungi have been reported for their ability to transform metal compounds into metal oxalates (Sayer, Kierans et al. 1997; Gharieb, Ali et al. 2004). In particular, this capability has been widely exploited to immobilize potentially toxic metals in the environment and in waste treatment (Tabak, Lens et al. 2005; Godlewska-Żyłkiewicz 2006). This could also represent an innovative application in the conservation of metal artefacts. In fact, for example, the presence of copper oxalate on bronzes exposed outdoor has already been identified (Nassau, Gallagher et al. 1987; Mazzeo, Chiavari et al. 1989), but it is not associated with the phenomenon of cyclical corrosion. Instead it creates compact patinas of an attractive green colour on the bronze surface. Since it also displays a high degree of insolubility and chemical stability even in particularly acid atmospheres (pH 3), it provides the surface with good protection (Marabelli and Mazzeo 1993). Therefore, the use of some species of fungi will enable the conversion of corrosion products, which are involved in active corrosion, such as chlorides and/or sulphates, into more stable and

insoluble oxalates. A real progress is expected in terms of durability, effectiveness and toxicity. Indeed, the chemically stable patina created may provide a very high protection to the artefacts and consequently, may contribute to stop the corrosion processes altogether.

II.3.1.c *Limewater*

The most damaging corrosion, known as 'Bronze disease', occurs when chlorides and moisture come into contact with copper alloys. At a first step, copper (I) chloride (nantokite) slurries develop at a pH of ~ 3.5 – 4.0 and are gradually transformed rapidly into a green precipitate of copper trihydroxychlorides (Tennent and Antonio 1981) according to the reaction 5 of oxidation and hydrolysis (ΔG_f = - 1510 KJ.mol^{-1}).

$$4\ CuCl + O_2 + 4\ H_2O \longleftrightarrow 2\ Cu_2(OH)_3Cl + 2\ H^+ + 2\ Cl^- \quad (5)$$

According to the Pourbaix diagram, nantokite should hydrolyse to copper (I) oxide at neutral conditions for pH and Eh (Figure 38). Thus, by adjusting pH of the corroded substrates towards alkalinity, further formation of copper trihydroxychlorides can be inhibited. In this respect, the use of limewater (pH= 8.5), acting as passivation agent through the formation of basic calcium carbonate, has been investigated.

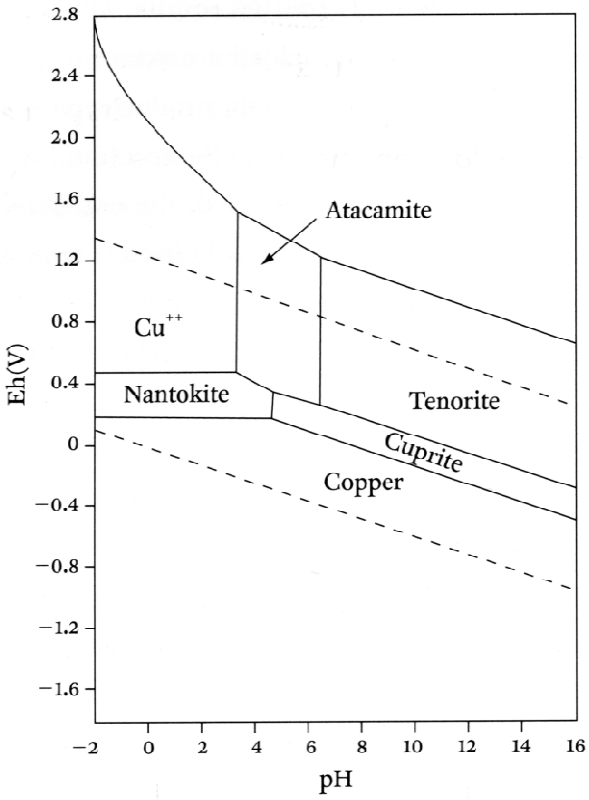

Figure 38 - Pourbaix diagram of the system Cu-Cl-H_2O at 25°C with a chloride ion concentration of 3550 ppm.(Scott 2002).

Standard bronze and copper coupons with three different types of patinas have been treated with the above-mentioned treatments. The patinas have been obtained after natural ageing in urban (UN, urban natural) and marine (MN, marine natural) environments or through a procedure[2] (Pichler process) capable of producing artificial brochantite (UA, urban artificial) on bronze. The corrosion resistance induced by the different treatments has been compared with those of reference treatments (Incralac, T_{ref} and benzotriazole, I_{ref}). Hence, a set of complementary analytical techniques (FTIR microscopy, ESEM, EIS and colorimetry) has been used to characterise the samples before and after treatment. Then, the treatments' performance has been evaluated periodically during an eighteen-month exposure of the coupons to both artificial and marine natural ageing. The monitoring of treatments' behaviour in a marine natural environment will be present in this chapter.

[2] *The Pichler and Vendl patination process, University of Applied Arts, Vienna, patent application in progress.*

II.3.2 Experimental methods

II.3.2.a *Bronze standards*

300 standards coupons (70 × 50 × 2.5 mm) have been prepared from an Rg5 bronze alloy (85% copper, 5% tin, 5% lead and 5% zinc). A single cast alloy sheet (400 × 300 mm) has been cutted and the coupons' surface and edges have been polished by the art foundry and carefully cleaned with technical acetone. The UA samples were prepared with a patented cuprite /brochantite surface layer by the Pichler process. In order to constitute the set of MN samples, the coupons have been exposed for one year to the marine environment of Cabo Raso (Portugal), which is characterised by a high-chloride atmosphere. The Cabo Raso site has a corrosivity class of C5 (according to ISO 9223) or superior in respect to copper as deduced from climatic and weight loss measurements respectively (table 6). The UN samples have been made of copper coupons exhibiting a green patina naturally produced during 80 years exposure to the Munich urban environment.

Time of wetness		Chloride salinity		Corrosivity class
h/year	class	mg/(dm^2.day)	class	C5
3854	τ4	851	S3	
Copper corrosion – weight loss (1 year)				Corrosivity class
6,8 µm/y				>C5

Table 6 - Classification of Cabo Raso corrosivity according to ISO 9223. Data collected during the year of exposure of MN samples.

II.3.2.b *Treatments*

II.3.2.b.1 *Treatments T1S and T2S*

The Dynasylan® F8263 (triethoxy(3,3,4,4,5,5,6,6,7,7,8,8,8-tridecafluoroctyl) silane ready-to-use solution in isopropanol, T1S) and Dynasylan® SIVOCLEAR (bi-component of fluoroalkylsilane K1 in isopropanol and catalyst K2, T2S) have been applied according with the manufacturer procedures (Chemspec, Degussa) on UN, UA and MN samples, previously dusted off, until saturation.

The presence of fluoroalkyl functional groups provide excellent hydrophobic and oleophobic properties to the surface.

II.3.2.b.2 *Reference treatment (T_{ref})*

The reference protective coating (Incralac, Tref) have been applied following the normal procedures. Incralac (solution of methyl methacrylate copolymer incorporating benzotriazole, Indestructible paint Co. Ltd.) have been prepared as a 7% solution in xylene and applied by brush.

II.3.2.b.3 *Treatment T4S*

Five wild fungal strains have been selected for their ability to transform copper oxides, copper hydroxysulphates and copper hydroxychlorides into copper oxalate: *Aspergillus niger* (1), *Penicillium* sp. (2), *Aspergillus alliaceus* (3), and two fungal strains isolated from vineyard soil in Switzerland, *Trichophyton* sp. (4) and *Fusarium* sp. (5). First, the formation of copper oxalate induced by fungi has been evaluated on different malt-agar (MA) media where powdered brochantite, atacamite and cuprite have been added. The copper oxalates formation has been then confirmed by ESEM as well as X-ray diffraction (XRD) and FTIR microscopy. Showing the best results, the strain 4 has then been inoculated onto a copper sheet covered with MA mixed with brochantite. Finally, strain 4 has been inoculated with MA and brochantite on UN and MN coupons without any sterilisation procedure and left to grow for one month. Then the medium has been allowed to dry and the fungi scraped off before analysing the samples. In all cases, brochantite has been added to prevent any contamination from other fungi susceptible to grow on the MA substrate.

II.3.2.b.4 *Corrosion inhibitors I1S and I_{ref}*

3% benzotriazole (I_{ref}) solution in ethanol have been used as reference corrosion inhibitor on both UN and MN samples by immersion for 4 min. In order to evaluate the inhibition capacities of limewater (I1S), MN samples have been immersed 30 min in different limewater solutions (I1S) at 0.1, 0.5, 1, 5, 10, 50%.

II.3.2.c *Colorimetric measurements*

Measurements of the colorimetric coordinates in the spaces CIEL*a*b* have been performed in order to evaluate possible chromatic alterations due to the application of superficial treatments and/or after outdoor exposition. A Minolta CM-508D colour measurement system has been used with an adjustment of illuminant D65 and a 10° observer, using CIELab 1976 colour space. On each sample six measurements have been carried out at six different spots of the sample and the mean value calculated.

II.3.2.d *Micro-ATR FTIR spectroscopy*

At the same time, microFTIR analyses have been performed in order to chemically characterise the patinas before and after the treatments. ATR spectra have been recorded between 4000 and 650 cm^{-1} on a Thermo-Nicolet Nexus 5700 spectrometer combined with a Nicolet Continuum FTIR microscope, fitted with a mercury-cadmium-telluride (MCT) detector and a x-y-z motorised stage with incremental steps of 1 µm. ATR Measurements have been made in reflection mode on the surface of the samples placed on the microscope stage, selecting the area with a 15x Thermo- Electron Infinity Reflachromat objective and a tube factor of 10x. A micro slide-on ATR with a silicon crystal (refractive index n = 3.4) has been connected to the objective and has been used with an aperture of 150 × 150 µm, resulting in investigated areas of about 44 × 44 µm. A total of 64 scans have been recorded at a resolution of 4 cm^{-1} and the resulting interferogram averaged. Acquisition and post-run processing have been carried out using Nicolet *Omnic* software.

II.3.2.e *Electron Impedance Spectroscopy*

EIS measurements have been performed on untreated samples and on 20 days old treated samples. A specific contact probe prototype (ST15) has been used on measured areas of 1,77 cm^2. A commercial cleaning cloth has been immersed for 120 min in mineral water (electrical conductivity 320 $\mu S.cm^{-1}$,

pH=7,9) before being fixed to the contact cell. The whole system has then been placed on the surface to be analysed. In order to stabilise the open circuit potential, the acquisition started at time t_o, 30min after the cell has been placed on the investigated area. A Gamry Femtostat FAS1, with Framework/EIS300 V3.11 software 1999 has been used in the frequency range 100 KHz - 10 MHz. EIS spectra with 10 points per decade have been acquired in potentiostatic mode with 10mV AC signal level at open circuit potential. Several areas have also been measured for each type of patinas and treatments in order to check the homogeneity and the repeatability of the results.

II.3.2.f *Scanning Electron microscopy*

To observe the copper oxalate crystals formed on samples treated with fungi, a Philips environmental scanning electron microscope (ESEM) has been used with an energy dispersive X-ray (EDX) analyser at an acceleration voltage of 20-25 keV, lifetime>50sec, CPS ≈2000 and working distance 34mm. The samples have been first lyophilised and gold sputtered, then observed in secondary electron (SE) mode.

II.3.2.g *X-ray Diffraction*

Non-destructive XRD analyses have been performed to analyse the mineralogical composition of the samples treated with fungi. A Philips diffractometer has been used for semi-quantitative mineralogical analyses, using cobalt Kα radiation and a speed of 0.05 º/s, from 3 to 74° = 2θ.

II.3.3 Results

II.3.3.a *Untreated samples*

The coupons' surfaces have been characterised by FTIR-ATR measurements. For the urban artificial (UA) patina, antlerite $Cu_3SO_4(OH)_4$ (3570, 3485, 1146, 1101, 1071, 752 cm^{-1}) with traces of brochantite $Cu_4(OH)_6SO_4$ (3375, 987, 943,

868, 854 cm^{-1}) has been detected (Figure 39a). This patina is also soft and poorly adherent to the metal substrate, while the urban natural (UN) patina, which mainly consists of brochantite (3586, 3563, 3381, 3271, 1089, 984, 941, 870, 849, 778, 732 cm^{-1}), presents a compact appearance (Figure 39b). Regarding the marine natural (MN) patina, the coupons' superficies are constituted of atacamite $Cu_2Cl(OH)_3$ (3326, 940 cm^{-1}) with traces of phosphates (1029, 822 cm^{-1}), silicates (1029, 1008 cm^{-1}) and malachite $Cu_2CO_3(OH)_2$ (3401, 1461, 1420, 875, 735, 700 cm^{-1}) as shown in figure 39c. It is worth saying that the presence of malachite may be attributed to an initial stage of corrosion of the one-year exposed MN coupons, and would probably disappear once the corrosion progresses forwards. Hence, its possible presence after the treatments' application can be used as a marker for evaluating their protective performances, indicating that no further corrosion has occurred.

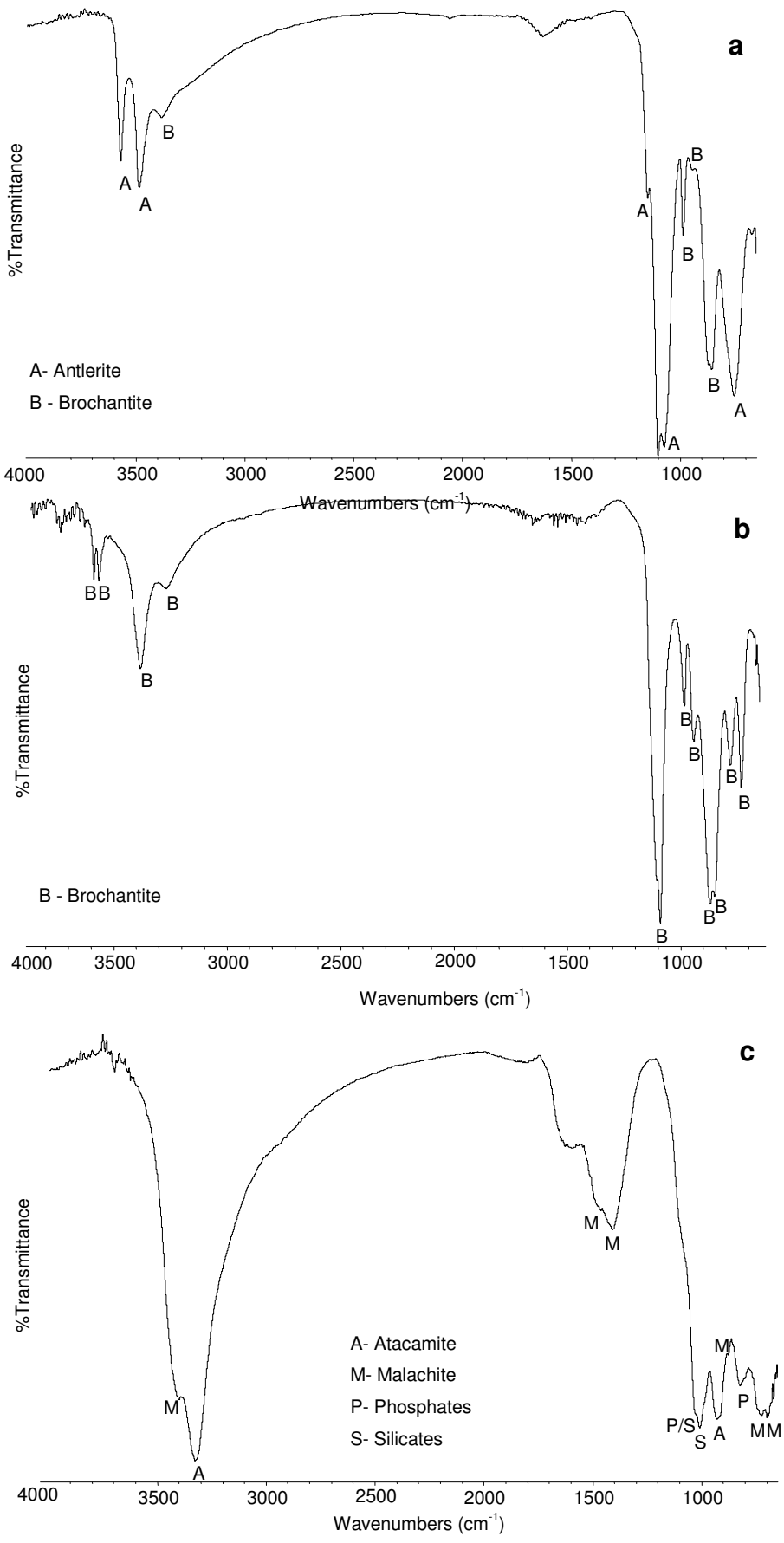

Figure 39 - a) μFTIR-ATR spectra (4000 - 650 cm^{-1}) of UA patina b) UN patina and c) MN patina.

XRD measurements have confirmed the FTIR results and permitted to better characterise cuprite and brochantite for the UA patina. The presence of atacamite, with some copper oxalate and copper oxide, has been also identified for the MN coupons. By colorimetry, all UA samples have exhibited very similar trends with a tendency towards pure green, certainly due to the chemical purity of their patinas, which has been synthesised following strict procedures. On the contrary, UN coupons have been characterised by a rather faint green colour and MN substrates have shown a quite unhomogeneous intermediate green colour (Figure 40).

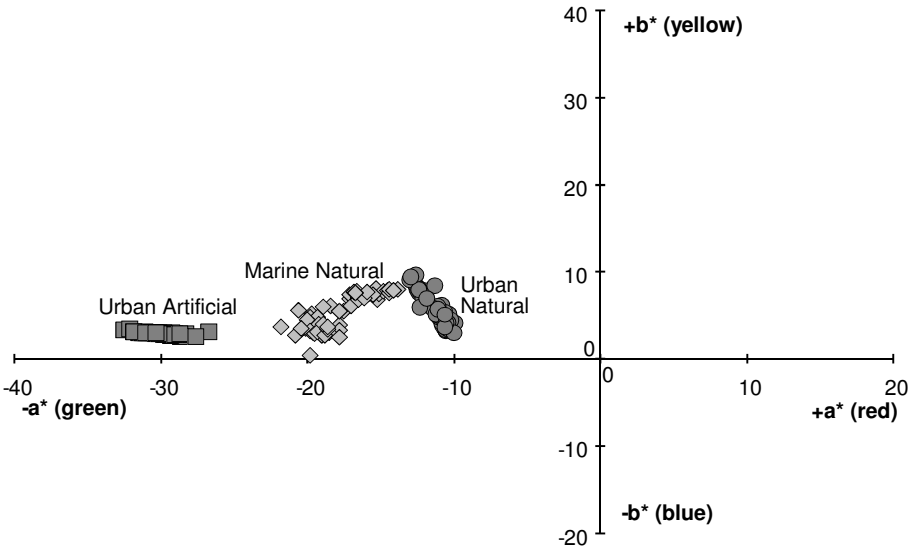

Figure 40 - Comparison of substrate groups UA, UN and MN by colour measurements in the CIELab color space.

Except for the artificially produced UA patinas, the wide dispersion of the EIS data has suggested poor patina homogeneity. An average low frequency impedance modulus has then been calculated with standard deviation for the different substrates. For UA patinas, $|Z|_{10mHz}$ = 29 ± 4 KΩ. For UN samples, $|Z|_{10mHz}$ = 69 ± 18 KΩ and for MN samples, $|Z|_{10mHz}$ = 5 ± 2 KΩ. Since the available patinas cover a rather wide range of impedance, they are expected to provide a good base for treatments testing.

II.3.3.b *Treated samples*

II.3.3.b.1 *Organo-silanes, treatments T1S and T2S*

T1S and T2S have been applied on all substrates (UN, UA and MN) and characterised 20 days after application. The analyses have then been repeated after further 9 months exposure in a marine environment (Genoa harbour, Italy). The EIS results obtained from treated coupons UN, UA and MN are summarised in figure 41.

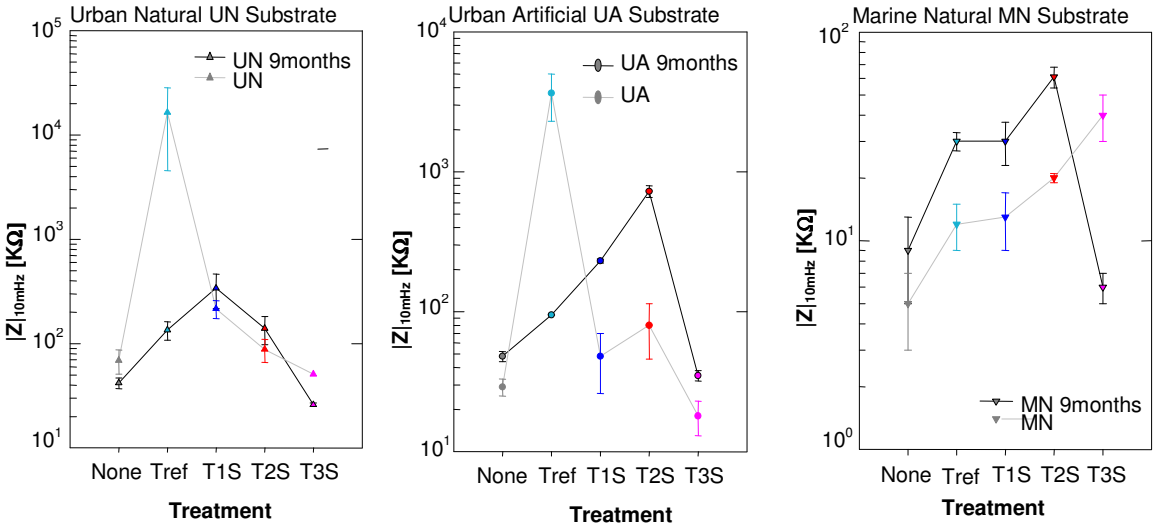

Figure 41 - EIS measurements performed on standard samples 20 days after the treatments' application (grey line) and on treated samples after 9 months exposure (black line). Tref Incralac; T1S: Dynasylan F8263; T2S: Dynasylan SIVO clear; T3S: artificial cuprite layer (not illustrated here).

At 20 days from the application, the high T_{ref} impedance modulus values can indicate an excellent protection achieved by the acrylic resin. However, these values are quite distant from those obtained for T1S and T2S, making their comparison difficult. Furthermore, the standard deviation for the impedance values of T_{ref} shows a huge dispersion of data when compared to that obtained with T1S and T2S. Therefore, the values for T1S and T2S can only be compared with the EIS values of untreated patinas, which have standard deviation from the same order. Some protection may be provided by T1S and T2S as their impedance values are always greater than for the untreated patinas. Since the polymerisation of silanes may require time, EIS

measurements have been repeated after two months. However, the results obtained have been significantly identical, suggesting the achievement of the polymerisation process. It is worth mentioning that, even if the protection performances of T1S and T2S are at this time lower than for T_{ref}, the more important data have been obtained from the evaluation of the protection properties of the different treatments during exposure. In particular, it is well known that the protection performance of T_{ref} decreases rapidly in the first months of exposure, and so an evaluation of new protective treatments can only be completed through data interpretation obtained after a natural ageing. In fact, after 9 months exposure, T_{ref} (Incralac) has showed a very marked impedance decrease while T1S and T2S have showed a very slight impedance increase. T1S has resulted to be the most protective treatment after 9 months exposure on UN substrate while the best results on UA and MN substrates have been observed with T2S. Comparing the colour measurements before and after treatment, the optical changes measured are not perceptible under visual observation and therefore they should be considered of minor importance. After 9 months exposure, no significant visual changes have been observed on UN and UA samples while the MN samples present a lighter and whitish aspect. These observations still need to be confirmed by colour measurements.

In order to characterise the supposed formation of the chemical bond Cu-O-Si between the silanes and the copper corrosion products with hydroxide groups (Figure 37), a first attempt has been made with µATR spectroscopy. However, the reduction of the O-H absorption intensity in the high frequency region can not confirmed the formation of a siloxy-copper bond as in ATR the low penetration depth at high wavenumbers may result in less intense or absent absorption bands. On irregular surfaces, a good contact of the surface with the ATR crystal may not be achieved and so result in low spectral quality in this region. The presence of fluorinated silanes has been identified at 1239 cm^{-1} ($\nu_{as}CF_2$; ρCF_2) and 1206 cm^{-1} ($\nu_{as}CF_2$ + $\nu_{as}CF_3$) but the Si-O-Cu fragment, which should absorbs at 980-950 cm^{-1} (Levitsky, Kokorin et al. 2000), is contaminated by the strong absorption bands of the substrate corrosion products (Figures 42-44). Future research is planned with the use of other more sensitive analytical techniques such as X-ray photoelectron spectroscopy (XPS)

or X-ray Absorption Spectroscopy (XAS) as suggested by a recent publication (Hoque, DeRose, *et. al.*, 2007).

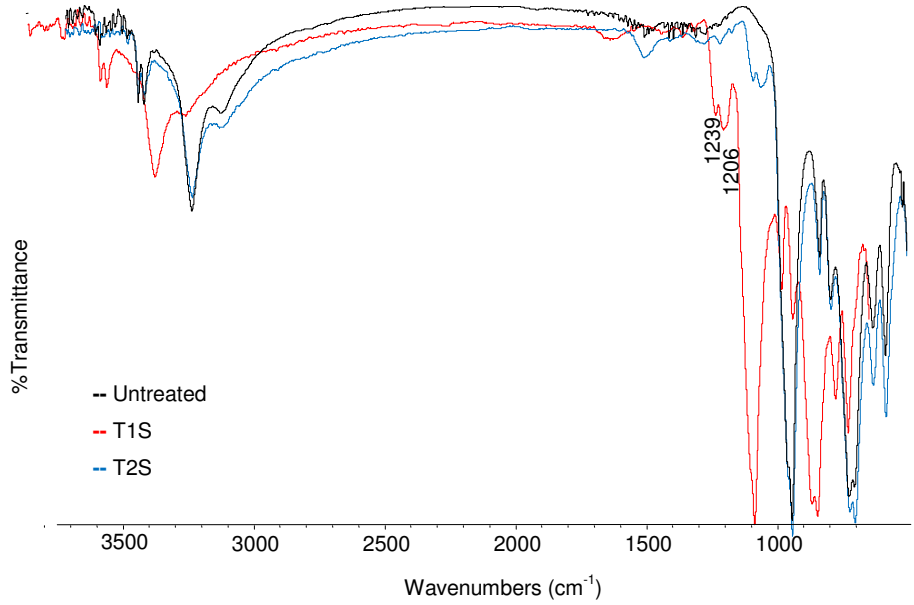

Figure 42 - µFTIR-ATR spectra (4000-650 cm^{-1}) of UN patina untreated or treated with T1S or T2S.

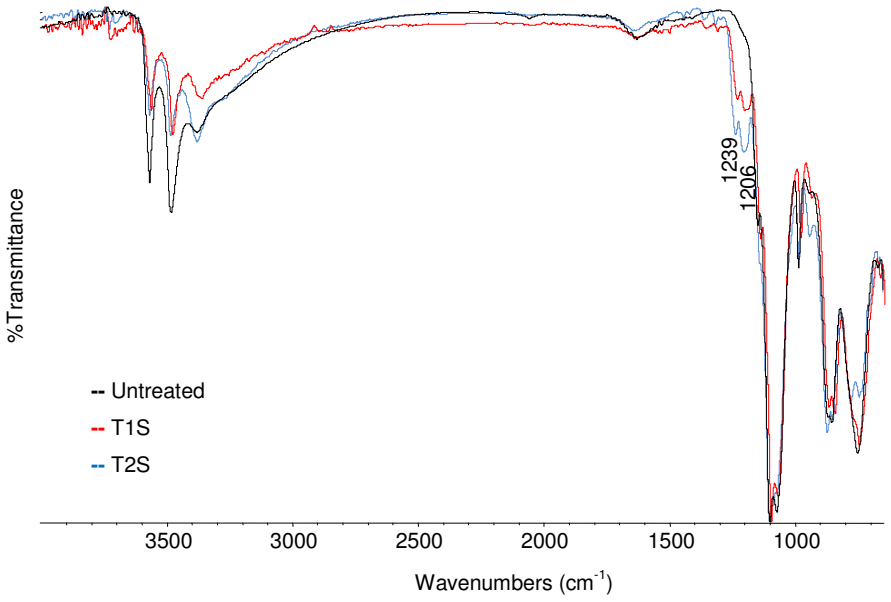

Figure 43 - µFTIR-ATR spectra (4000-650 cm^{-1}) of UA patina untreated or treated with T1S or T2S.

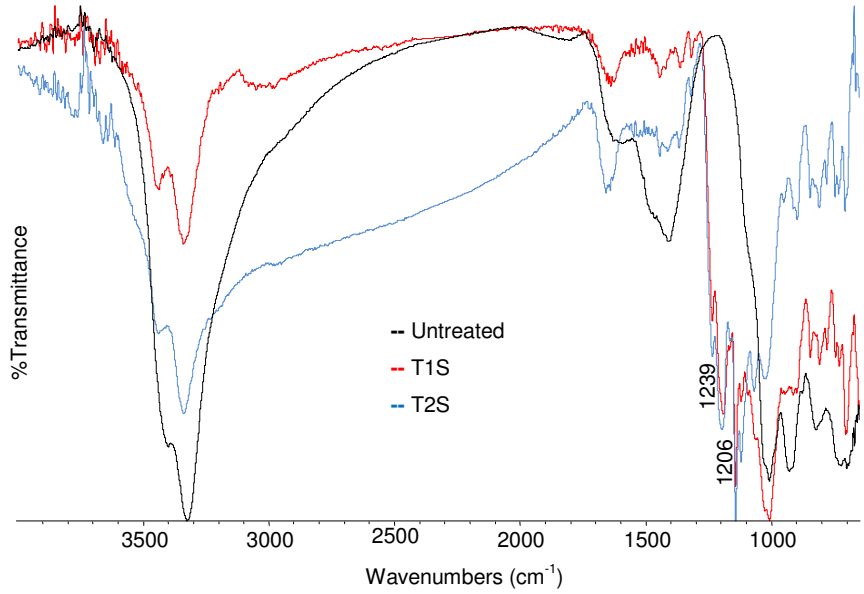

Figure 44 - µFTIR-ATR spectra (4000-650 cm^{-1}) of MN patina untreated or treated with T1S or T2S.

II.3.3.b.2 *Artificial copper oxalates, treatment T4S*

After the investigation of five different fungal strains for the transformation of existing copper hydroxysulphates and copper hydroxychlorides into copper oxalates, the best performances in terms of formation rate and production of copper oxalates have been obtained with *Trychophyton sp.* After one month in contact with the surface of MN and UN coupons, nearly all the respective atacamite or brochantite substrate has been converted into moolooite ($CuC_2O_4 \cdot nH_2O$ with n<1) as confirmed by microFTIR, ESEM analyses and XRD measurements (Figure 45).

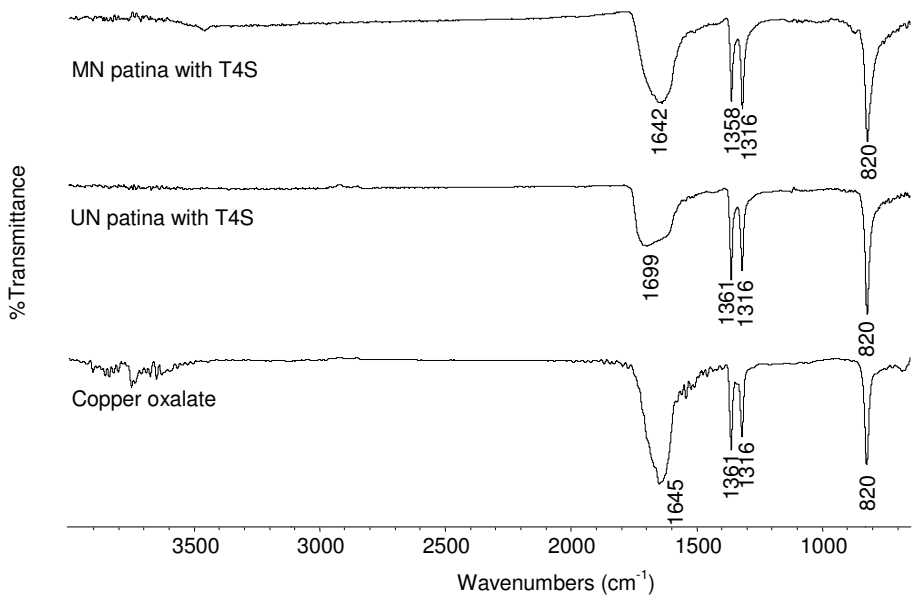

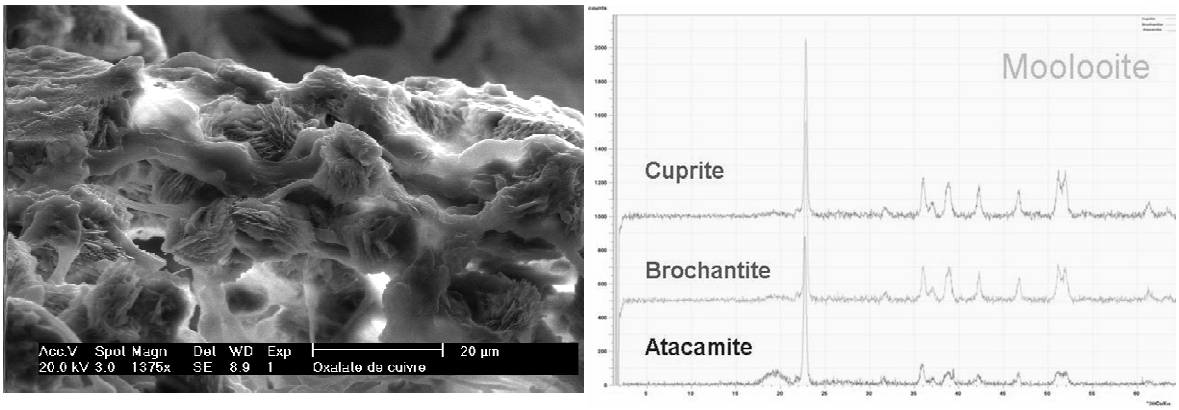

Figure 45 – a) µFTIR-ATR spectra (4000-650 cm^{-1}) of MN/UN patinas transformed by T4S with a reference spectrum of copper oxalate. b) Secondary electron image showing mooloite crystals formed by Trichophyton sp. on brochantite substrate. c) XRD spectra on brochantite, atacamite and cuprite powders transformed into mooloite by Trichophyton sp.

At this stage of the research, few hypotheses can be formulated. It seems that oxalic acid is involved in the formation mechanism. Indeed, parallel experiments have been carried out on copper sheets in presence of malt-agar mixed with 0.1 M oxalic acid solutions and also in this case, the formation of copper oxalates has been observed. However, the mechanisms involved in the assimilation of metal ions and production of metal oxalates have to be deeply investigated. Leaching tests will be also foreseen in order to evaluate the adhesion properties of the produced copper oxalates to the substrate. Moreover, after 2 weeks, the growth of *Trychophyton sp.* may be affected by an eventual contamination from extraneous biological agents such as *Trichoderma.* This important feature will

be further studied to evaluate the optimal spacing between each inoculation point in order to rapidly create a dense network of copper oxalates.

II.3.3.b.3 *Limewater, treatment I1S*

For our purpose 0.1, 0.5, 1, 5, 10, 50 % limewater solutions have been prepared and applied on some marine natural (MN) aged samples by immersion of 30 minutes. The formation of calcium carbonate has been determined by the presence of a band at 875 cm^{-1} in the FTIR spectrum (Figure 46) as the vibrational bands from the untreated MN patina spectrum covered the other characteristic bands of calcium carbonate (1400, 715 cm^{-1}). A 5% concentration has been chosen for the I1S treatment since in this case, the calcium carbonate formation is not associated with any whitening of the surface (Figure 47).

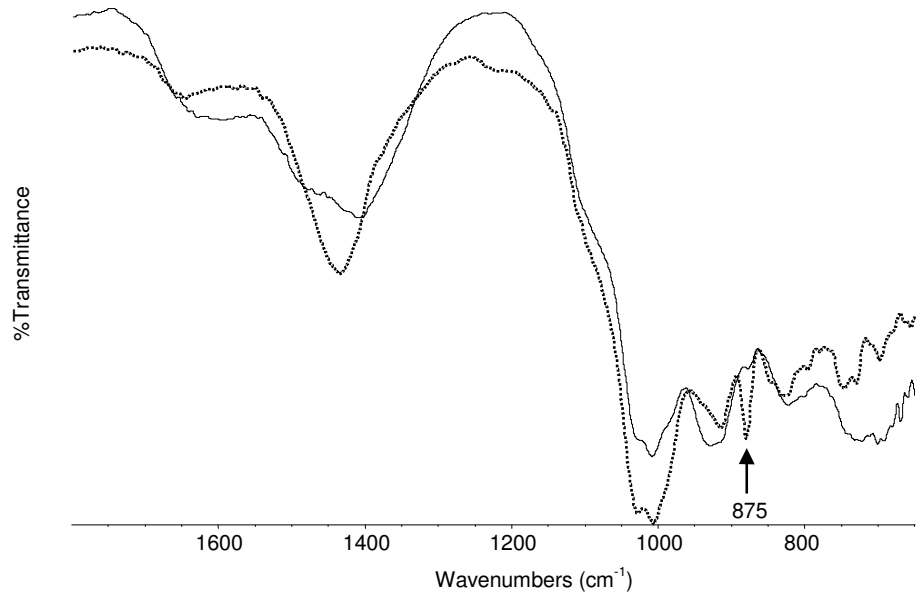

Figure 46 - µFTIR-ATR spectra (1800-650 cm^{-1}) of MN patina untreated or treated with I1S.

Figure 47 - Samples UN (left) and samples MN (right) treated by 30 minutes immersion into 5% limewater solution.

The same treatment has been applied on UN samples. EIS measurements have shown an opposite inhibition behaviour for I1S and I_{ref} (benzotriazole). In fact, I1S give the best protection on MN patina and poor performance on UN substrate, while I_{ref} give very good protection on UN patina and the worst performance on MN substrate (Figure 48).

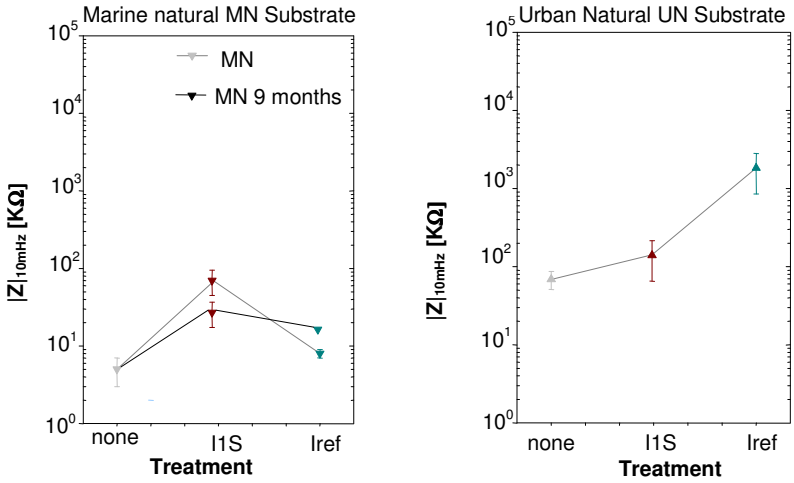

Figure 48 - EIS measurements performed on standard samples 20 days after the treaments' application (grey line) and on treated samples after 9 months exposure (black line). I_{ref}: BTA; I1S 5% limewater solution.

As mentioned above, only the MN samples have been exposed to a marine natural environment in Cabo Raso (P) and will be developed below. For the monitoring, visual observation, thickness and EIS measurements have been performed after 6 and 12 months exposure. The surface changes visually

observed for the samples treated with inhibitors (I1S, I_{ref}) have been similar to those of the untreated samples. There is also a general trend to increase surface layer thickness with exposure time. The first EIS data have shown how I1S has exhibited the most significant decrease of impedance value with exposure while I_{ref} has increased its own, reaching a value close to I1S. An exact explanation cannot be provided for the interpretation of EIS results and these different features need certainly to be completed by the data obtained after 18 months exposure.

II.3.4 Conclusions

This research can be considered as a first attempt made to underline the need to develop and adopt specific treatments in response to specific corrosion behaviours and characteristics exhibited by outdoor bronze monuments. The possibilities offered by FTIR-ATR microscopy for monitoring and localising corrosion products has been demonstrated as well as the integration of complementary techniques to obtain a full characterisation of new alternative inhibition and protective treatments as indicated by the preliminary results. These innovative treatments, based on organo-silanes, copper oxalate biopatinas and limewater have been tested through a natural ageing in a marine environment. However, all treatments need certainly further research studies in terms of protective and inhibition performance as well for the application procedures. In fact, EIS measurements have clearly established the different intrinsic protection capability of the untreated patinas which may affect the treatments' application procedures and performances. Therefore, the monitoring campaign has been conducted over a period of 18 months and further data will integrate the first evaluation achieved so far. In particular, micro-destructive analyses on selected cross-sectioned samples will follow in order to evaluate the effective quality or penetration of treatments. An artificial ageing has been also foreseen with different exposure cycles, which consist of 2 weeks exposure to UV radiation in a Xenon-arc chamber followed by 2 weeks exposure in the salt spray chamber. Generally, this research has also highlighted how clear and standard analytical procedures must be developed and followed by

conservation scientists for evaluating the applicability and long-term performance of new protection and inhibition treatments.

II.3.5 Acknowledgements

This research has been carried out with the support of the European Union, within the VI Framework Programme (Contract: Eu-ARTECH, RII3-CT-2004-506171).

III ADVANCES IN RESEARCH

III.1 Characterisation and localisation of organic substances in paint cross-sections

This chapter illustrates the possibilities offered by micro ATR-FTIR spectroscopy for the stratigraphic study of organic substances employed in the realisation of painted artworks. As non-destructive analysis, this technique represents a real improvement over traditional bulk analyses, such as chromatographic methods or mass spectroscopy, which are conventionally used for the detection of organic substances. Different paint cross-sections are therefore analysed with a mapping system in order to evaluate the distribution of the identified compounds in the different layers. With the intention of avoiding the contamination of polymer mounting resin in FTIR spectra, the use of infrared transparent salts as embedding materials for cross-sections is here proposed as a new alternative method. The typical spatial resolution (20 μm) obtained with this method can however be limitative for thin organic layers and therefore an imaging system with a focal plan array detector (FPA) is also presented. Thus, the high spatial resolution achieved enables organic compounds present in layers measuring less than 10 μm to be identified. FTIR chemical images of organic substances have been obtained using either univariate analyses, integrating specific absorbances for each identified compound, than chemometric methods applied on the whole spectroscopic data set.

III.1.1 Introduction

Paintings consist of complex multi-layer systems where organic materials (binding media and varnishes) are distributed in an inorganic (mainly pigments) matrix. Accurate chemical characterisation of the individual components as well as their stratigraphic location within the paint structure is of the outmost importance for understanding the painting technique adopted and the ongoing degradation processes. The results obtained guide stakeholders in deciding the most appropriate conservation-restoration measures to be adopted.

Over the last few years, different techniques, such as FTIR microscopy imaging (van der Weerd, Brammer et al. 2002), imaging secondary ion mass

spectrometry (SIMS) (Keune and Boon 2004) and microspectrofluorimetry (G.Bottiroli, A.Gallone et al. 2005) have successfully been applied to identify organic substances directly on paint cross sections. Regarding FTIR microscopy, the development of micro-sampling accessories and in particular of miniaturised ATR crystals for ATR spectroscopy has allowed the micro-destructive analysis of smaller quantities (Messerschmidt and Harthcock 1988; Humecki 1995; Katon 1996). Moreover, the recent introduction of mapping/imaging equipment has authorised to collect a large number of FTIR spectra on a surface and perform a distribution map of the identified compounds. The advantages and drawbacks of each system have been already reported by Bhargava who pointed out the differences between the two FTIR microspectroscopic techniques (Bhargava, Wall et al. 2000).

FTIR mapping is a single-point data collection which makes use of adjustable apertures to select the area under investigation. In the case of specular reflection mode, the spatial resolution is related to the aperture's dimension which cannot be lower than the theoretical diffraction limit of about 10 µm without loss of information. Compared to reflection mode, ATR configuration provides an improvement of the spatial resolution due to the high refractive index of the ATR crystal, which gives a higher spatial resolution according to the Rayleigh criterion (Reffner and Martoglio 1995; Lewis and Sommer 1999). So far, ATR–FTIR microspectroscopic mapping has been mainly used for surface analyses in different fields, such as industrial film polymers and pharmaceutical (Meana-Esteban, Lete et al. 2006; Planinsek, Planinsek et al. 2006; Crupi, Ficarra et al. 2007; Popelka, Machová et al. 2007). Few applications to heritage materials have been reported and all of them have been using ATR mode directly performed on the objects' surface (Colombini, Carmignani et al. 2004; Marengo, Liparota et al. 2005) and not on cross-sectioned samples.

In opposition, FTIR imaging is a simultaneous and therefore faster data collection. Since no aperture is present, the high spatial resolution is related to the focal plane array (FPA) detector pixel dimension of about 6 µm, but unfortunately this means also a poor S/N ratio. In order to characterise thin organic layers, such as varnishes or mordants present in as thin films in paint cross sections, imaging ATR-FTIR microscopy a represents a great opportunity to obtain chemical images with an enhanced spatial resolution (Chan and

Kazarian 2003; Chan, Kazarian et al. 2005). So far, ATR-FTIR microspectroscopic imaging has been used in different fields, such as pharmaceutical (Chan, Hammond et al. 2003; Ricci, Nyadong et al. 2007), biomedical (Colley, Kazarian et al. 2004; Chan, Kazarian et al. 2005), forensic (Ricci, Chan et al. 2006) or polymers (Zhang, Otts et al. 2002; Kazarian, Andrew Chan et al. 2004) studies. Few examples related to cultural materials have been reported in the literature: the study of albumen photographs (Ricci, Bloxham et al. 2007), painting cross sections (Spring, Ricci et al. 2008) and the identification of mineral components in a Maya paint (Goodall, Hall et al. 2008).

This chapter aims at illustrating the possibilities offered by ATR-FTIR microspectroscopic mapping and imaging in the characterisation of both inorganic and organic constituents used in different artistic techniques: oil and egg tempera painting, paper and gilt decoration. The different components' spatial distribution has been established using both univariate and multivariate analyses.

It is well known that absorbance bands from the polymer embedding resin may contaminate FTIR spectra. In alternative, different preparation methods using IR transparent salts (silver chloride AgCl or potassium bromide KBr) have been reported for thin sections (Pilc and White 1995; Langley and Burnstock 1999) and in a recent publication, a sample embedded in KBr has also been polished on both sides until a thin slide remains (van der Weerd, Heeren et al. 2004). Nevertheless, difficulties in the preparation of layered samples have been reported or, in the case of AgCl, darkening and accelerated corrosion have necessitated a rapid examination of the samples. To this purpose, a variation of the already reported KBr thin section preparation method is proposed together with other infrared transparent salts for the analysis of cross sections in ATR mode and its efficacy evaluated.

III.1.2 Experimental methods

III.1.2.a *Paint samples*

Five real samples have been collected from: a) a green decoration (sample T2) from the Thubchen Lhakhang temple mural paintings (15th century A.D.) located in Lo Manthang, upper Mustang, Nepal (Figure 49a), (b) a blue painted area (sample Fe2) of a 14th century A.D. Italian polychrome sculpture belonging to a private collection, (c) the wooden support (sample BC1) of a celestial globe (17th century A.D.) made by Vincenzo Coronelli (Figure 49b), d) the blue angel's wing (sample MCR13) of Mattia della Robbia's terracotta altarpiece "*Assumption of Virgin between S. Sebastian and S. Rocco*" (1527-1532 A.D.) located in the collegiate church of S. Maria Assunta in Montecassiano (Macerata, Italy) (Figure 49c) and e) a star's ray (sample 22L) from the vault of the frescoes painted by Giotto in 1305 A.D. and located in the Scrovegni chapel (Padua, Italy) (Figure 49d).

It has to be underlined that sample 22L was collected by a scalpel and then held with glue in order to be first submitted to non destructive X-Ray fluorescence analyses aimed at analysing the chemical composition of the metal leafs. In this particular case the potential of ATR imaging in discriminating between the original organic material and the contamination caused by the glue has been evaluated. All samples have been first carefully observed under a binocular stereo microscope Leica MZ6. T2 and Fe2 samples have been embedded in a polyester resin support (SeriFix resin, Struers), then cross-sectioned and submitted to wet polishing with conventional methods using silicon carbide cards with successive grid from 120, 400, 800, to 1000. With the purpose to evaluate the contaminating role played by the polyester resin embedding system, an alternative method which made use of KBr as embedding material has been tested with all samples.

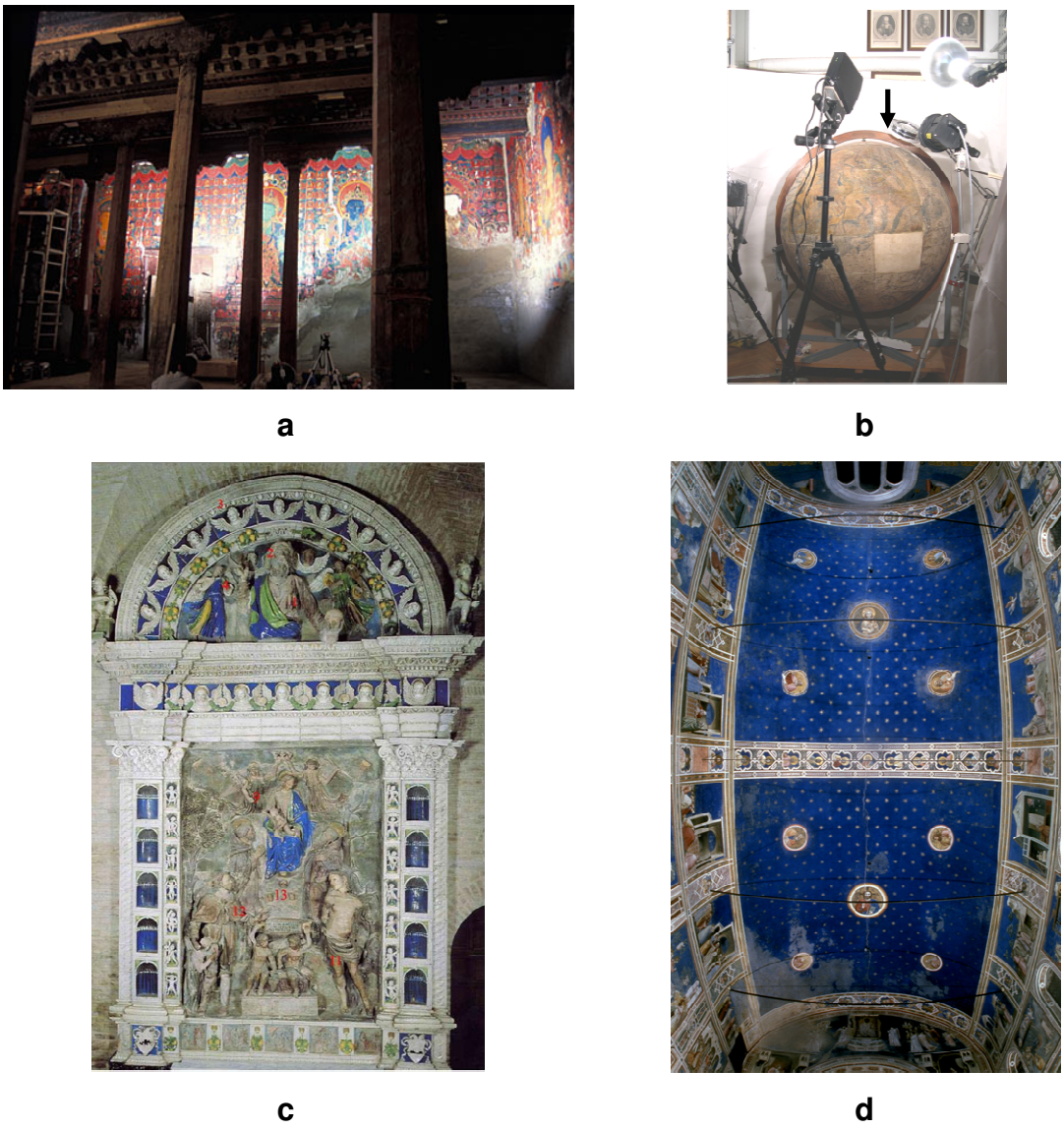

Figure 49 – (a) Thubchen Lakhang monastery, Assembly Hall; (b) Vincenzo Coronelli's celestial globe while submitted to multi spectral imaging analysis. The arrow indicates the place on the wooden globe support from which sample MC1 has been collected; (c) Mattia della Robbia's terracotta altarpiece "Assumption of Virgin between S. Sebastian and S. Rocco" (1527-1532 A.D.) in Macerata. (d) Giotto's frescoes of the Scrovegni Chapel in Padua, ceiling after restoration.

III.1.2.b *Optical microscopy*

This examination plays an important role in the documentation of the stratigraphic morphology of the paint cross-sections under both visible and ultraviolet light. In particular, the observations under UV light allow to detect and locate the presence of organic materials (binding media, varnishes, etc.) thanks to the fluorescence effects generated by such materials when submitted

to a UV radiation source.Dark field observations of cross-sectioned samples have been performed using an optical microscope Olympus BX51M equipped with fixed oculars of 10x and objectives with different magnifications (5, 10, 20, 50 and 100x). Visible and ultraviolet light have been respectively provided by a 100W halogen projection lamp and an Ushio Electric USH102D lamp. Cross sections' photomicrographs have been recorded with a digital scanner camera Olympus DP70 directly connected to the microscope.

III.1.2.c *ATR-FTIR microscopy*

III.1.2.c.1 *Mapping*

For samples T2, Fe2 and BC1, a Nicolet Nexus 5700 spectrometer combined with a Nicolet Continuum IR microscope has been employed in these experiments. The system is fitted with a mercury-cadmium-telluride (MCT) type A detector cooled by liquid nitrogen and a X-Y-Z motorized stage. Spectra have been acquired with a micro slide-on ATR silicon crystal (n=3.4), aperture of 150 µm x 150 µm (analysed area ~ 40 x 40 μm^2), in the range of 4000-650 cm^{-1}, at a spectral resolution of 4 cm^{-1}. A total of 64 scans were recorded and the resulting interferogram averaged. Data collection and post-run processing were carried out using a Nicolet Omnic-Atlµs software. A step size of 20 µm has been used in order to verify the possible detection of thin layers. Each false colour image obtained from the map data set results from the selection of the area of one or a range of specific chemical vibrational bands (peak area map) plotted against the spatial position of each spectrum in the data set. The chemical images were obtained by attributing a colour to each pixel according to the absorbance of a characteristic spectral band corresponding to a given compound.

III.1.2.c.2 *Imaging*

For samples MCR13 and 22L, a FPA detector (Santa Barbara, USA) comprising 16384 small pixels arranged in a 128 x 128 grid format has been used to measure FT-IR images with a spectrometer operating in continuous scan mode.

Spectra have been collected with 8 cm^{-1} spectral resolution in the range 3800–900 cm^{-1} using 128 scans. In the micro ATR configuration, the spectrometer and the FPA detector are coupled with an infrared microscope with a 20X cassegrainian objective and a Ge ATR objective. The imaging ATR spectrometer is patented by Varian (Burka and Curbelo 2000). In the optical arrangement used, the spatial resolution is approximately 5 µm (Chan, Kazarian et al. 2005; Chan and Kazarian 2007; Ricci, Bloxham et al. 2007). The imaging area measured using this accessory and this particular FPA detector is 63 x 63 μm^2. The chemical images can be obtained in the same manner as for mapping but, due to the large amount of data generated by a imaging experiment, multivariate analysis is carried out using a special data handling software, ISys® 4.0 (Spectral Dimensions Inc., MD). Furthermore, multivariate methods can overcome the difficulties which may appear in the generation of chemical images using univariate analysis (Budevska, Sum et al. 2003; Chan and Kazarian 2007). In fact, absorbance bands may overlap when different components have similar chemical features (functional groups) resulting in inaccurate images. In particular, principal component analysis (PCA) has been employed to find the minimum number of causal influences (*m* variables) using all the variables simultaneously. In the newly defined *m*-dimensional space, each spectrum (object) can be described by a colour in the red-green-blue (RGB) scale and the whole set data cube as a multitude of coloured points. The first principal component covers as much of the variation in the data set as possible. The second principal component is orthogonal to the first with the maximum possible variance and so on until all m axes are defined. The main results from PCA are the score and loading plots. The score plot shows how the objects (spectra) are related to each other, while the loading plot shows how the variables relate to each other.

III.1.2.d *SEM-EDX*

A scanning electron microscope, Philips XL 20 model SEM-EDX equipped with an energy dispersive X-ray analyzer has been used on the cross-sectioned samples. The elemental composition has been carried out at an acceleration voltage of 25-30 keV, lifetime>50sec, CPS ≈2000 and working distance 34mm.

EDX-4 software equipped with a ZAF correction procedure for bulk specimens has been used for semi-quantitative analyses of X-ray intensities.

III.1.3 Results and discussion

III.1.3.a *Embedding systems in transparent infrared salts*

The use of infrared transparent salts as embedding material for cross sections has been developed in order to avoid the contamination of the embedding resin and to improve the detection of organic substances. A first attempt with the use of potassium bromide (KBr), which is commonly employed for the preparation of transmission pellets, has given very promising results. Using a macro-micro pellet die, KBr cross sections have been successfully prepared with a simple procedure. First, 300 mg of KBr has been pressed into a pellet under low pressure (2 tons for 30 seconds) in order to achieve a soft base where to transfer the multi-layer fragment. A paint reconstruction fragment of known composition (malachite layer on gypsum preparation layer) has then been positioned with its surface parallel to this base and other 300 mg of KBr added on. After a second low pressure application (3 tons for 2 minutes), the pellet (13 x 2 mm) has carefully been extracted and been inserted in a polyester resin support in order to be more easily handled (Figure 50). Finally the KBr cross-sections have carefully been dry-polished transversally using aluminium oxide Micro-Mesh® sheets with successive grid from 2400 to 4000, 6000, 8000 and 12000, in order to achieve a smooth surface. The resin support allows also more sample stability during ATR measurements.

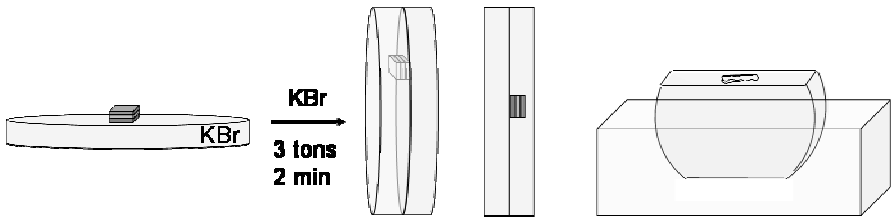

Figure 50 - Preparation of paint cross-sections embedded in KBr into a macro–micro pellet die: the sample is positioned parallel to a KBr pellet previously gently pressed. Some KBr powder is added to cover the sample and all the system is pressed into a new pellet which is further inserted in a polyester resin support and polished.

However, KBr is a very hygroscopic material and the spectral quality gets worse during time acquisition particularly in the first 20 minutes of FTIR measurements, as illustrated in the following graphic based of the signal-to-noise ratio (S/N) value between 4000 and 3800 cm^{-1}, measured during 2 hours on the preparation layer of the malachite paint reconstruction (Figure 51).

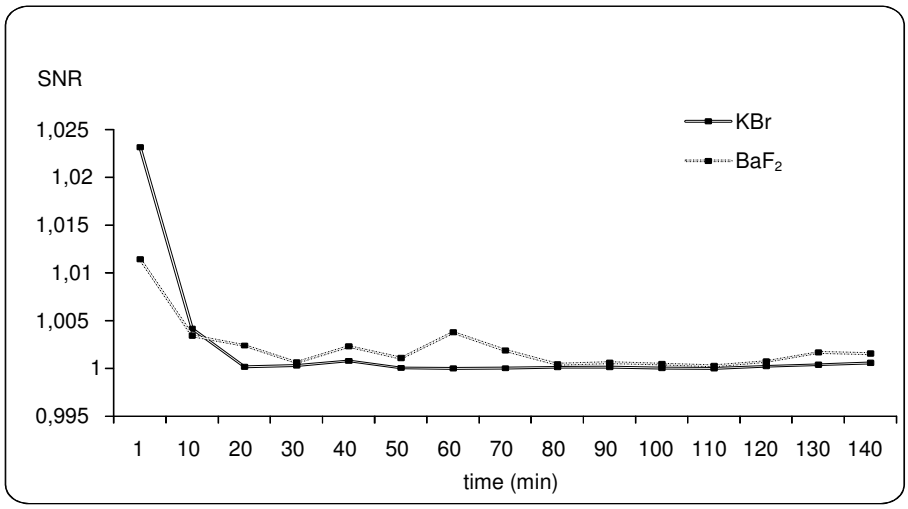

Figure 51 – Variation of the signal-to-noise ratio (SNR) with time for FTIR spectra acquired on the preparation layer of the malachite paint reconstruction embedded in KBr or BaF_2.

Therefore, other infrared salts with a minor hygroscopicity have been also investigated (Table 7). As already presented in literature (Pilc and White 1995), silver chloride is sensitive to the light and the preparation may so resulted difficult to achieve without viewing the fragment to section. Zinc sulphide and zinc selenide present fluorescence and phosphorescence respectively under ultraviolet lighting system and may compromise the optical microscopy observations of such cross sections. Due to its excessive cost, diamond has been excluded as well as thallium bromoiodide (KRS-5) for its red colour. Consequently, further tests have been carried out with calcium fluoride (CaF_2) and barium fluoride (BaF_2).

IR Material	Solubility (g/100g H_2O)
KBr	53.5
AgCl	0,00015
ZnSe	insoluble
ZnS	0,00069
Diamond	insoluble
KRS-5	0,05
CaF_2	0,0013
BaF_2	0,17

Table 7 – Solubility of infrared optics materials.

In both cases, the procedure adopted for KBr has been modified since it has been possible to compact the salts in pellet forms following the one mentioned above. First, 300 mg of BaF_2 (CaF_2) has been pressed (5 tons for 1 min) into a pellet adding 10 µL of H_2O in order to obtain a compact base. The paint fragment has then been positioned and other 300 mg of BaF_2 (CaF_2) added on with 10 µL of H_2O. After a second pressure application (7 tons for 4 min), the pellet (13 x 2 mm) has been extracted with much attention due to their fragility and brittleness and been inserted in a polyester resin support. Pellets have been dried overnight before polishing and FTIR analysis. Nevertheless, the results achieved with CaF_2 have not been successful as the paint fragment embedded into was not visible. For BaF_2 cross section, the S/N value between 4000 and 3800 cm^{-1} has been measured in the same conditions as for KBr (Figure 51). However, the results obtained seem to indicate a rather low improvement of the spectral quality. Hence, KBr cross sections represent the best results so far achieved, which may be further improved controlling the atmosphere under the FTIR microscope stage during measurements.

An evaluation of the effect of the pressure applied during the pellet formation on the integrity of the paint layers structure has been performed on a real oil painting sample which has been divided in two pieces and embedded either in polyester resin or potassium bromide. In both cases, the average value of the paint layer thickness is 50-80 µm, suggesting that KBr embedding procedure does not alter the paint structure, as showed in figure 52a-b. In literature (Fernández-Bertrán and Reguera 1996; Günzler and Gremlich 2002; Braga and

Grepioni 2004), possible mechanochemical reactions have been reported during the preparation of KBr pellets but in our case, no differences have been observed in the FTIR spectra registered at the interface between sample's surface and either KBr or polyester resin embedding. In addition, the KBr embedding system also leads to better optical microscopy observations under ultraviolet illumination thanks to the absence of the resin fluorescence contribution. In fact, the fluorescence of the paint layer is more evident on the microphotograph of the KBr cross section than for the polyester resin one (Figure 52c-d).

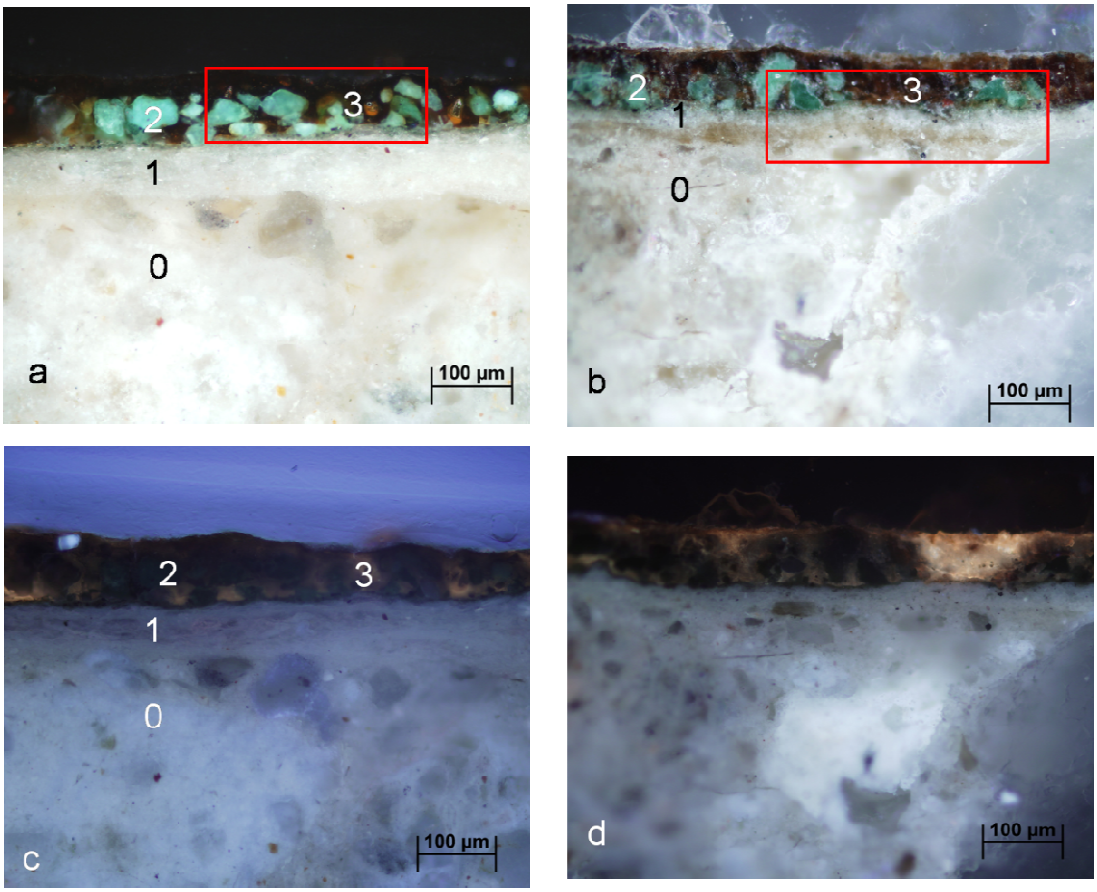

Figure 52 - Cross-section photomicrographs in visible light (original magnification 200 x) of sample T2 embedded in a) polyester resin and b) KBr. Cross-section photomicrographs under ultraviolet illumination (original magnification 200 x) of T2 sample embedded in a) polyester resin and b) KBr. The red box indicated the selected areas for ATR mapping. Each layer is numbered with: 0 (ground layer), 1 (white preparation), 2 (green), 3 (transparent brownish).

III.1.3.b *Green decoration from Nepal Thubchen Lhakhang temple mural paintings (sample T2)*

III.1.3.b.1 *ATR mapping of T2 cross-section in polyester resin*

Under optical microscopy observation, sample T2 is constituted of a ground layer (0) covered by a finely grounded white preparation (1), on which a single green layer and a superficial transparent brownish layer are superimposed (Figure 52a). A very bright fluorescence typical of siccative oil is also revealed under ultraviolet illumination in the surface layer and surrounding the pigment particles in the paint layer (Figure 52c).

Micro-ATR mapping measurements have been carried out on a representative area of the sample (300 × 100 μm^2) indicated with a red box in figure 52a, in order to identify and localise the different constituents (Figure 53). Malachite, a natural basic copper carbonate, has been localised in the paint layer integrating the carbonate out-of-plane bending band at 815 cm^{-1} (Figure 53a) and the preparation layer resulted to be constituted of clay using the bands at 990 cm^{-1} (ν Si-O) (Figure 53b). However the binding media have not been characterized in the paint and surface layers as all FTIR spectra were relatively contaminated by the absorption bands of the embedding resin (1727, 1285, 745 cm^{-1}) which overlap with eventual fatty esters and carboxylic acids bands. On the contrary in the preparation layer, amide I (1641 cm^{-1}) and amide II bands (1539 cm^{-1}) have been evidenced and suggested the presence of a proteinaceous binder (Figure 53b), even if it has not been possible to obtain a corresponding chemical image.

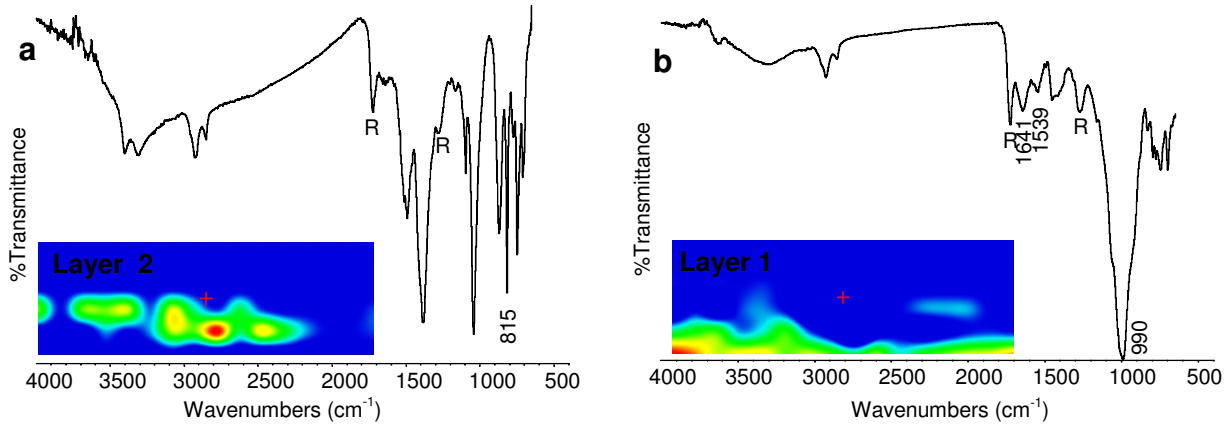

Figure 53 - FTIR false colour plots of the different paint components and ATR-FTIR (4000-650 cm^{-1}) spectra obtained from the higher intensity area (indicated in red) in the false colour plots of (a) malachite (peak area map of 815 cm^{-1} band and (b) clay (peak area map of 990 cm^{-1}). R: embedding resin.

III.1.3.b.2 *ATR mapping of T2 cross-section in potassium bromide*

In order to avoid the contamination effect from the polyester resin, ATR measurements have been attempted directly on the surface of the paint fragment before its embedding. In this way, the components of the outermost external layer have been characterised. In particular, together with calcium carbonate (1408, 872 cm^{-1}) and fatty ester (νC=O, 1735 cm^{-1}), carboxylic acids (νC=O, 1710 cm^{-1}) and copper carboxylates (νCOO^-, 1585–1550 cm^{-1}) have been individuated as degradation products derived from the triglycerides hydrolysis associated with the interaction of malachite (figure 54). As already reported in chapter II-2 from the conservative point of view, degradation processes important consequences, such as whitening phenomena and protrusions formation. In addition, ATR analysis performed on the fragment's recto has permitted to identify the presence of clay and calcite in the ground layer, suggesting the use of a "secco" technique as for the majority of the Far East Asian mural paintings (Mazzeo, Baraldi et al. 2004; Mazzeo 2006).

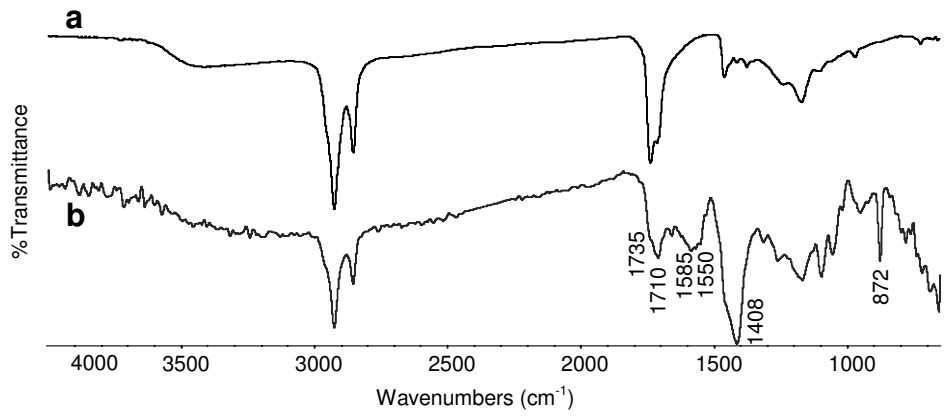

Figure 54 – ATR-FTIR spectra (4000-650 cm^{-1}) of a) 10 years old linseed oil reference spectrum and b) the surface of sample T2.

On the KBr cross section, ATR mapping has been performed directly on a selected area (345 × 90 μm^2) (figure 52b). In particular, a better characterisation and localisation of the organic substances has been possible with the acquisition of FTIR spectra free of absorption bands from the polyester resin (figure 55). In fact, a chemical image has been obtained using the carbonyl stretching band at 1710 cm^{-1} for the lipidic binder, which is spatially located both in the brown external layer and in the malachite layer (figure 55a). As for the ATR analysis before embedding, the presence of free fatty acid is predominant, confirming the ongoing degradation of the binding medium. Regarding the proteinaceous material identified in the white preparation layer (figure 55c), the absence of a contemporary C=O stretching band, which would have indicate the use of egg tempera, may suggest that a glue has been employed instead, even though, due to the low intensity of the amide I and II bands it was not possible to obtain a significative map profile. Concerning the inorganic materials, the presence of malachite (figure 55b) and clay (figure 55c) has been confirmed in the respective paint and preparation layers as well as calcite in the ground layer, which has been detected thanks to the wider area submitted to mapping (figure 55d).

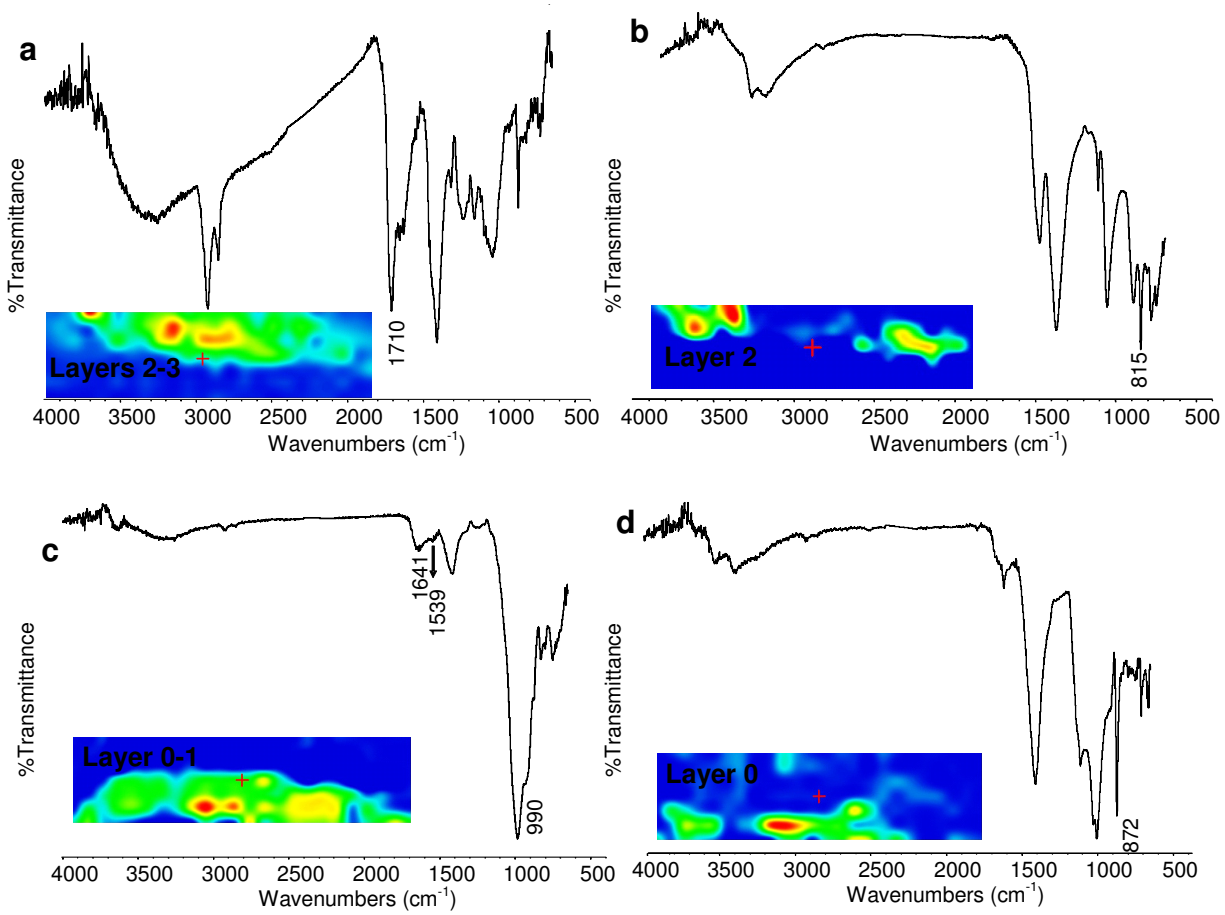

Figure 55 - FTIR false colour plots of the different paint components and ATR-FTIR (4000-650 cm^{-1}) spectra obtained from the higher intensity area in the false colour plots of (a) siccative oil (1710 cm^{-1}) (b) malachite (815 cm^{-1}),(c) clay (990 cm^{-1}) and d) calcite (872 cm^{-1}).

III.1.3.c *Blue painted area from Italian polychrome sculpture (sample Fe2)*

III.1.3.c.1 *ATR mapping of Fe2 cross-section in polyester resin*

Under optical microscopy observations of sample Fe2 (Figure 56a), a complex stratigraphy is visible. First, an outer dark blue layer (thickness of 30–65 µm) and a light blue paint layer (48 µm) constituted of a mixture of blue and white pigment particles are applied over a gold leaf. Under this latter, a red gilding ground (10 µm) and a white ground layer are visible. Moreover, UV illumination has evidenced a thin external layer (layer 4) with a characteristic yellowish fluorescence as well as the presence of a strong fluorescence for both the light blue and the ground layer (Figure 56b).

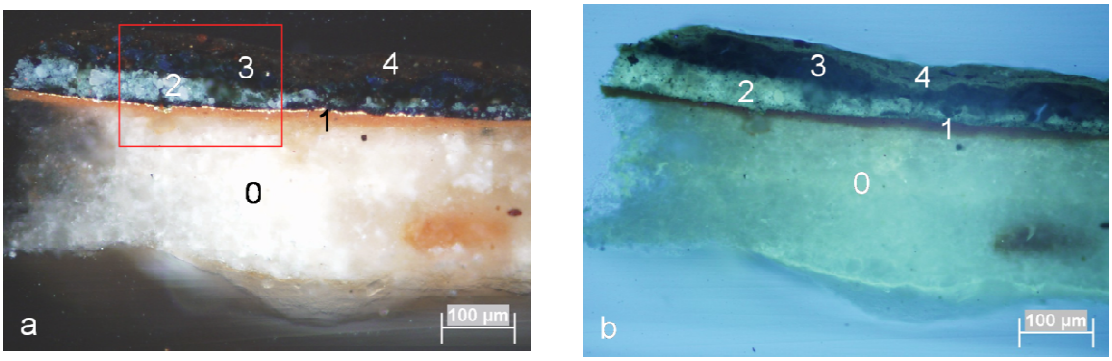

Figure 56 - Sample Fe2 cross-section photomicrographs (original magnification 200 x): a) visible microscopic image and b) fluorescent image after UV illumination. The red box indicated the selected area for the ATR mapping. Each layer is numbered with: 0 (ground), 1 (red gilding ground + gold leaf), 2 (light blue), 3 (deep blue) and 4 (thin external layer).

A selected area (220 x 160 µm^2) of the cross-section has then been submitted to ATR mapping with the aim to spatially locate the employed pigments and binding media (figure 57). Azurite $2CuCO_3{\cdot}Cu(OH)_2$ ($\nu_{as}CO_3^{-2}$, 1493 cm^{-1}) represents the main pigment used for the deep blue layer (layer 3), whereas a silicate based blue pigment mixed with few lead white $2PbCO_3{\cdot}Pb(OH)_2$, constitute the light blue paint layer (layer 2) as showed by the respective chemical images obtained using the 1035 cm^{-1} (νSi-O) and 1399 cm^{-1} ($\nu_{as}CO_3^{-2}$) bands in figures 57a-c. The gold leaf was applied over a layer made of a fine red bole (layer 1, $Al_2O_3{\cdot}SiO_2$ with Fe_2O_3, commonly used as an ingredient in grounds for gold leaf) whose related spectra have been easily obtained with only contamination of the gypsum $CaSO_4{\cdot}2H_2O$ ground and embedding resin

(figure 57d). The characteristic O-H stretching bands showed by the bole at 3697, 3651 and 3619 cm^{-1} made possible its detection even below the ATR crystal spatial resolution limit (20 µm). Finally gypsum ($\nu_{as}SO_4^{-2}$, 1109 cm^{-1}) has been identified in the white ground (layer 0) (figure 57e). In this case, the binding medium used for the ground has not been individuated probably due to the high absorbance generally showed by gypsum, which occurs in the same spectral range (1700–1600 cm^{-1}) of the amide I band, and the presence of the embedding resin. In contrast, amide I (1636 cm^{-1}) and amide II (1528 cm^{-1}) bands, which can be ascribed to proteinaceous material, have been observed in the red bole and light blue paint layers 1and 2 (figure 57f). However, for the layer 2, the exact attribution to a specific painting material is compromised by the contemporary presence of the C=O stretching band at 1724 cm^{-1} that can be assigned either to the polyester resin or the triglycerides. In fact, this band together with the amide I and amide II bands may suggest the presence of an egg tempera binder, but they could also be assigned to glue contaminated by the polyester embedding resin. Also for the composition of the outermost brown layer, its attribution has been possible only by ATR measurements carried out on the fragment's surface before being embedded and this has resulted to be constituted of proteinaceous material.

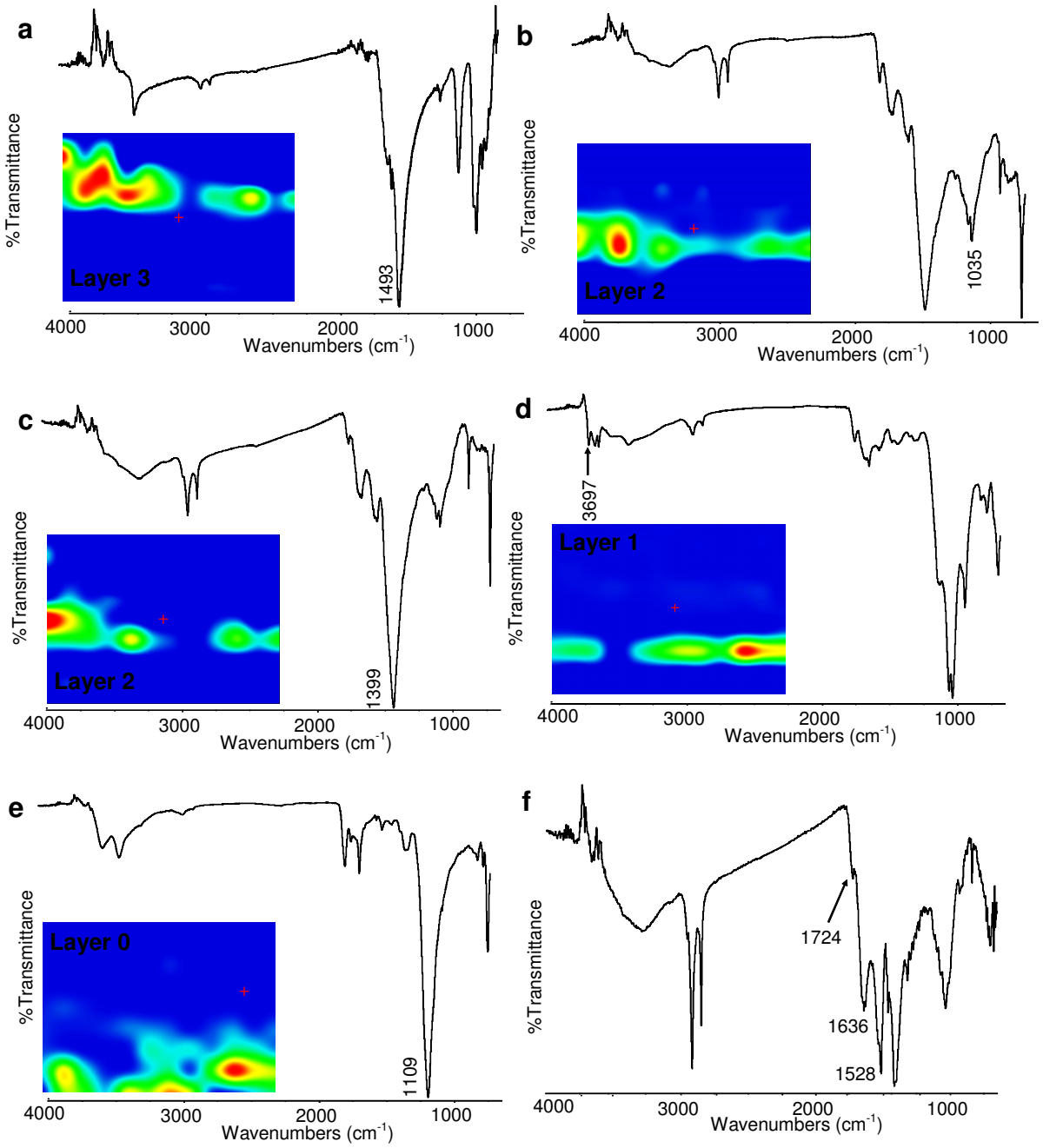

Figure 57 – ATR-FTIR (4000-650 cm^{-1}) spectra obtained from the higher intensity area (indicated in red) of the enclosed false colour plots displaying the intensity of the vibrational bands used as markers for the different paint components: a) azurite, b) silicate based blue pigment, c) lead white, d) bole, e) gypsum and f) ATR-FTIR (4000-650 cm^{-1}) spectrum obtained from the layers 1-3 attributable to the use of egg tempera technique or to the embedding resin's contamination.

III.1.3.c.2 *ATR mapping of Fe2 cross-section in potassium bromide*

In order to better clarify the nature of the organic substances, ATR mapping has been performed on a selected area (200 x 180 μm^2) of the sample embedded in KBr, as indicated by the red box shown in visible light microphotograph of sample Fe2 (Figure 58).

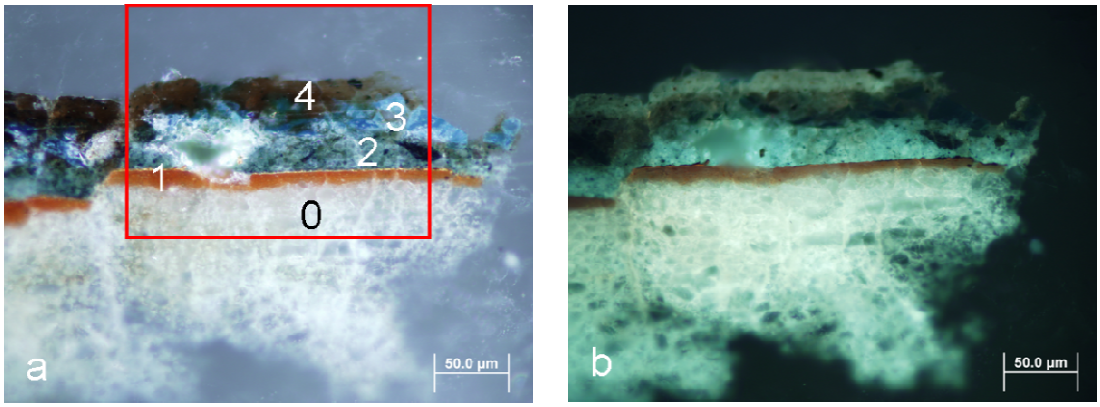

Figure 58 - Cross-section photomicrographs of sample Fe2 embedded in KBr (original magnification 500 x): a) visible microscopic image and b) fluorescent image after UV illumination. The red box indicated the selected area for the ATR mapping. Each layer is numbered with: 0 (ground), 1 (red gilding ground + gold leaf), 2 (light blue), 3 (deep blue) and 4 (thin external layer).

In this case, the KBr embedding system has provided with a better identification of the organic components located in dark blue and external layers 3–4 (Figure 59) where the presence of a proteinaceous material (amide I, 1636 cm^{-1}) and triglycerides (νC=O, 1726 cm^{-1}) has allowed the attribution to egg tempera as binding medium. The shoulder of the lipidic compounds observed in the FTIR spectrum can be the result of natural ageing of the binder, as already reported by Meilunas (Meilunas, Bentsen et al. 1990). In particular, layers 3 and 4 are characterised by a sharp amide II band (1528 cm^{-1}) more intense than the amide I (1636 cm^{-1}). The common FTIR spectrum of proteinaceous molecules, which is represented by an amide II band intensity lower than for the amide I band, is here not observed and this feature may suggest a additional contribution from metal carboxylates as confirmed by the contemporary presence of a band at 1575 cm^{-1} (νCOO^-) (van der Weerd, Brammer et al. 2002). Regarding the light blue paint layer 2, the only presence of amide I and

amide II bands have allowed us to exclude the use of an egg tempera binder. Nevertheless, FTIR spectroscopy is intrinsically limited to distinguish between analogous proteinaceous binders, such as egg white, animal glue and casein, the exact nature of the binder can so only be attributed based on historical information. In fact, the use of egg white or “glair” has been limited to paint finishing, whereas animal glue has been extensively reported as binder for both paint layers and grounds (Thompson Jr 1954). Even if casein tempera may also have been used, it has the tendency to produce brittle paint films, which is not the case of the examined polychrome sculpture. Hence, other micro-destructive chromatographic techniques, such as GC–MS or HPLC, can certainly be more appropriate in this case.

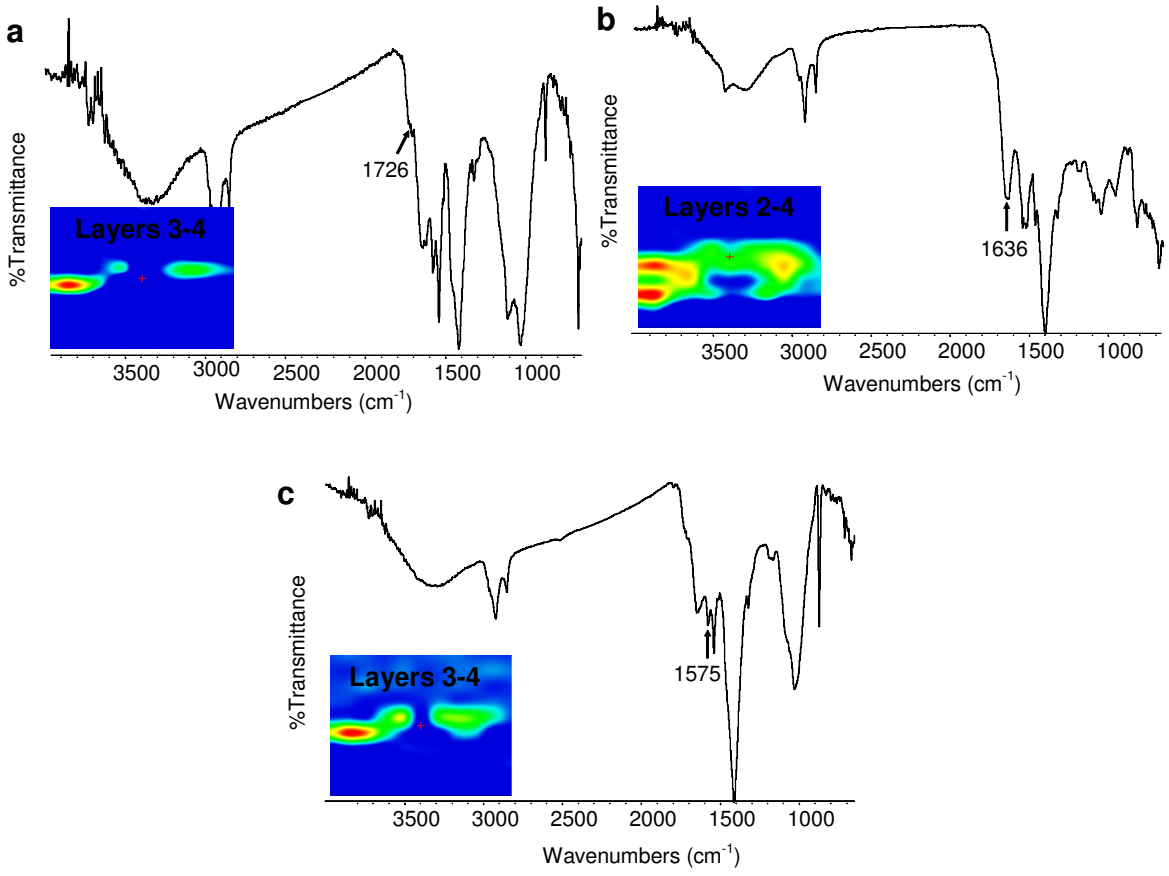

Figure 59 - ATR-FTIR (4000-650 cm^{-1}) spectra obtained from the higher intensity area (indicated in red) of the enclosed false colour plots displaying the intensity of the vibrational bands used as markers for the different paint components: (a) fatty acids, (b) proteinaceous material, (c) copper carboxylates.

III.1.3.d *Paper decoration from Vincenzo Coronelli globe (sample BC1)*

Another sample (BC1) collected from the wooden support of the Coronelli's celestial globe has been embedded in KBr and analysed. In order to prepare the wooden support's surface, a first thick sheet of paper is applied with a natural resin giving water-resistant proprieties and then a thinner printed sheet, which represents the drawing, is smooth out with the same sizing (Gettens and Stout 1966). Due to their characteristic fibrous cellulose structure, the two layers of paper, respectively layer 0 (350 µm thick) and layer 2 (150 µm thick) can be easily observed under either visible or ultraviolet light, as showed in the microphotographs of figure 60. On top are present a thin grey layer (layer 3, 20 µm thick) and a second white (layer 4, 15 µm thick), which also strongly fluorescents under UV light. In both the paper layers, the use of an organic size is also revealed by the strong yellow fluorescence observed under UV light.

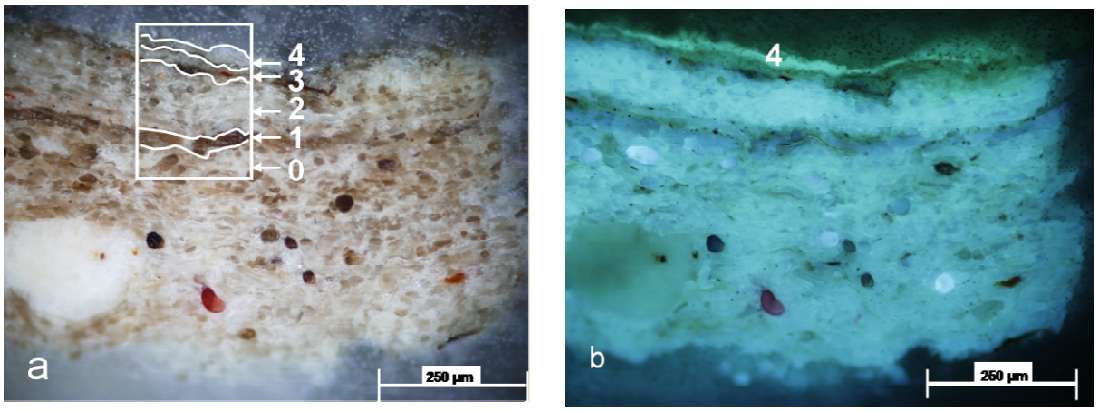

Figure 60 - Cross-section photomicrographs of sample BC1 embedded in KBr (original magnification 200 x): a) visible microscopic image and b) fluorescent image after UV illumination. The red box indicated the selected area for the ATR mapping. Each layer is numbered with: 0 (paper substrate), 1 (brown), 2 (paper), 3 (white), 4 (transparent fluorescent under UV light).

In this case, ATR mapping, performed on an area of 220 x 300 µm^2 (Figure 60a), has allowed distribution maps to be obtained for the different components (Figure 61). A part from the two layers of cellulose (Figure 61a) individuated integrating the 990-1090 cm^{-1} region (νC-O + γOH), the use of shellac (Figure 61b), characterised by absorption bands at 1250 cm^{-1} (νC-O) and 1740-1690 cm^{-1} (νC=O), as sizing has been confirmed (Derrick 1989). Nevertheless, the corresponding chemical image cannot be perfectly correlated to the real

distribution of shellac within the layers as the high porosity (presence of surface voids) of the paper substrates does not allow a good contact with the ATR crystal. The presence of gypsum ($\nu_{as}SO_4^{-2}$, 1145-1110 cm^{-1}) has been characterized in the layer 3 and can be explained by the sampling, which has been performed close to an area plastered during past restoration interventions aiming at filling a paper detachment (Figure 61c). At this occasion, a protective varnish has been further applied as a finish and result also to be constituted of shellac (layer 4 in figure 61b). The potential of KBr embedding system is really demonstrated in this case since a so thin external layer would have certainly be analysed with difficulties on a sample embedded with the conventional system.

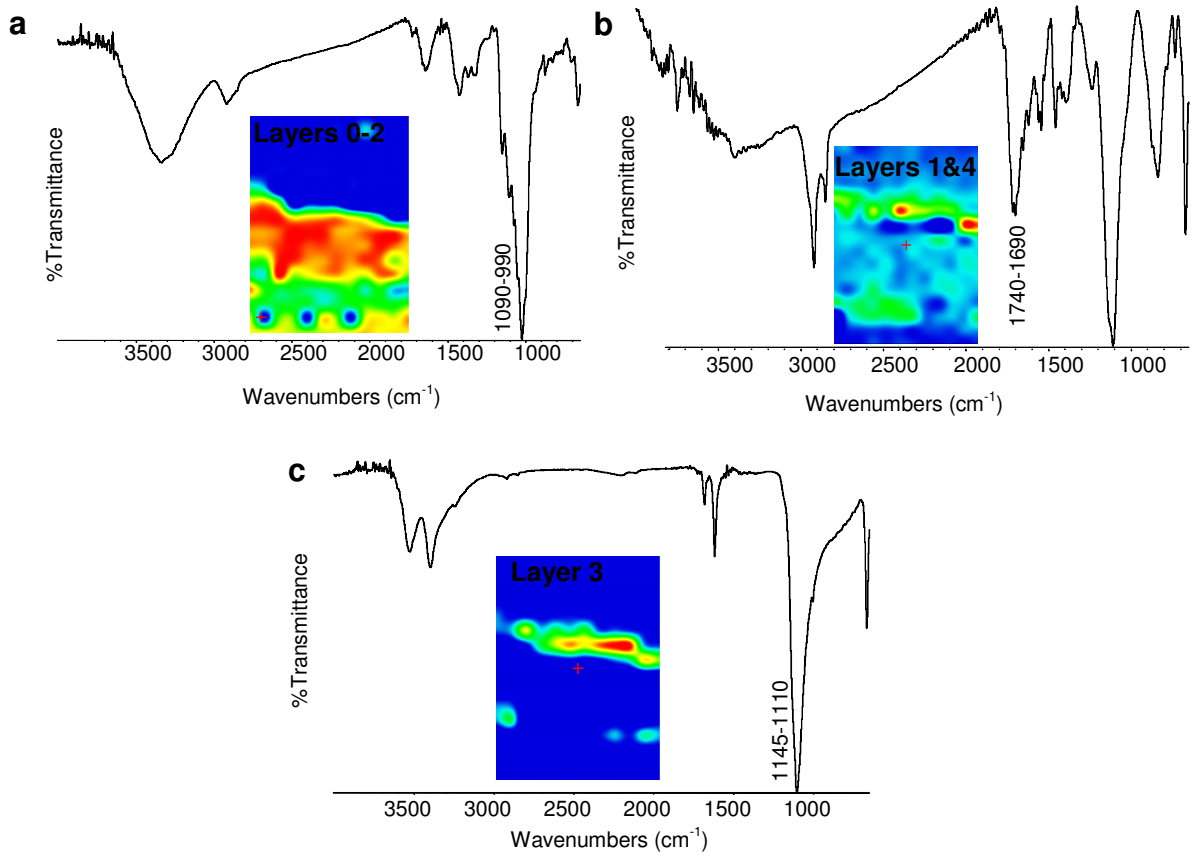

Figure 61 - ATR-FTIR (4000-650 cm^{-1}) spectra obtained from the higher intensity area (indicated in red) of the enclosed false colour plots displaying the intensity of the vibrational bands used as markers for the different paint components: a) cellulose, b) shellac, c) gypsum.

III.1.3.e *Mordant gilding on the Mattia della Robbia's altar-piece (sample MCR13)*

Most of the della Robbia's altar-piece consists of glazed terracotta while approximately 30% is composed by polychrome "cold painting" (*pittura a freddo*) terracotta (Pappalardo, Costa et al. 2004). Moreover, few studies have been reported on this uncommon *secco* technique as well as the gilding technique adopted for paint terracotta. Therefore here is proposed a sample, which may characterise the gilding technique adopted by della Robbia. Under optical microscopy observations of sample MCR13, a light blue and a white paint layers (layer 5 and 4, 20-50 µm and 30 µm thick respectively) are visible on a gold leaf (layer 2), under which a brownish gilding mordant (layer 1, 4-14 µm thick) and a white ground (layer 0, 20-60 µm thick) are present (Figures 62 a-b). Deposition materials are also present as a thin dark layer (layer 3) over the gold leaf, indicated in the secondary electron (SE) image illustrated in figure 53c. This may suggest that the blue layer is repaint and the angel's wing, from which the sample has been collected, has been originally gilt.

Observations under UV light can give us a first appreciation of the different organic material present in the stratigraphy. In fact, while the white ground and the repainted layers are characterised by a strong bright yellow fluorescence, the gilding mordant shows just a pale bluish one (Figure 62b). The documentation of the fluorescence effects takes real advantage from the UV-inactive KBr embedding system if compared with the conventional embedding into a synthetic polymer, which also generates fluorescence phenomenon. Furthermore, a detachment between the organic mordant and the lower white paint layer has been highlighted in the SE image (figure 62c) referred as a blue box in the visible image (figure 62a). Even if the reasons of such detachment are unknown, this feature can outline a different physical behaviour for the gilding mordant and the underneath binding material, which should be linked to different chemical compositions.

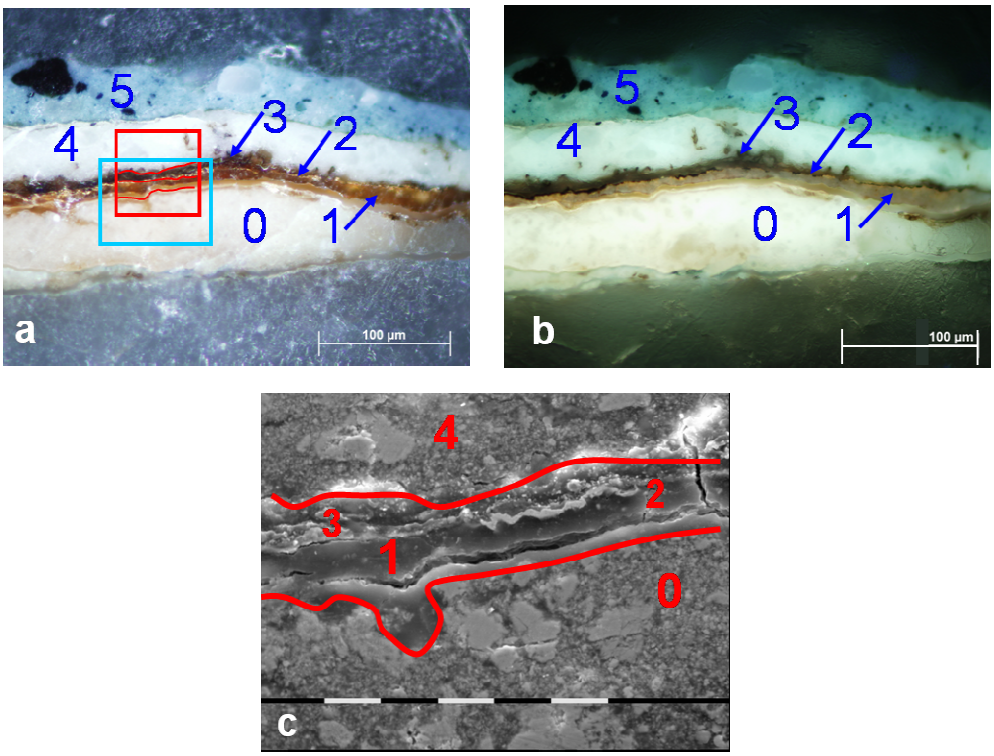

Figure 62 - Cross-section of sample MCR13 embedded in KBr: a) visible light microscopic image. b) UV light microscopic image; c) SE image (original magnification 1600x): the detachment occurring between the white ground layer (0) and the gold leaf (2) is visible.

The whole data cube generated by ATR imaging performed on an area (63 x 63 μm^2) marked with a red box in figure 62a, has been analysed in order to obtain chemical images for each identified painting material as illustrated in figures 63a-c. In particular, the binding medium used for layers 0 and 3 has been identified as siccative oil whereas the presence of an adhesive sizing of proteinaceous nature represents the main component of the brownish layer applied as mordant gilding. Figures 63a and b show the chemical images of the oil and proteinaceous material which have been obtained by integrating the absorbance of the characteristic vibrational bands of respectively the C=O fatty ester asymmetric stretching at ca. 1730 cm^{-1} (the integration range used was 1750 cm^{-1} to 1700 cm^{-1}) and the amide I at ca. 1640 cm^{-1} (integration range 1680-1610 cm^{-1}). It has been also possible to identify silicates (1070-970 cm^{-1}) in the mordant layer, even though a significative distribution plot has not been obtained (Figure 63d). The use as mordant gilding of proteinaceous material, probably glue, mixed with silicates is in accordance with the literature. In fact ancient treatises mention either the use of mixture of siccative oil and natural

resins or a glue size mixed with red bole. The presence of siccative oil in the white ground under the mordant seems to be in accordance with the hypothesis that the detachment has occurred between them due to their differences in chemical composition and response to physical stresses. Concerning the stratigraphic identification of the pigments used, lead white (basic lead carbonate) was detected as the main constituent of both layers 0 and 3 and its FTIR image has been obtained by selecting the integrated absorbance of the CO_3^{2-} asymmetric stretching at ca.1395 cm^{-1} (the integration range used was 1500 cm^{-1} to 1300 cm^{-1}) (Figure 63c). These results highlight the great advantage of using FTIR imaging and ATR mode for the characterisation of this thin gilding mordant layer. In fact, the spatial resolution is here related to the pixel dimension of the detector and is approximately of 5 µm.

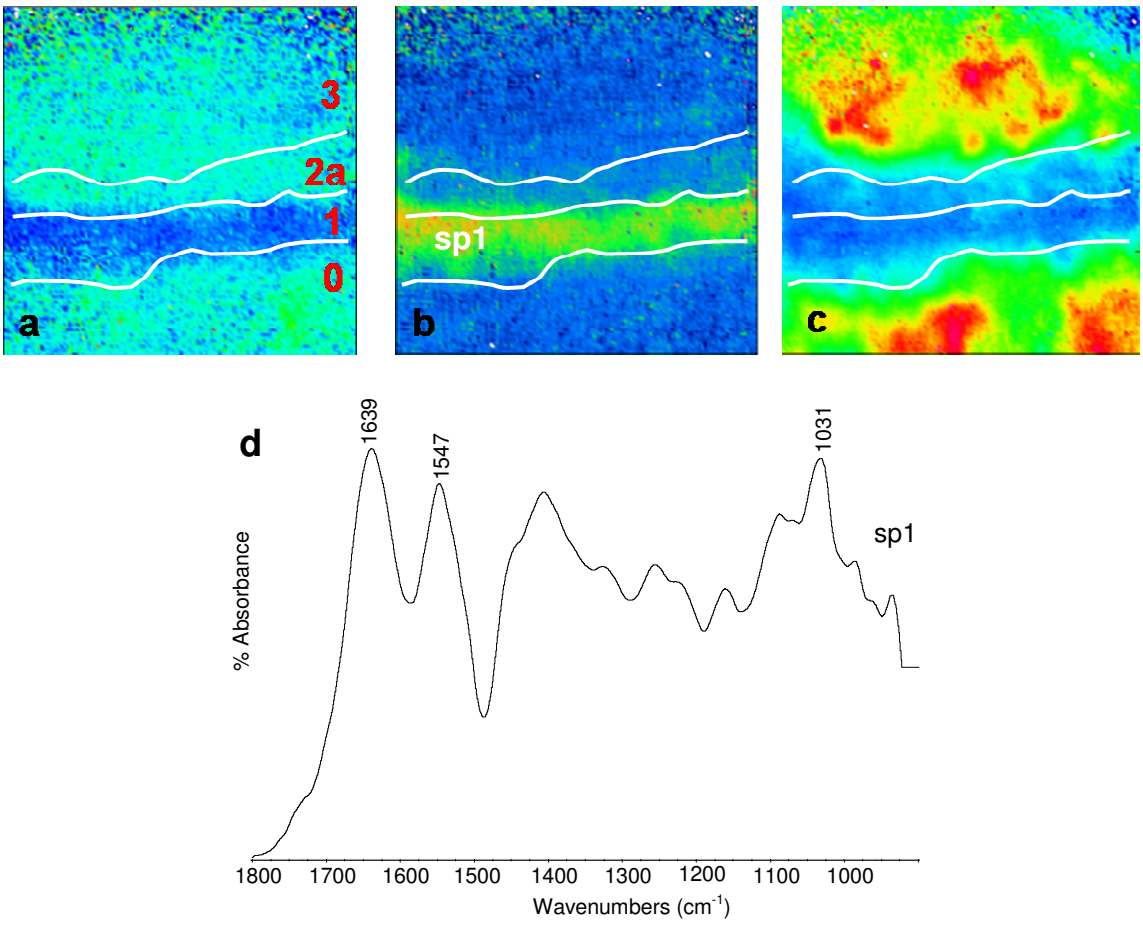

Figure 63 - a) FTIR image representing the integrated absorbance of the asymmetric carbonyl stretching band between 1750 and 1700 cm^{-1}; b) FTIR image representing the integrated absorbance the amide I band between 1680 and 1610 cm^{-1}; c) FTIR image representing the integrated absorbance of the carbonate band between 1500 and 1300 cm^{-1}; d) FTIR spectrum (1800-900 cm^{-1}) extracted from the higher intensity area of d, marked sp1.

III.1.3.f *Mordant gilding on the star ray's fragment from the Giotto frescoes in the Scrovegni Chapel (sample 22L)*

In the attempt to characterise the constitution of the mordant gilding used by Giotto in the decoration of the ceiling of the Scrovegni Chapel mural paintings a micro sample has been collected from a ceiling star ray's. The visible light microscope image together with the UV light and back-scattered image of the sample in the scanning electron microscope (Figure 64) have been used to help interpret and complement the ATR-FTIR imaging results. The first optical and scanning electron microscope observations indicate that a golden tin technique has been adopted. In literature (Thompson Jr 1954; Tintori 1982), there are different definitions of *stagno dorato (*golden tin): it can be understand as a cheap substitute for gold, made of tin tinted with a golden varnish, or as a fine real gold foil laminated with tin. In this case, gold laminated with tin has been used. In fact, sample 22L shows a complex stratigraphy which results to be composed of nine layers with a total of 75 microns thickness (Figure 64c). A gold leaf (Figure 64c: layer 8) has been applied over a tin leaf (figure 64c: layer 6) with a mordant gilding (Figure 64c: layer 7), which appears black in the BSE image and fluorescent in the UV light image (Figure 64b). In this sample, we are in presence of a superimposition of two golden tin layers as the same sequence is repeated under with gold (layer 4), mordant (layer 3) and tin (layer 2). This feature may suggest that the sample has been collected from an area of two contiguous golden tin applications. Hence, another mordant is also visible between the two golden tin systems (Figure 64c, layer 5) as well as a thin layer under the first golden tin layer (layer 1, Figures 64bc) in order to adhere to the mural. Furthermore, an external thin bluish fluorescent layer (Figure 64b) is also visible in the UV image and can be associated with the above mentioned contamination induced by the glue used to hold the sample during the XRF analyses. SEM-EDX elemental analyses have confirmed the use of a golden tin technique and have permitted identifying both tin and gold as constituents of the leafs, which appear respectively grey and white in the BSE image (Figure 64c) (Cesareo, Castellano et al. 2002; Cesareo, Castellano et al. 2004; Cesareo, Castellano et al. 2005; Marabelli, Santopadre et al. 2005).

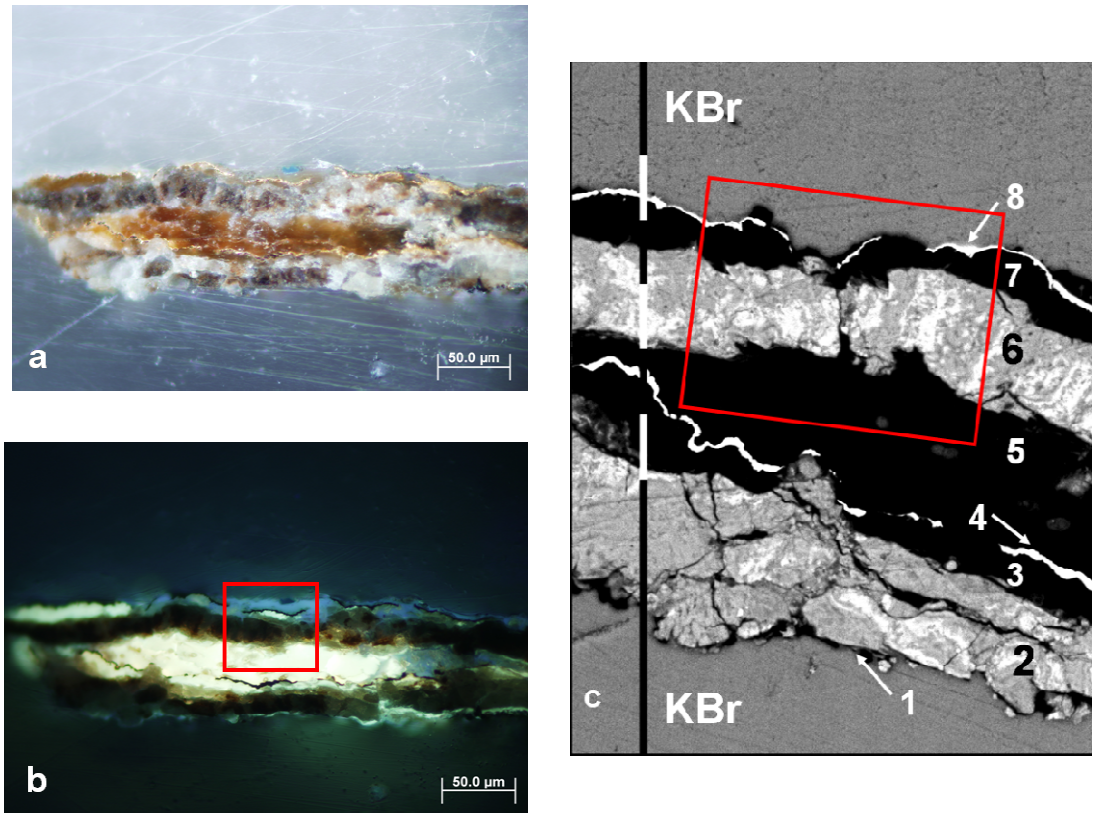

Figure 64 - Cross-section of sample 22L embedded in KBr: a) visible light microscopic image; b) UV light microscopic image; c) BSE image (original magnification 1300x): the different layers are numbered from 1 to 8. The red box indicates the area imaged by ATR-FTIR.

In order to spatially characterise the different organic materials constituting the mordant layers, ATR-FTIR imaging has been performed directly on the cross-section on a representative area (63 x 63 μm^2) of the upper golden tin layer (red box in Figure 64a). As illustrated in figure 56, the resulting image obtained with the univariate analysis plotting the intensity of the C=O asymmetric stretching absorbance band (range between 1760 cm^{-1} and 1700 cm^{-1}) has allowed localising the different organic substances. Even though no single image has been obtained for each mordant layer, the different FTIR spectra extracted from the data cube have suggested the presence of a mixture of siccative oil with natural resin in both the gold mordant and tin mordant layers (Figures 65ab and Figure 64, layers 7 and 5). On the other hand, the blue fluorescent layer (layer 9) in the ultraviolet light image has been identified as polyvinyl acetate (Figure 65c). Calcium oxalates, which may be derived by organic compounds' degradation, have been also identified on the surface and in the different organic layers (Figure 65d). The distribution of carboxylates as degradation

products has been also plotted using the integrated asymmetric COO^- stretching absorbance at ca. 1550 cm^{-1} (Figure 65e). Although less defined, the green zones coincide with the inner tin mordant layer. Moreover, PCA carried out in the spectral range between 1800-1000 cm^{-1} has pointed out the presence of a layer 5-10 µm thick, as it is possible to appreciate in Figure 66. The corresponding loading shows the presence of two intense bands at 1739 cm^{-1} and 1234 cm^{-1}, which are ascribable to the polyvinyl acetate.

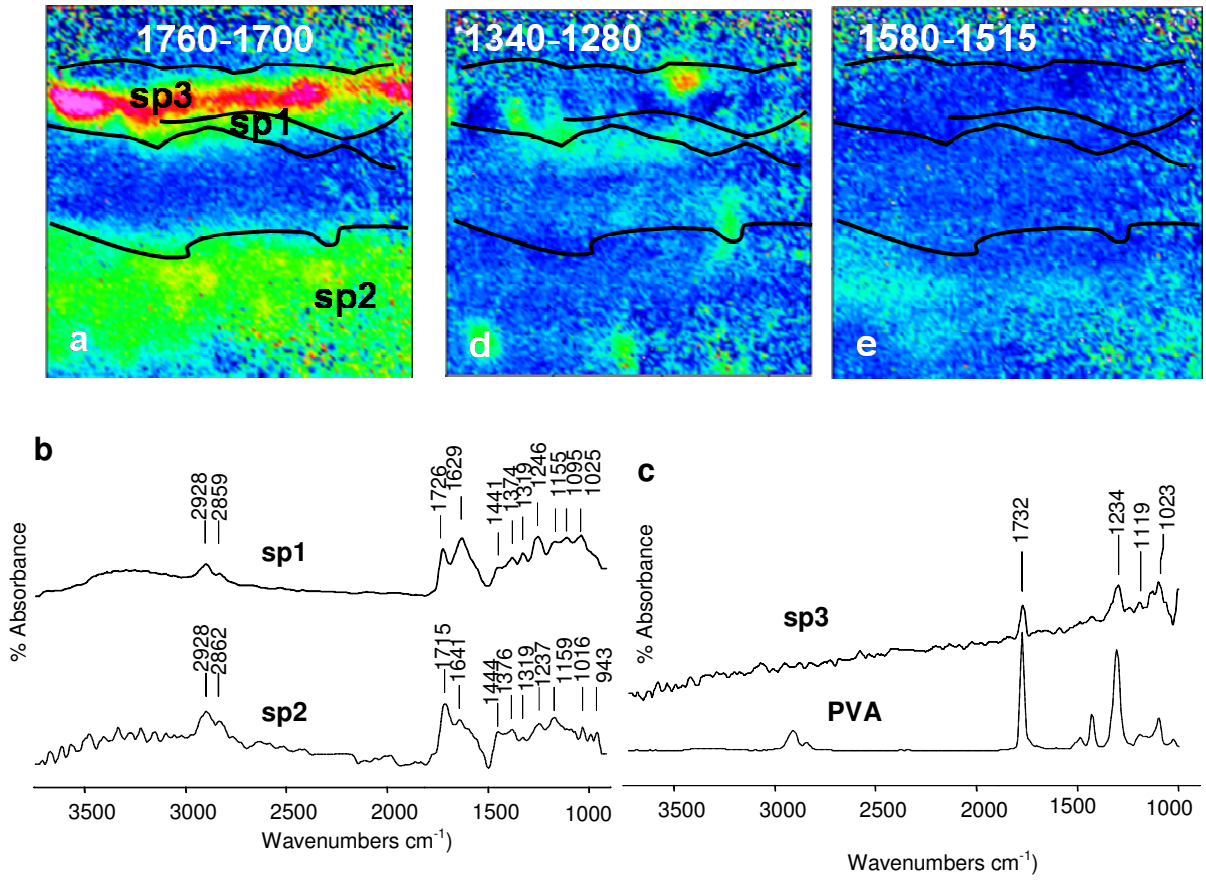

Figure 65 - FTIR images of the area indicated by a red box in figure 4, representing the integrated absorbance of a) the asymmetric carbonyl stretching band between 1760 and 1700 cm^{-1}, d) the oxalates band between 1340 and 1280 cm^{-1} and e) the carboxylates band between 1500 and 1600 cm^{-1}. b) FTIR spectra extracted from mordant layer 7, marked sp1 in a and from mordant 2 area, marked sp2 in b; c) FTIR spectrum extracted from one of the red regions of the image in g, marked sp3, compared with a reference spectrum of polyvinyl acetate.

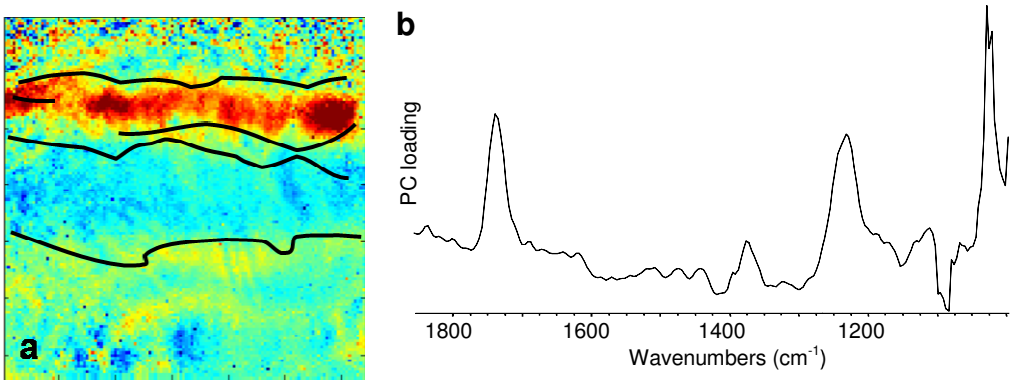

Figure 66 - a) score plot and b) PC loading of the micro-ATR-FTIR imaging data obtained for the sample 22L in the spectral region 1850-1000 cm^{-1}.

III.1.4 Conclusions

This study illustrates the possibilities offered by ATR-FTIR microspectroscopy for the stratigraphic characterisation of inorganic species but also of organic substances present in lower proportions. Since the conventional resin embedding system does not allow their unambiguous detection given the contamination effects in FTIR spectra, micro-ATR analysis directly performed on the surface of the sample before its embedding has been tested but resulted limited to the identification of organic substances located on the outermost paint surface. Therefore, an alternative KBr embedding system for the production of paint cross-sections has been also proposed and evaluated comparing polyester resin and KBr cross sections of the same sample. Either for proteinaceous, lipidic or resinaceous materials, not only their identification but also their distribution has been evidenced. In comparison with specular reflectance mode, the higher quality of ATR-FTIR spectra obtained here indicates the great advantages of this analytical technique for determining the spatial distribution of the identified chemical compounds in a paint cross-section. However, the opacity of the silicon crystal does not allow accurate localisation of thin layers and, due to spatial resolution about 20 µm, thinner layers can only be detected if they are composed of highly absorbent inorganic substance such the bole layer identified in sample Fe2. Thus, the enhanced spatial resolution achieved with the particular combination of FTIR

microspectroscopy with an ATR germanium crystal and a FPA detector can help in the analysis of very thin layers below 10 µm as the gilding mordants of samples MCR13 and 22L. Moreover, the univariate method, which provides valuable information on the composition of the paint cross-sections for both inorganic and organic compounds, can be further confirmed or completed by multivariate analyses performed on the whole set data cube, extracting principal components as representative variables. Both ATR mapping and imaging are non-destructive methods, which can be further combined with optical microscopy and SEM-EDX elemental analysis to obtain complementary information and depict a complete characterisation of painted artworks.

III.1.5 Acknowledgements

This research has been partially carried out with the support of the European Union, within the VI Framework Programme (Contract: EU-ARTECH, RII3-CT-2004-506171). The ATR imaging results have been obtained during a short research period in the laboratory of Prof. S. Kazarian (Imperial College of London, UK). Dr. C. Ricci is thanked for assistance with FTIR imaging microscope and multivariate analysis data interpretation. The authors gratefully acknowledge Dr. P. Santopadre and Dr. M. Ioele (Instituto Superiore per la Conservazione e il Restauro, Rome, It) for providing the sample 22L from the Scrovegni chapel and permitting the presentation of the results in this thesis. Mrs. M. Quaranta is also thanked for the preliminary experiments on the KBr embedding system.

III.2 Macroscopic ATR-FTIR imaging of paint cross-sections

Macro attenuated total reflectance Fourier transform infrared (ATR-FTIR) spectroscopic imaging is presented as non-destructive analytical methodology for the study of paint surfaces. This chapter illustrates new opportunities offered by a conventional diamond ATR accessory coupled with a focal plane array detector to obtain chemical images of multi-layered paint cross-sections. The use of a large internal reflection element permits to increase the field of view of the imaging area up to 770 x 550 μm^2 and to obtain FTIR imaging of the sample's complete stratigraphy. Applied for the first time to cultural heritage, this approach becomes a versatile analytical tool to determine the composition of the inorganic and organic painting materials present and get information on their distribution within the different layers. In the optical arrangement used, a spatial resolution of approximately 15 µm is achieved without the use of any infrared microscope objectives. This study demonstrates the possibilities offered by macro ATR-FTIR imaging for a rapid and simple identification of the different compounds present in paint cross-sections before performing further molecular and elemental analyses which may be time consuming or require particular sample preparation.

III.2.1 Introduction

Fourier transform infrared (FTIR) spectroscopy is commonly used for the characterisation of the inorganic and organic paintings' components and represents a useful analytical tool in the understanding of painting techniques, state of conservation and causes of degradation. The characterisation of the interactions and degradation processes taking place within the complex multi-layered paint structures is generally carried out on cross-sectioned micro samples collected from paintings. FTIR imaging, which makes use of a focal plane array detector, is one of the few methods, providing both spectral and spatial information on the different painting materials present within each individual paint layer constituting a complex heterogeneous matrix. In particular

the combination of attenuated total reflection (ATR) FTIR spectroscopy and an imaging system provides an improvement of the spatial resolution due to the high refractive index of the ATR crystal, which gives a higher spatial resolution according to the Rayleigh criterion (Sommer, Tisinger et al. 2001; Chan and Kazarian 2003). So far, ATR-FTIR imaging has been used in different fields, such as pharmaceutical (Chan, Hammond et al. 2003; Chan and Kazarian 2007; Ricci, Nyadong et al. 2007), biomedical (Colley, Kazarian et al. 2004; Chan, Kazarian et al. 2005), forensic (Ricci, Chan et al. 2006; Patterson, Havrilla et al. 2007; Ricci, Phiriyavityopas et al. 2007) or polymers (Zhang, Otts et al. 2002; Kazarian, Andrew Chan et al. 2004) studies. Only few examples related to cultural artefacts have been reported in the literature: the study of albumen photographs (Ricci, Bloxham et al. 2007), painting cross sections (Spring, Ricci et al. 2008) and the identification of mineral components in a Maya paint (Goodall, Hall et al. 2008). Recently the use of large internal reflection elements has been developed and the possibilities of increasing the imaging area has been demonstrated elsewhere (Chan and Kazarian 2003; Colley, Kazarian et al. 2004; Patterson and Havrilla 2006; Chan and Kazarian 2007; Patterson, Havrilla et al. 2007; Ricci, Phiriyavityopas et al. 2007). Despite the improvement of the analysed area achieved with these accessories, problems of contact uniformity between sample and crystal may sometimes arise, especially in the case of hard or non-easily deformed samples. Due to its hardness which allows a high pressure to be applied, diamond is often used as material for ATR-FTIR accessories. Using such arrangement, reproducible spectra of hard materials are successfully measured with a uniform contact between sample and crystal (Chan and Kazarian 2003). In this work, the potentialities offered by macro diamond ATR-FTIR imaging to the study of paint cross-sections, in terms of characterisation and localisation of the compounds present, are illustrated.

III.2.2 Experimental methods

III.2.2.a *Paint samples*

Three real samples have been collected from a) a gilt decorated leather (17-18th century D.C) manufactured in central Italy (sample CD), b) the Madonna's blue robe (sample Fe2) of a 14th century A.C. Italian polychrome sculpture belonging to a private collection and c) the Madonna's red robe (sample MCR8) of the Andrea della Robbia's terracotta altar-piece "*Assumption of Virgin between S. Sebastian and S. Rocco*" located in the collegiate church of S. Maria Assunta in Montecassiano (Macerata, Italy). All samples have been first carefully observed under a binocular stereo microscope Leica MZ6. Samples MCR8 and Fe2 have been embedded in a polyester resin support (Serifix. Struers), then cross-sectioned and submitted to wet polishing with conventional methods using silicon carbide cards with successive grid from 120, 400, 800, to 1000.

III.2.2.b *Optical microscopy*

Dark field observations of cross-sectioned samples have been performed using an optical microscope Olympus BX51M equipped with fixed oculars of 10x and objectives with different magnifications (5, 10, 20, 50 and 100x). Visible and ultraviolet light were respectively provided by a 100W halogen projection lamp and an Ushio Electric USH102D lamp. Photomicrographs have been recorded with a digital scanner camera Olympus DP70 directly connected to the microscope. The observations under UV light are commonly used as a first tool to qualitatively detect and stratigraphically locate the presence of organic materials (binding media, varnishes, etc.) thanks to the fluorescence effects generated by such materials when submitted to a UV radiation source.

III.2.2.c *ATR-FTIR spectroscopic imaging*

An FPA detector has been used to measure FT-IR images with an FT-IR spectrometer operating in continuous scan mode together with a diamond ATR accessory (Golden gate™, Specac Ltd.). The imaging ATR spectrometer is patented by Varian (Burka and Curbelo 2000). In the optical arrangement used, the spatial resolution is approximately 15 μm (Chan and Kazarian 2003). Spectra have been collected with 8 cm^{-1} spectral resolution in the range 4000–900 cm^{-1} and 64 scans. The FPA detector comprised 4096 small pixels arranged in a 64 x 64 grid format with each of the pixels measuring an infrared spectrum; thus, 4096 spectra are acquired in a single measurement. A plot of the distribution of the absorbance of a specific spectral band corresponding to a particular substance in the imaged area of the sample produced the chemical image for that particular substance. A colour scale from high value (red) to low value (blue) is employed. The imaging area measured using this accessory and this particular FPA detector was 770 x 550 μm^2. To ensure that good contact has been established between the cross sections and the crystal, a drop of water has been added, acting as reflective medium for the infrared radiation and compensating the micro irregularities of the surface. The eventual water absorbance bands present in the spectrum has been further subtracted.

III.2.3 Results and discussion

III.2.3.a *Macro ATR-FTIR imaging of non embedded fragment*

Leather gilding has been originated in Spain and in particular from Cordoba but it has also been manufactured in Italy. The typical golden aspect is achieved by the application of a metal leaf (tin, silver or copper) on the leather with some glue. The metal surface is then brushed with little egg white in order to avoid metal oxidation. A final finishing (“*mecca”)* made up of a natural varnish containing yellow organic pigments (saffron, aloe) is then applied to achieve the golden colour. In the attempt to characterise the outermost varnish layer of sample CD, macro ATR measurements have been performed directly on the

surface of the gilt leather fragment. A view of the leather fragment is shown in figure 67a. The FTIR image created by integrating the C-O fatty ester stretching absorbance band between 1270 and 1210 cm^{-1}, which is considered as marker for the presence of a natural resin (Omecinsky and Carriveau 1982), is presented in figure 67b. The spectrum extracted from the higher intensity area points out the presence of free fatty acids (Figure 67h), probably from shellac (1698, 1453, 1415, 1237, 1167 and 1038 cm^{-1}) as confirmed by the distribution plot obtained with the integrated C=O carbonyl asymmetric stretching absorbance band between 1720 and 1685 cm^{-1} (Figure 67c).

Vibrational bands assignable to the presence of calcium oxalates have also been identified in the spectrum. The varnish distribution does not appear homogeneous and some degradation products have been recognized in the blue areas of the varnish distribution plot, corresponding to zones where the metal leaf has turned black by corrosion (Figure 67d-f). Spectra extracted from these areas indicate the contemporary presence of calcium oxalates ($\nu_{sym}COO^-$ at 1373, 1318 cm^{-1}), sulphates ($\nu_{asym}SO_4^{2-}$ at 1198 cm^{-1}) and silicate deposition materials (νSi-O at 1076, 1035 cm^{-1}). Moreover, in the same areas, a proteinaceous material (amide I, 1617 cm^{-1} and amide II, 1535 cm^{-1}) has been individuated and can probably be assigned to the glair originally applied to avoid the metal leaf's oxidation (Figure 67g, i). In this example, diamond ATR-FTIR imaging measurements have allowed the contemporary characterisation of the original natural resin as well as the degradation products and deposition material in a non-destructive way towards the sample. This analytical technique can therefore be used not only for the material characterisation but also, being non-destructive, repeated at different periods of time opening up novel analytical possibilities in the monitoring of ongoing deterioration processes and restoration materials' performance.

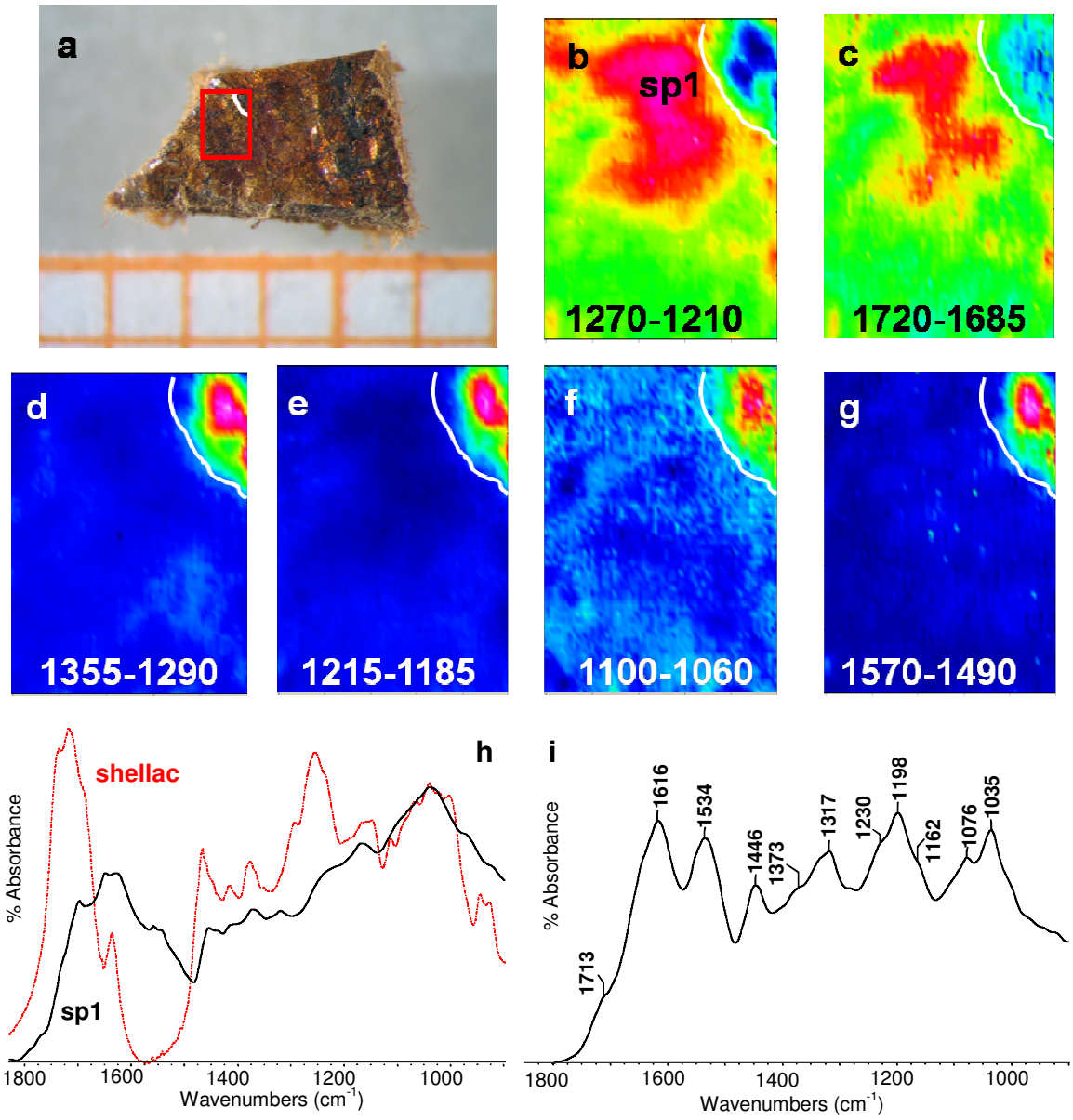

Figure 67 – a) Stereomicroscope view of sample CD. FTIR images of the area indicated by a red box in a, representing the integrated absorbance of b) the natural resin band between 1270 and 1210 cm^{-1}, c) the natural resin band between 1720 and 1685 cm^{-1}, d) the oxalates band between 1355 and 1290 cm^{-1}, e) the sulphates band between 1215 and 1185 cm^{-1}, f) the silicates band between 1100 and 1060 cm^{-1}, g) the amide II band between 1570 and 1485 cm^{-1}. h) FTIR spectrum extracted from the top central area of b, marked sp1 and compared with a reference spectrum of shellac. i) FTIR spectrum extracted from the top right corner of d, marked sp2. The size of the FTIR images is 770 × 550 μm^2.

III.2.3.b *Macro ATR-FTIR imaging of cross-section in polyester resin*

III.2.3.b.1 *Blue painted area from Italian polychrome sculpture*

Sample Fe2 shows a complex stratigraphy with two different blue paint layers (thickness of ~ 30 and ~20 µm respectively for the inner light blue layer 2 and the outer dark blue layer 3) applied over a gold leaf (layer 2) under which a red gilding ground (layer 1, 10 µm thick) and a white ground layer 0 are visible (figure 68a). Under UV illumination, an external brownish layer (layer 4, 15 µm thick), which is observed with difficulties in the reflected light microphotograph, fluoresces yellowish and a strong fluorescence is also evident in the white ground and light blue layers (figure 68b).

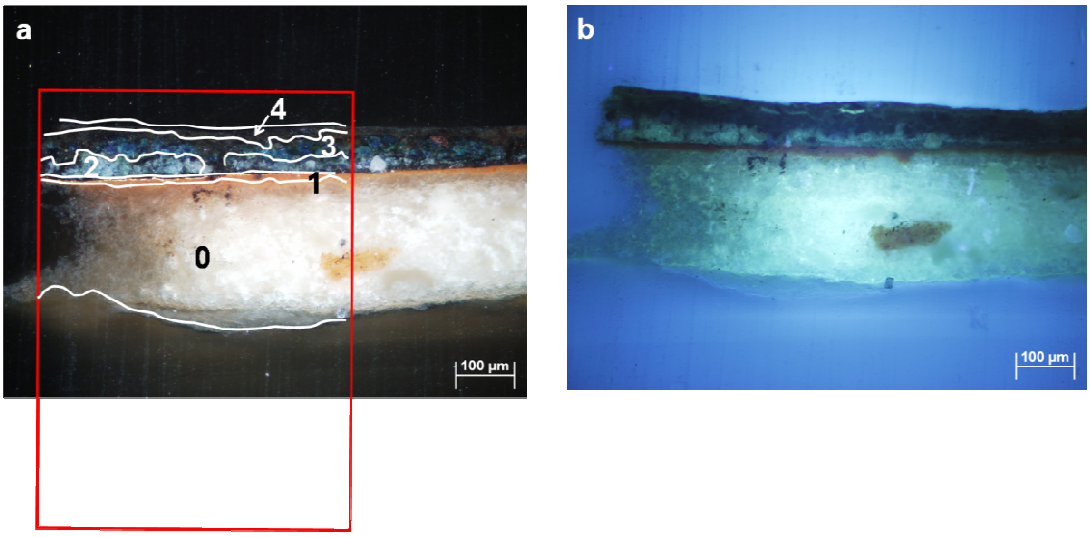

Figure 68 - Sample Fe2 cross-section photomicrographs (original magnification 200 x): a) visible microscopic image and b) UV light microscopic image. The red box indicated the selected area for the macro ATR imaging. Each layer is numbered with: 0 (ground), 1 (red gilding ground + gold leaf), 2 (light blue), 3 (deep blue) and 4 (thin external layer).

Macro ATR-FTIR imaging measurements have been performed and the whole data cube has been analysed in order to obtain chemical images for each identified painting material. In order to determine the area of the cross-section which was analysed, an FTIR image was also created for the polyester embedding resin integrating the 1253 cm^{-1} (νC-O) absorbance band (figure 69a). The integrated absorbance of the Si-O stretching band occurring between 1050 and 1000 cm^{-1} has been used to characterise a silicate based blue pigment (figure 69b). Azurite (a natural basic copper carbonate blue pigment)

has been defined by integrating the C=O bending at ca. 950 cm^{-1} (figure 69c). Finally a distribution plot of lead white (a lead basic carbonate), which has been already characterised by the authors in a previous work (Mazzeo, Joseph et al. 2007), has been obtained by integrating the C=O asymmetric stretching band between 1440 and 1340 cm^{-1}. The carbonate absorbance bands of lead white and azurite are overlapped, resulting in an inaccurate image for the localisation of lead white, which represent also the distribution of azurite (figure 69d). On the other hand, the integration of the amide II band at ca. 1530 cm^{-1} has been used to plot the distribution of a proteinaceous binder (figure 69e) which seems to be present in all painting layers. The spectra collected from the dark blue outer layer 3 are characterised by an carbonyl band at 1730 cm^{-1}, associated with triglycerides, suggested the use of egg tempera as binding medium (figure 69f). The same band is visible in the outermost layer 4 and a mixture of siccative oil and natural resin seems to have been used as varnish. To confirm this identification, a spectrum extracted from the red area in the layer 4 is also shown in figure 69g. However, the presence of lipidic substances cannot be ascertained due to the use of a polyester resin as an embedding system. Moreover, the thickness of the painting layers respect to the dimension of the imaging area does not permit to establish the exact localisation of the identified components between the different blue layers. We met some difficulties in identifying compounds present in the area of the sample under the gold leaf (red and white ground layers) and only the absorbance bands of water (used for contact) were present in the spectrum. It is probably due to material discontinuities within the different layers, which have been generated during the polishing procedure used for the cross-section preparation, resulting in a non perfect ATR crystal/surface contact. However, even if the interpretation of these ground layers has not been yet resolved this method could certainly be useful for other case studies. The polishing procedure could also be improved paying attention at using Micro-Mesh® polishing tissues with no abrasion fluid instead of water (van Loon, Keune et al. 2005).

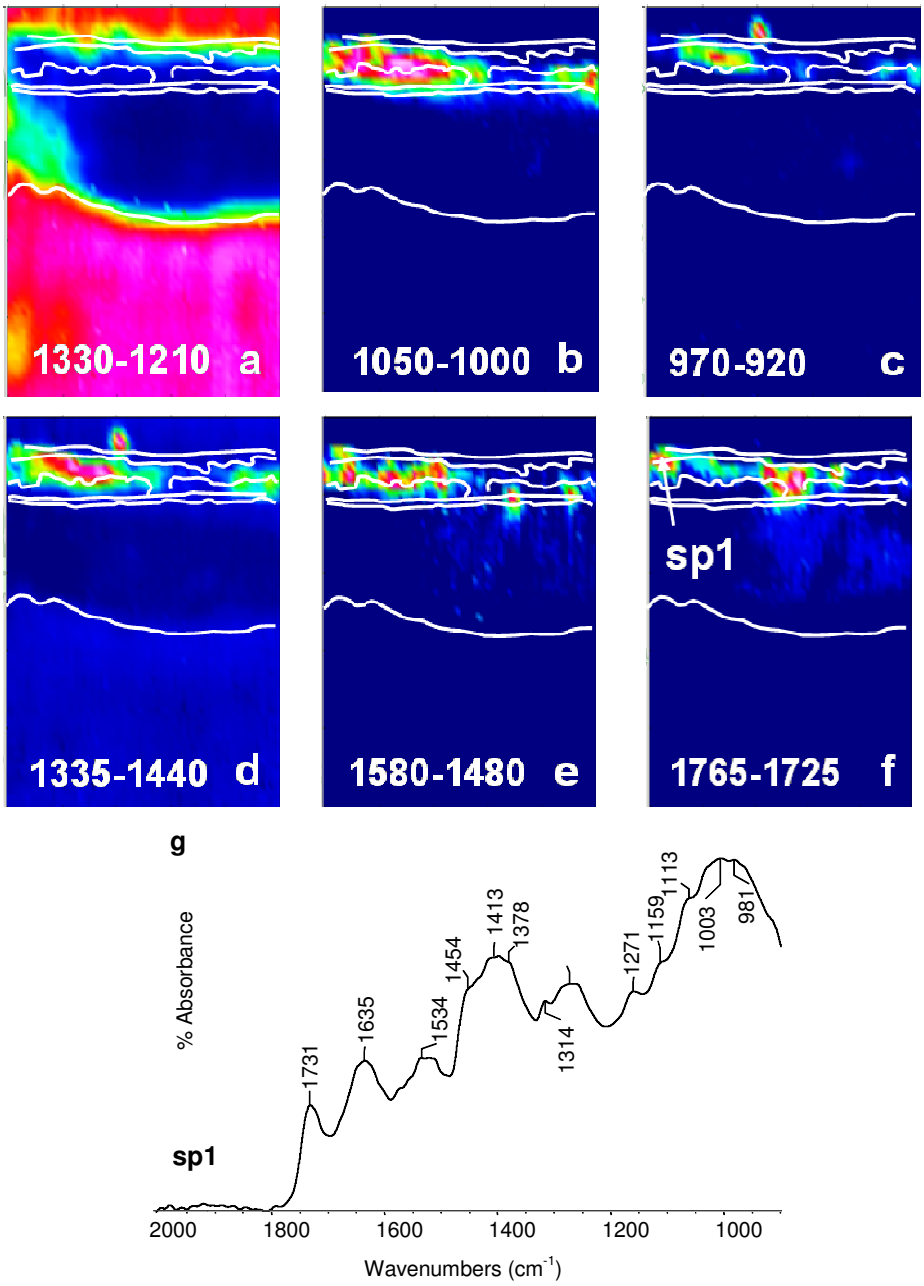

Figure 69 – a) FTIR image created by plotting the integrated absorbance of the embedding resin band between 1330 and 1200 cm^{-1}; b) FTIR image showing the distribution of the silicate integrated absorbance between 1050 and 1000 cm^{-1}; c) FTIR image showing the distribution of the azurite integrated absorbance between 970 and 920 cm^{-1}; d) FTIR image showing the distribution of the carbonate integrated absorbance between 1335 and 1440 cm^{-1}; e) FTIR image showing the distribution of the amide II integrated absorbance between 1580 and 1480 cm^{-1}; f) FTIR image showing the distribution of the triglerides integrated absorbance between 1765 and 1725 cm^{-1}; g) FTIR spectrum extracted from the right area of f, marked sp1.The size of the FTIR images is 770 × 550 μm^2.

III.2.3.b.2 *Red painted area from Italian terracotta altar-piece*

A complex stratigraphy is visible under the optical microscope observations of the sample MCR8, which is subdivided in nine layers as shown in figure 70. A white layer with red-orange inclusions (layer 8, thickness of 65-110 µm) is laid over a thin orange layer (layer 7, 20-50 µm thick) and a pink layer with white and red particles (layer 6, thickness ca. 60 µm). Below, a transparent brownish layer (layer 5, 15-35 µm thick) is applied over a light pink layer with bright red inclusions (layer 4, thickness of 15-40 µm) and a discontinuous thin transparent layer (numbered 3) is visible on the right part of the figure 70a. A transparent red layer (layer 2, 25-45 µm thick) is then superimposed to an dark orange layer (35-80 µm thick, layer 1) and a white layer with some orange particles (layer 0). Under UV illumination, the layers 3 and 5 showed a light blue fluorescence and in all others layers a bright fluorescence is evident (Figure 70b).

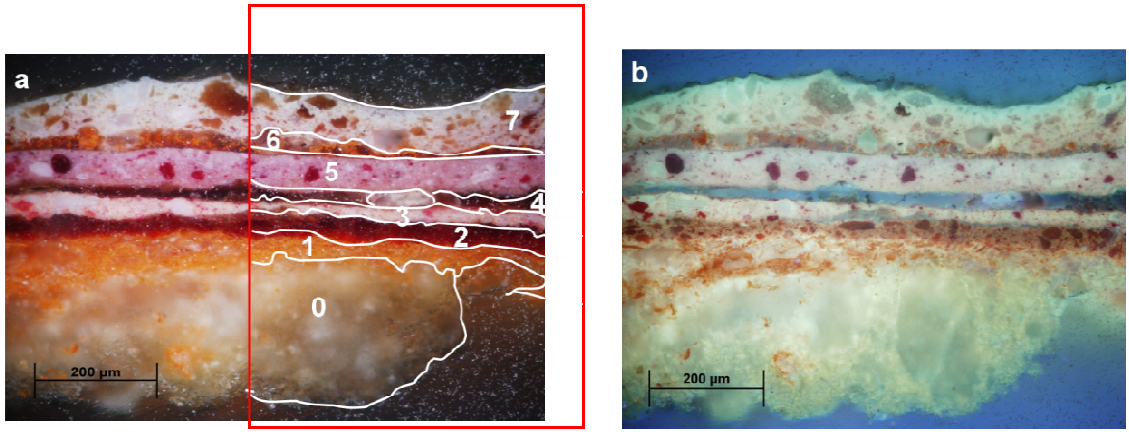

Figure 70 - Detail of a cross section from the terracotta altar-piece (MCR8): a) visible microscopic image; b) image of sample under ultraviolet light.

Macro ATR-FTIR imaging has been performed on the cross-section and the resulting chemical images are illustrated in figure 71. The distribution of the embedding resin has been plotted using the integration of the C-O stretching band at ca. 1235 cm^{-1} to evidence the area of the cross-section which was studied (Figure 71a). Several inorganic compounds have been identified and distribution plots were obtained integrating characteristic spectral bands for each component (Figure 71b-c): gypsum (SO_4^{2-} asymmetric stretching 1145-1110 cm^{-1}) and carbonates using the CO_3^{2-} asymmetric stretching 1440-1340

cm^{-1}. However, distinction between calcium and lead carbonate has not been possible since their asymmetric stretching principal bands are closed together and the bending ones (875 and 835 cm^{-1} respectively for calcite and lead white) are absent from the spectral region investigated (4000-900 cm^{-1}). More interesting is the localisation of organic substances. The integrated absorbance of amide II band at ca. 1530 cm^{-1} has been used to plot the distribution of a proteinaceous binding medium (Figure 71d). Although it is widely distributed among the different painting layers, the spectra collected from the outer layers 5-7 are characterised by an more intense amide II band than the amide I (1636 cm^{-1}) band. In the fingerprint profile showed by proteinaceous molecules, the intensity of the amide II band is lower than that of the amide I as shown from the spectra extracted from the inner layers 1-3 in figure 71f. Therefore this feature may suggest a contribution from metal carboxylates for the external layers 5-7. The distribution plot of triglycerides using the integrated absorbance of C=O ester asymmetric stretching 1760-1720 cm^{-1} shows also the presence of lipidic compounds in all layers numbered from 1 to 7, allowing the attribution to egg tempera as binding medium in these layers (Figure 71e).

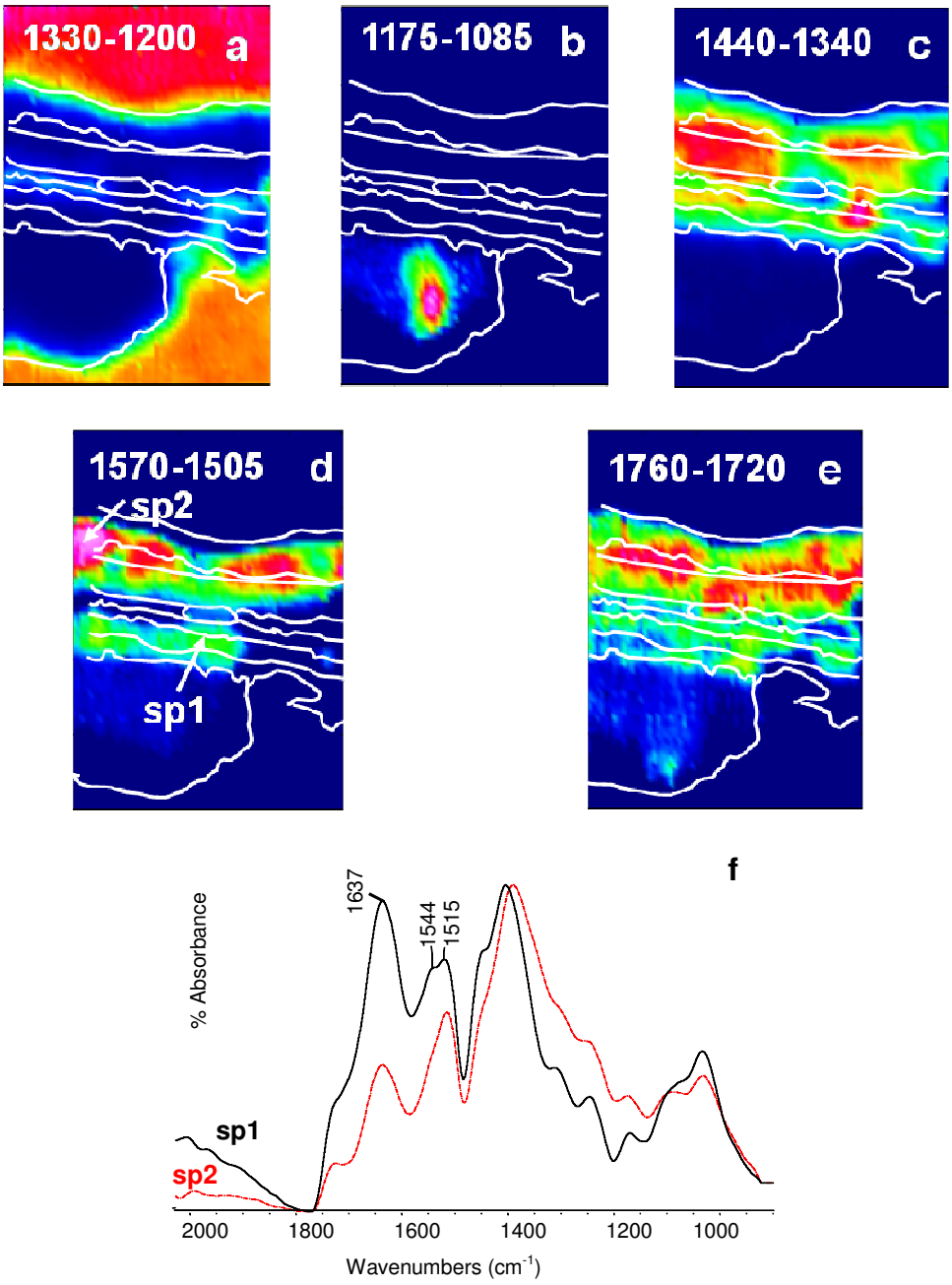

Figure 71 - FTIR images representing the integrated absorbance of a) the natural resin band between 1330 and 1200 cm^{-1}, b) the gypsum band between 1175 and 1085 cm^{-1}, c) the carbonate band between 1440 and 1340 cm^{-1}, d) the amide II band between 1570 and 1505 cm^{-1}, e) the fatty ester band between 1760 and 1720 cm^{-1}. F) FTIR spectra of different areas of d, extracted from the inner layers 1-3, marked sp1 and from the top layers 5-7, marked sp2.The size of the FTIR images is 770 × 550 μm^2.

III.2.4 Conclusions

This study highlights the possibility of performing macro ATR-FTIR spectroscopic imaging on paint cross sections for the characterisation and localisation of either inorganic compounds or organic substances present as painting materials. ATR measurements can be performed in an easy way and the only requirement is to achieve a good contact between the sample and the diamond crystal. In order to obtain contact uniformity, water has been successfully used on the cross sections embedded in polyester resin. In only few cases where the absorbance bands of water have been prominent in the spectrum, spectral subtraction has been employed. The study will be further extended to the use of chlorine solvents, such as carbon tetrachloride or tetrachloroethylene, which have no absorbance bands in the spectral region investigated (4000-900 cm^{-1}). Hence, the same procedure could also certainly be applied to cross sections embedded in KBr, transparent to mid-IR radiation. In fact the traditional embedding polyester resin does not allow the identification of the organic substances, in particular for those of lipidic nature with any certainty. Moreover in the spectral range of the FPA detector (4000-900 cm^{-1}), absorbance bands may overlap when different components have similar chemical features (functional groups) resulting in inaccurate images. In order to overcome these difficulties, further multivariate analyses are foreseen to extract images that represent the variables which are assumed to originate some underlying pattern in the data set, instead of the intensity of single absorbance bands.

However, the method presented is a fast qualitative analysis which can be performed without the use of an infrared microscope and can represent the first non-invasive step of an analytical approach including further elemental and molecular analyses. These first promising results open up future applications, also dealing with other conservation issues, such as the corrosion behaviour of metallic objects and the characterisation of the corrosion products present.

III.2.5 Acknowledgements

This research has been partially carried out with the support of the European Union, within the VI Framework Programme (Contract: EU-ARTECH, RII3-CT-2004-506171). The ATR imaging results have been obtained during a short research period in the laboratory of Prof. S. Kazarian (Imperial College of London, UK). Dr. C. Ricci is thanked for assistance with FTIR imaging spectrometer. The authors gratefully acknowledge Dr. M. Ioele (Instituto Superiore per la Conservazione e il Restauro, Rome, It) for providing the sample of gilt leather CD and permitting the presentation of the results in this thesis.

III.3 Comparison studies of mapping, imaging and synchrotron techniques

Different FTIR microspectroscopic techniques in attenuated total reflection (ATR) mode, using single-element mercury-cadmium-telluride (MCT) detector (mapping), focal plane array (FPA) detector (imaging) or multi-element MCT detector (raster scanning), are compared together for the characterisation of inorganic compounds and organic substances in paint cross sections. As the embedding resin may interfere in the FTIR spectra, all measurements have been performed on paint cross sections embedded in potassium bromide, a transparent salt in the mid-infrared region, in order to better identify the organic materials. Mapping system combined with a synchrotron source, which has been used on a compressed paint sample in a diamond anvil cell, is also included as it offers sample free of any contamination. The limitations and advantages of the different FTIR analytical tools are illustrated in terms of spatial resolution achieved, data quality (signal-to-noise ratio S/N) and chemical information obtained. In particular, this chapter highlights the recent introduction of multi-element detector, which may represent a good compromise between mapping and imaging systems.

III.3.1 Introduction

For the characterisation of the paintings materials, FTIR microscopy have been widely applied as one of the few techniques providing spatially chemical information about both inorganic and organic compounds as well as their degradation products. In particular, different detectors have been developed for a systematic and large data collection: single-element mercury-cadmium-telluride (MCT) detector (mapping), focal plane array (FPA) detector (imaging) or multi-element MCT detector (raster scanning) (Bhargava and Levin 2007). On a selected sample area, specific spectral information can thus be obtained as distribution plots using the intensities of characteristic absorption bands against their spatial position (Treado and Morris 1993; Krishnan, Powell et al. 1995).

The mapping system involves sequential data collection with the selection of the investigated area through adjustable apertures. In order to allow a sufficient radiation throughput, the aperture dimensions and the related spatial resolution cannot be lower than 10 x 10 μm^2. A redundant aperture minimizes the diffraction effects, but may also result in less spectral quality than a single aperture. However, higher spatial resolution down to ~ 5 µm and high spectral quality can be obtained using ATR mode, with the crystal acting as beam condenser (Lewis and Sommer 2000) or coupling the FTIR microscope with a synchrotron (SR) source (Reffner, Martoglio et al. 1995b; Dumas and Miller 2003). Moreover, overlapping between two adjacent sampling areas during data collection allows further increasing the spatial resolution (Harthcock and Atkin 1988b; Krishnan, Powell et al. 1995; Bhargava, Wall et al. 2000). The main drawback of mapping system is the acquisition time required of the order of hours, which may, however, not be relevant dealing within rare cultural heritage samples.

Recently, linear array detectors have been developed combining together several mercury cadmium telluride (MCT) detectors. As for mapping, this system, so-called raster scanning, analyses sequentially large sample areas but has an acquisition time reduced by a factor of *m*, corresponding to the number of detector elements. The individual elements are 25 µm in size and thus permit to obtain spectra with a good spectral quality (Levin and Bhargava 2005; Bhargava and Levin 2007). Respect to mapping system, where geometrical apertures are used, the spatial resolution is here determined by the system's optics. In transmission or reflection mode, the achieved resolution of 25 µm can be reduced to 6.25 µm using optical zoom of 4x magnification. In ATR mode, due to the magnification factor of the germanium crystal, the operative spatial resolution is ~ 6 µm.

On the contrary, FTIR imaging consists of a simultaneous and therefore faster data collection, which makes use of a multichannel detector where small pixels of about 6 µm are distributed over a grid pattern (FPA, focal plane array) (Ebizuka, Wakaki et al. 1995; Lewis, Treado et al. 1995; Burka and Curbelo 2000). In this system, the spatial resolution is related to the pixel dimension, but unfortunately this means also a poor spectral quality (low S/N), as the received photons quantity is subdivided in the various pixels and is thus inversely

proportional to the number of pixels. Nevertheless, the ATR configuration can provide increased lateral resolution of approximately 5 µm compared to transmission or reflection imaging (Sommer, Tisinger et al. 2001; Chan and Kazarian 2003; Chan, Kazarian et al. 2005).

FTIR spectra obtained with reflectance measurements show a rather poor quality and may be difficult to interpret. In consequence, very few publications have been reported for the study of paint cross sections (Bruni, Cariati et al. 1999; van der Weerd, Brammer et al. 2002). In contrast, transmission mode offers a higher spectral quality but the sample preparation for a multilayered paint fragment requires, for example, thin sections which are quite arduous to obtain by microtoming or polishing (Derrick, Stulik et al. 1999; Zieba-Palus 1999; van der Weerd, Heeren et al. 2004). Therefore only methods, such as ATR or diamond anvil cell, which allow the analysis of such samples but with an easiest preparation (embedded cross section or squeezing respectively), will be evaluated in this chapter. In fact, the use of compression cell for studying organic materials is preferred to microtoming as it avoids the contamination of the embedding resin in the FTIR spectra.

Hence, ATR mapping, raster scanning and imaging systems with conventional sources are compared with transmission mapping system available with a synchrotron radiation at European Synchrotron Radiation Facility (ESRF). In particular, limitations and advantages of each FTIR technique are presented for the characterisation of thin organic layers in paint cross sections. An alternative embedded system in potassium bromide has been used in order to avoid the interference of the embedding resin in the FTIR spectra, as demonstrated elsewhere (van der Weerd, Heeren et al. 2004; Mazzeo, Joseph et al. 2007).

III.3.2 Experimental methods

III.3.2.a *Paint samples*

All paint fragments have been taken from the blue angel's wing (sample MCR13) of Mattia della Robbia's terracotta altarpiece "*Assumption of Virgin between S. Sebastian and S. Rocco*" (1527-1532 A.D.) located in the collegiate

church of S. Maria Assunta in Montecassiano (Macerata, Italy). After careful observation under a binocular stereo microscope Leica MZ6, a paint fragment has been embedded in potassium bromide (KBr) and polished using aluminium oxide Micro-Mesh® polishing cloths up to the finest mesh (12000), following the procedures illustrated in chapter III-1. This cross section has been used for optical microscopy, FTIR microscopy with conventional source and single-element or multichannel detectors. Another paint fragment has been squeezed in a diamond anvil cell and analysed with a FTIR microscope and a synchrotron light source, available at ESRF. In order to better illustrate the advantages and limitations of each FTIR technique presented, two additional examples are developed hereafter: an angel's halo of the Universal Judgement (sample 3L) from the frescoes painted by Giotto in 1305 A.D. and located in the Scrovegni chapel (Padua, Italy) and the Madonna's halo of the "*Virgin and Child with Saints* ", a XV century easel painting attributed to Rondinelli (sample ROND13), both embedded in potassium bromide and analysed respectively with ATR and SR transmission microspectroscopic mapping.

III.3.2.b *Optical microscopy*

Dark field observations of cross-sectioned samples have been performed using an optical microscope Olympus BX51M equipped with fixed oculars of 10x and objectives with different magnifications (5, 10, 20, 50 and 100x). Visible and ultraviolet light have been respectively provided by a 100W halogen projection lamp and an Ushio Electric USH102D lamp. Cross sections' photomicrographs have been recorded with a digital scanner camera Olympus DP70 directly connected to the microscope.

III.3.2.c *SEM-EDX microscopy*

A scanning electron microscope, Philips XL 20 model SEM-EDX equipped with an energy dispersive X-ray analyzer was used on the cross-sectioned samples. The elemental composition was carried out at an acceleration voltage of 25-30 keV, lifetime>50sec, CPS ≈2000 and working distance 34mm. EDX-4 software

equipped with a ZAF correction procedure for bulk specimens was used for semi-quantitative analyses of X-ray intensities.

III.3.2.d *FTIR microscopy*

For all configurations, the chemical images have been obtained as false-colour distribution plots using the integrated absorbance of a characteristic spectral band for each chemical compound present. A colour scale from high value (red) to low value (blue) is employed.

III.3.2.d.1 *Mapping with single-element detector*

Globar source at M2ADL

A Thermo-Nicolet Nexus 5700 spectrometer has been used coupled to a Nicolet Continuμm IR microscope fitted with an MCT detector cooled by liquid nitrogen and a 15x Thermo-Electron Infinity Reflachromat objective with a tube factor of 10x. ATR spectra have been acquired in the range 4000–650 cm^{-1}, at a spectral resolution of 4 cm^{-1}, using a slide-on ATR objective with a hemispherical silicon crystal. A total of 64 scans have been recorded and the resulting interferogram averaged. For ATR mapping on a selected area (120 x 230 μm^2) of sample MCR13, a step size of 20 μm in x direction and 10 μm in y direction has been chosen with an aperture of 100 μm x 100 μm, relative to an investigated area of ~ 29 x 29 μm^2 in ATR mode. Data collection and post-run processing were carried out using Nicolet Omnic-Atlμs software.

A Nicolet iN™10MX imaging microscope, fitted with an MCT detector cooled by liquid nitrogen, has also been used in order to perform ATR mapping. The measurements have been performed using a slide-on ATR objective with a conical germanium crystal, in the range 4000–680 cm^{-1}, at a spectral resolution of 4 cm^{-1} and with 16 scans. The selected areas (30 x 120 μm^2 for sample MCR13 and 36 x 126 μm^2 for sample 3L) have been mapped with an aperture of 20 μm x 20 μm and a step size of 3 μm results in a investigated area of 5 x 5 μm^2. Data collection and post-run processing were carried out using Nicolet Omnic-Atlμs software.

Synchrotron source at ESRF

FTIR microscopy has been performed on the ID21-infrared end station, at the ESRF (*http://www.esrf.eu/UsersAndScience/Experiments/Imaging/ID21*). The instrument is a Nexus spectrometer coupled with a Nicolet Continuμm IR microscope. Transmission spectra are made of an average of 50 scans acquired in the range 4000–700 cm^{-1} with a spectral resolution set to 4 cm^{-1}. The map areas (145 x 200 μm^2 for sample MCR13 and 248 x 200 μm^2 for sample ROND13) have been acquired with beam spot from 8 x 8 to 5 x 5 μm^2 and step size from 8 to 5 respectively. Working in the conditions does not maintain the beam flux constant over the all infrared domain (4000-650 cm^{-1}) and the spectra have therefore low spectral quality under 800 cm^{-1}. Data collection and post-run processing were carried out using Nicolet Omnic-Atlμs software.

III.3.2.d.2 *Imaging with focal plan array detector*

A FPA detector (Santa Barbara, USA) comprising 16384 small pixels arranged in a 128 x 128 grid format has been used to measure FT-IR images with a spectrometer operating in continuous scan mode. Spectra have been collected with 8 cm^{-1} spectral resolution in the range 3800–900 cm^{-1} using 128 scans. In the micro ATR configuration, the spectrometer and the FPA detector are coupled with an infrared microscope with a 20X cassegrainian objective and a Ge ATR objective. The imaging ATR spectrometer is patented by Varian (Burka and Curbelo 2000). In the optical arrangement used, the spatial resolution is approximately 5 μm (Chan, Kazarian et al. 2005; Chan and Kazarian 2007; Ricci, Bloxham et al. 2007). The size of the images obtained with the microATR objective is 63 x 63 μm^2. Data collection and post-run processing were carried out using Bruker Opus software.

III.3.2.d.3 *Raster scanning with linear array detector*

A Nicolet iN™10MX imaging microscope, fitted with an 16-element MCT detector array cooled by liquid nitrogen, has been used with a slide-on ATR objective euipped with a conical germanium crystal. In this configuration, the spatial resolution is 6.25 µm. ATR measurements have been performed on a selected area (225 x 130 μm^2) with 8 scans, at a spectral resolution of 4 cm^{-1}, in the range 4000–720 cm^{-1}. Data collection and post-run processing were carried out using Nicolet Omnic-Atlµs software.

III.3.3 Comparative studies of a paint fragment

III.3.3.a *ATR mapping on a embedded cross section*

III.3.3.a.1 *ATR mapping with FTIR microscope Continuµm*

The KBr cross section of MCR13 presents a clear overview of the stratigraphy (figure 72a). A light blue paint layer (layer 5, 20-50 µm thick), composed of a mixture of white pigment with some blue particles, and a white one (layer 4, 30 µm thick) are superimposed to a gold leaf (layer 2), under which a brownish gilding mordant (layer 1, 4-14 µm thick) and a white ground (layer 0, 20-60 µm thick) are visible. A thin dark layer (layer 3), which is probably deposition materials, can also be observed over the gold leaf and suggests that the angel's wing has been originally gilt and later on repainted with a light blue paint layer. Under UV illumination, the white ground and the repainted layers are characterised by a strong bright yellow fluorescence while the gilding mordant shows just a pale bluish one (figure 72b). It is worth mentioning that the KBr embedding system also leads to a better documentation of the fluorescence effects if compared with the conventional embedding into a synthetic polymer, which also generates fluorescence phenomenon under ultraviolet illumination. Furthermore, a detachment between the organic mordant and the lower white paint layer has been highlighted in the SE image (figure 72c) referred as a blue box in the visible image (figure 72a). Even if the reasons of such detachment are unknown, this feature can outline a different physical behaviour for the

gilding mordant and the underneath binding material, which should be linked to different chemical compositions.

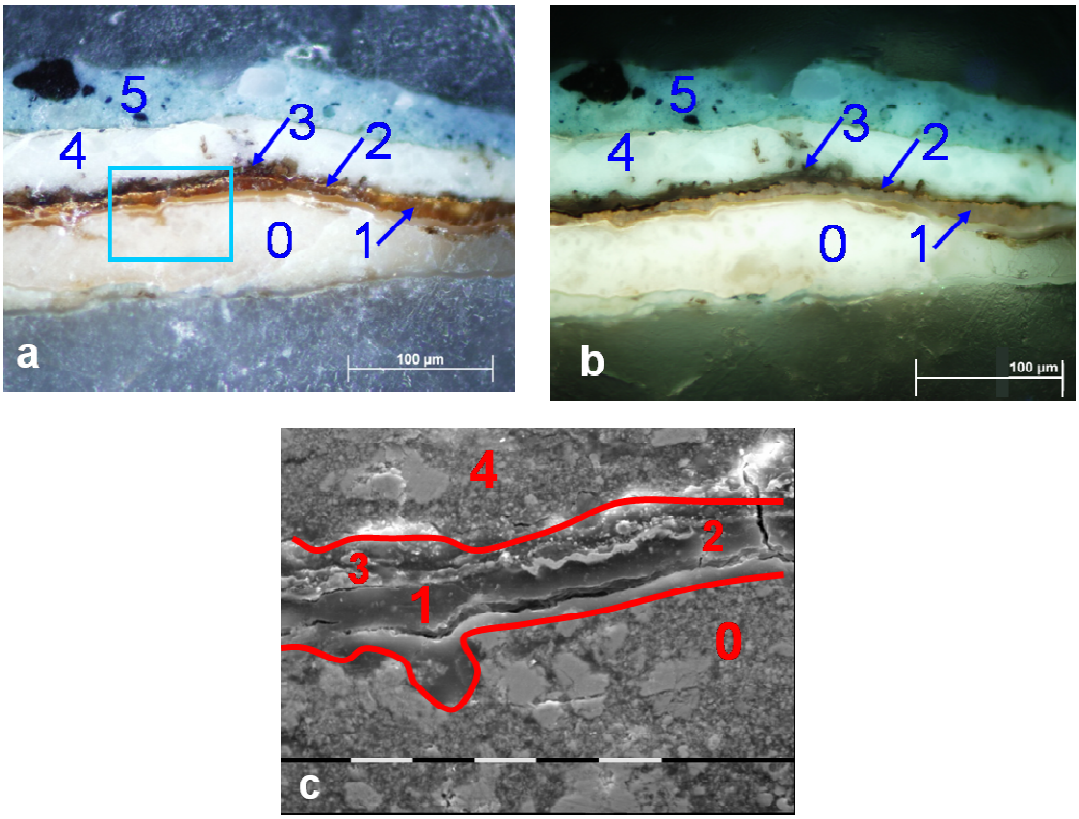

Figure 72 - Cross-section photomicrographs of sample MCR13 embedded in KBr: a) visible light microscopic image: the blue box indicated the selected area for the SEM-EDX analysis. b) UV light microscopic image; c) SE image (original magnification 1600x): the detachment occurring between the white ground layer (0) and the gold leaf (2) is visible.

Micro-ATR mapping measurements have been carried out on a representative area of the sample (120 × 230 µm^2) indicated with a red box in figure 73a, using a conventional source with a microscope Nicolet Continuµm (Figure 73). Lead white (basic lead carbonate $2PbCO_3 \cdot Pb(OH)_2$) has been localised in both white layers 0 and 4 and in the light blue layer 5, integrating the CO_3^{2-} in-plane bending band at 679 cm^{-1} (Figure 73b). A similar profile has been obtained with the OH stretching band at 3530 cm^{-1}, typical of basic lead carbonate (Figure 73c). In particular, the white layer 0 is enriched in cerusite (lead carbonate) as it can be appreciated integrating the CO_3^{2-} out-of-plane bending band at 839 cm^{-1} (Figure 73d). A different source for the two white pigments can explain this feature and may be correlated to a past intervention of repaint. The fine dark

blue particles probably result from indigo, an organic pigment which has a strong hiding power and therefore requires few quantity of pigment to obtain the wanted tonality. Thus, its detection is difficult in presence of highly absorbant inorganic compounds, such as lead carbonate. Moreover, gypsum (SO_4^{2-} asymmetric stretching, 1112 cm^{-1}), which could represent the dark layer 3 as deposition material, is not precisely located in this layer but its distribution plot seems also incorporate the mordant layer 1 (Figure 73e). On the other hand, the characterisation of the different binding media has been successfully achieved. In fact, the distribution of a lipidic binder has been obtained in the repainted layers and in the white ground, using the ester C=O stretching band at 1732 cm^{-1} (Figure 73f). Integrating the amide I absorbance band at 1638 cm^{-1}, proteinaceous material has been observed in the thin mordant layer 1 but also in the thin dark layer 3 over the gold leaf (Figure 73g). Unfortunately, oxalates have also absorbance bands in the same region and therefore the distribution plot at 1638 cm^{-1} is not specific for protein. In fact, the presence of oxalates has been confirmed in the central layer 1 and 3 but also in layer 4, integrating the characteristic O-C-O stretching band at 1319 cm^{-1}, as shown by the resulting map in figure 73h. The same overlapping occurs between carboxylates and amide II band in 1600-1550 cm^{-1} region. Nevertheless, the presence proteinaceous material has been confirmed in both layers 1 and 3 performing a correlation map with a reference spectrum of glue (Figure 73i). The same profile has been achieved for silicates (correlation map with bole) and their presence as deposition material and/or inert material added to give bulk to the mordant layer 1 is not clear since they are localised in both the dark layer 2 and mordant layer 1 (Figure 73j). In fact for gilding mordant, ancient treatises mention either the use of mixture of siccative oil and natural resins or a glue size mixed with red bole (a natural ferruginous aluminium silicate red pigment). The presence of siccative oil in the white ground under the mordant seems to be in accordance with the hypothesis that the detachment has occurred between them due to their differences in chemical composition and response to physical stresses. One of the main drawbacks of working in ATR with a hemispherical crystal is problems of contact arising from a non perfectly planar surface and the preparation of KBr cross section should thus be carefully

achieved, paying attention to apply a gentle and constant pressure during the polishing procedures.

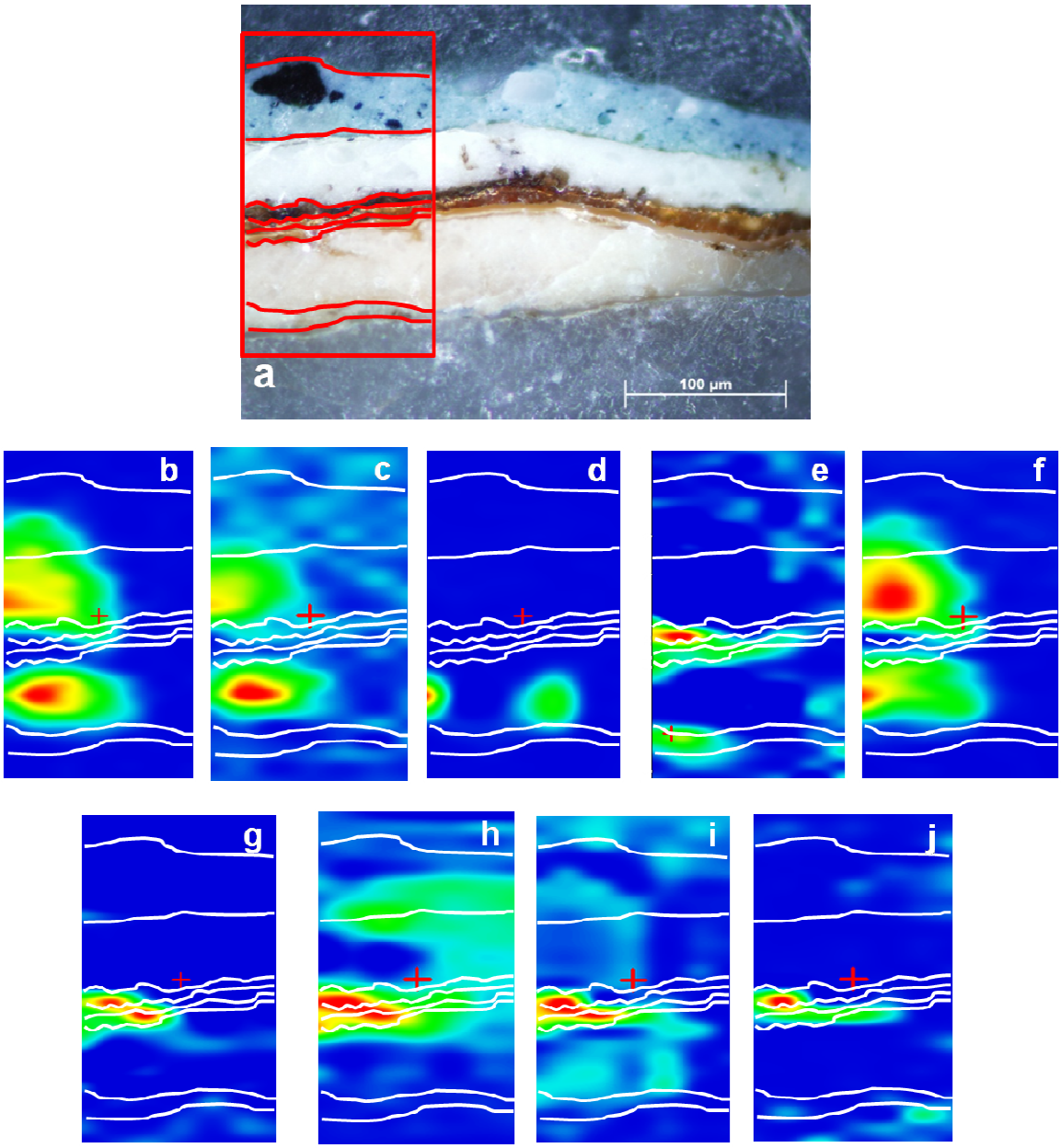

Figure 73 - a) visible light microscopic image of sample MCR13 embedded in KBr: the red box indicated the selected area for the ATR mapping. FTIR false colours plots representing b) lead white (peak area 679 cm^{-1}), c) lead white (peak area 3530 cm^{-1}), d) cerusite (peak area 839 cm^{-1}), e) gypsum (peak area 1112 cm^{-1}), f) siccative oil (peak area 1732 cm^{-1}), g) amide I (peak area 1638 cm^{-1}), h) oxalates (peak area 1319 cm^{-1}), i) proteinaceous material (correlation map with a reference spectrum of glue) and j) silicates (correlation map with a reference spectrum of bole).

III.3.3.a.2 *ATR mapping with FTIR microscope iN10X*

MCR13 KBr cross section

The same KBr cross section has been submitted to micro-ATR mapping measurements on a newly developed system in which a spectrometer is integrated to a FTIR microscope in a unique instrumentation. The chemical maps obtained from an area of 30 × 120 μm^2 and shown in figure 74, are rather consistent with the results obtained on the microscope Nicolet Continuμm. The distribution of lead white has been observed in layers 0, 4 and 5 by plotting the integrated absorbance value of the CO_3^{2-} asymmetric stretching band at 1395 cm^{-1} (Figure 74b). In the same layers, the presence of lipids has been localised using the ester C=O stretching mode absorption band at 1734 cm^{-1} (Figure 74c). In the same manner as for ATR mapping performed with the conventional FTIR microscope, cerusite has been individuated only in the white layer 0 (Figure 74d). On the contrary, gypsum (SO_4^{2-} stretching, 1111 cm^{-1}) has been here identified and precisely localised in the thin dark layer 3, validating its presence as deposition material (Figure 74e). Figure 74f has been obtained plotting the 1636 cm^{-1} band, which represents, as stated above, the proteinaceous material and oxalates. In fact, a similar chemical map has been obtained for only oxalates using the characteristic O-C-O stretching band at 1319 cm^{-1} (Figure 74g). Moreover carboxylates absorb also in the same region as amide II and therefore the 1550 cm^{-1} band cannot be used too. Fortunately, the location of proteinaceous material has been accurately assigned to the thin mordant layer 1 using other methods such as correlation map or multivariate curve resolution (MCR). First, a correlation map has been achieved between the reference spectrum of glue and the complete data set of the recorded FTIR spectra. Its presence has only been individuated in the FTIR spectra corresponding to the layer 1 as illustrated in figure 74h. Elaborating a correlation map with bole, the same distribution plot is obtained for silicates (Figure 74i). Moreover, MCR has pointed out the presence of a layer 7-12 μm thick, as it is possible to appreciate in figure 75. The corresponding loading shows the presence of two intense bands at 1623 cm^{-1} and 1550 cm^{-1}, which are ascribable to proteinaceous material. In particular, the amide II band

presents a sharp profile indicating the contemporary presence of carboxylates. Characteristic bands for oxalates and silicates are also visible. Respect to ATR mapping with conventional FTIR microscope, the chemical information obtained in this case is substantially the same. However, the chemical maps are more accurate and, in particular the presence of proteinaceous material and silicates is confined to the thin mordant layer, while gypsum appears as deposition material in the above dark layer.

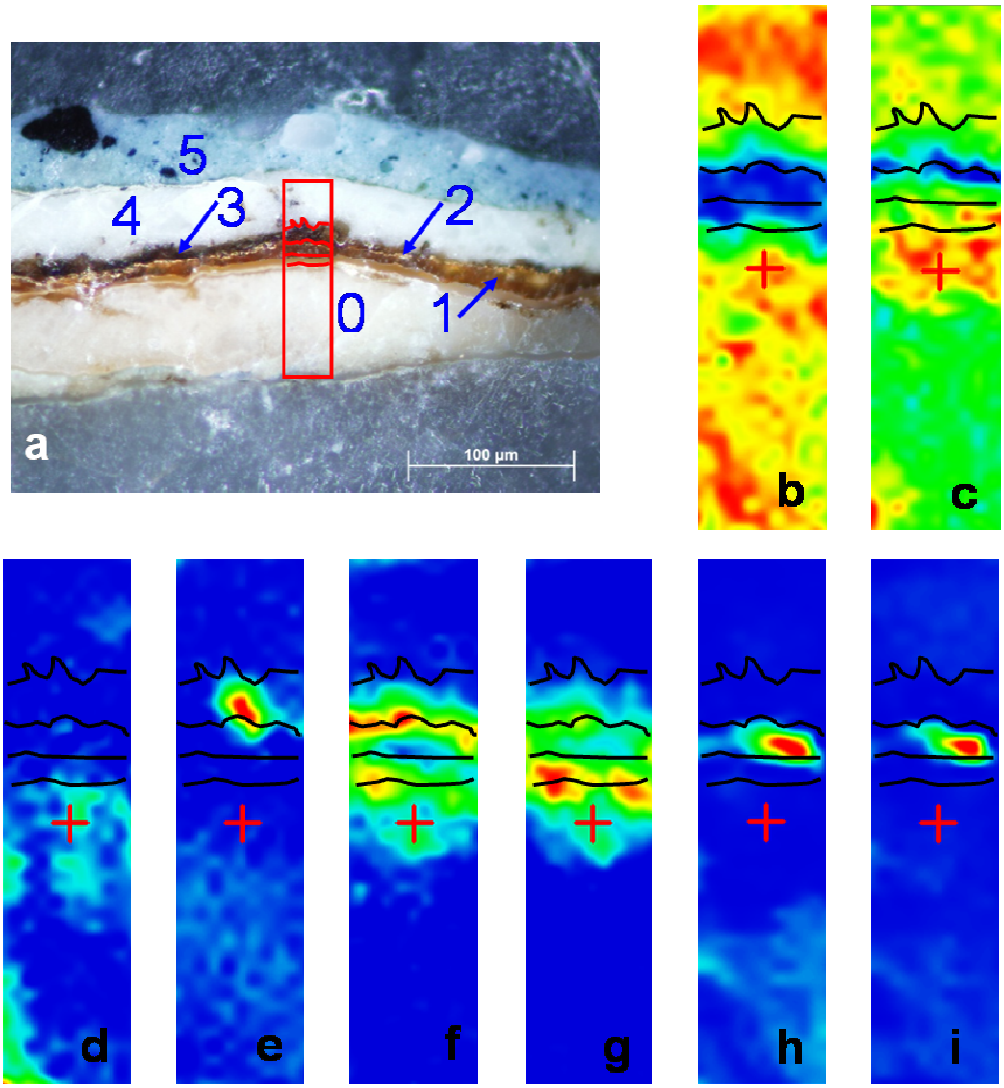

Figure 74 - a) visible light microscopic image of sample MCR13 embedded in KBr: the red box indicated the selected area for the ATR mapping. FTIR false colours plots representing b) lead white (peak area 1395 cm^{-1}), c) siccative oil (peak area 1734 cm^{-1}), d) cerusite (peak area 839 cm^{-1}), e) gypsum (peak area 1111 cm^{-1}), f) amide I (peak area 1636 cm^{-1}), g) oxalates (peak area 1319 cm^{-1}), h) proteinaceous material (correlation map with a reference spectrum of glue) and i) silicates (correlation map with a reference spectrum of bole).

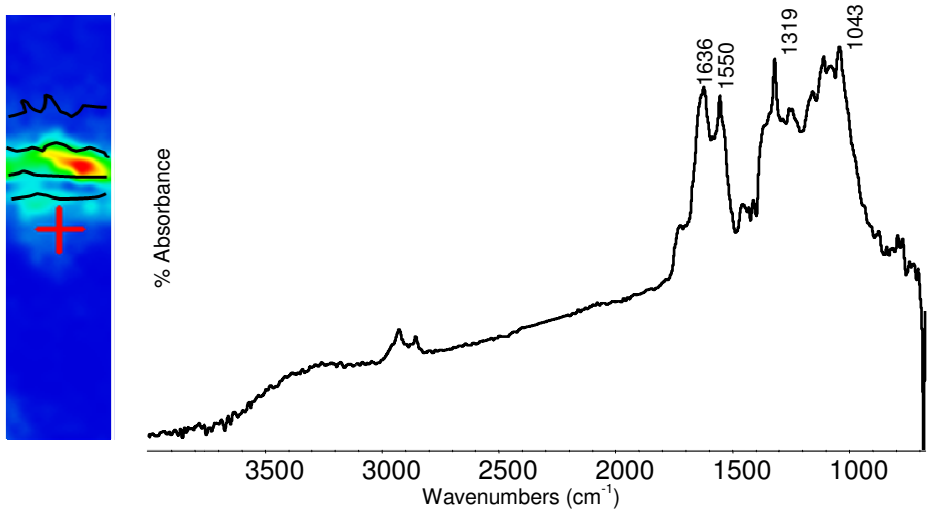

Figure 75 – Distribution plot and spectrum of one component obtained by MCR on the micro-ATR-FTIR mapping data of the sample MCR13 in the spectral region 4000-650 cm^{-1}.

3L KBr cross section

In order to help interpret and complement the ATR-FTIR mapping results, the 3L cross section has been first observed under optical microscope. The visible light and UV light images illustrated in figure 76 indicate that a golden tin technique has been adopted. Despite different definitions of *stagno dorato* (golden tin) are reported (Thompson Jr 1954; Tintori 1982), the case present here is a fine real gold foil laminated with tin instead of a tin foil tinted with a golden varnish, commonly used as a cheap substitute for gold. A gold leaf (layer 3) has been applied over a tin leaf (layer 1) with a thin mordant gilding (layer 2, 3-5 µm thick), which appears fluorescent in the UV light image (figure 76b). The tin foil itself is fixed to the mural by means of another mordant layer (layer 0, 15-50 µm thick), with also shows a bright yellow fluorescence under UV illumination. The use of a golden tin technique has been confirmed by SEM-EDX elemental analyses performed of a similar fragment (sample 22L). Both tin and gold have been identified in the different metal leaves, appearing respectively grey and white in the BSE image (figure 76c) (Cesareo, Castellano et al. 2002; Cesareo, Castellano et al. 2004; Cesareo, Castellano et al. 2005; Marabelli, Santopadre et al. 2005).

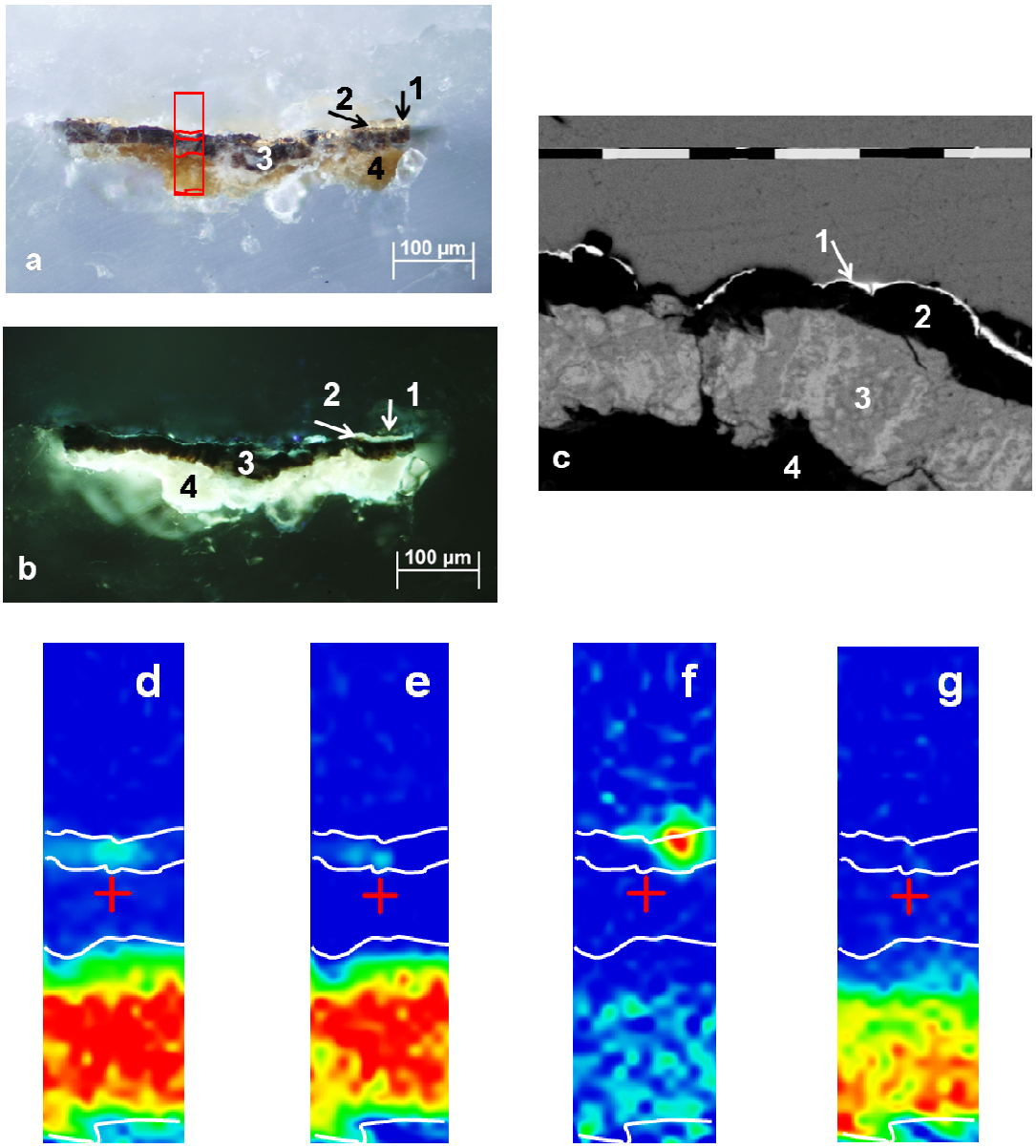

Figure 76 - Cross-section of sample 3L embedded in KBr: a) visible light microscopic image: the red box indicated the selected area for the ATR mapping; b) UV light microscopic image; c) BSE image (original magnification 1300x) of sample 22L with a similar structure: the different layers are numbered from 1 to 4: gold leaf (1), gold mordant layer (2), tin leaf (3) and tin mordant layer 4. FTIR false colours plots representing d) aliphatics CH (region of interest 2990 - 2830 cm^{-1}), e) fatty acids (peak area 1707 cm^{-1}), f) oxalates (peak area 1320 cm^{-1}) and g) carboxylates (peak area 1555 cm^{-1}).

ATR-FTIR mapping has been performed directly on the KBr cross-section on a representative area (36 x 126 μm^2) marked with a red box in figure 76a. As illustrated in figure 76d, the resulting image obtained plotting the intensity of the CH aliphatic stretching absorbance bands between 2990 and 2830 cm^{-1} has allowed localising the different organic substances. The distribution plot of the

acid C=O asymmetric stretching band at 1707 cm^{-1} (figure 76e) and the FTIR spectra extracted from the different areas have suggested the presence of a mixture of siccative oil with natural resin in both the gold mordant and tin mordant layers (layers 2 and 0 respectively). Calcium oxalates, which may be derived by organic compounds' degradation, have been also identified in the different organic layers integrating the O-C-O stretching band at 1320 cm^{-1} (Figure 76f). The distribution of carboxylates as degradation products has been also plotted using the integrated asymmetric COO^- stretching absorbance at ca. 1555 cm^{-1} (Figure 76g) and coincided with the inner tin mordant layer. It is worth saying that this sample has been also analysed with ATR microscopic mapping and imaging systems but without the thin mordant layer of 5 µm being determined. In fact, as the optical path length between source and objective is reduced, the integrated system iN10X benefits from higher energy output and permits working with lower apertures (20 x 20 $µm^2$), which therefore result in a better spatial resolution. Higher quality FTIR spectra are also obtained with a better signal-to noise ratio or with a reduced acquisition time (16 scans).

III.3.3.b *Synchrotron (SR) Transmission mapping on a fragment*

MCR13 KBr cross section

A first attempt has been achieved to perform the analyses in attenuated total reflectance (ATR) mode on the sample embedded in potassium bromide (KBr) and prepared in cross-sections. However, after adjustment of the beam alignment with the ATR objective, the measurements did not succeeded due to energy's loss as soon as a contact was established with the sample's surface. In fact, the achieved pressure, even is low, may slightly change the position of the ATR objective of few micrometers, resulting in a beam out of focus. Therefore, the analyses have been performed in transmission with beam spot of ~5×5 $µm^2$ and step size of 5 µm in order to keep a high spatial resolution. After careful positioning on a diamond window following by pressing into a micro-compression cell, the stratigraphy of sample MCR13 is obviously damaged (Figures 77ab). However, as for the embedding in KBr, a better characterization of the organic substances will be allowed thanks to the absence of the

embedding resin contribution in the FTIR spectra. On the other hand with this setting, the beam flux decreases in the low wavenumbers region and so the useful infrared domain is from 4000 to 800 cm^{-1}. Either inorganic compounds and organic subtances have been characterised and localised within the stratigraphy through the use of 2D-mapping on a selected area (145 x 200 μm^2) (Figures 77b-e). In the white layers (layers 0 and 4), lead white has been identified using the carbonate asymmetric stretching band at 1424 cm^{-1}. In the central layers (mordant layer 1 and dark deposits layer 3), either gypsum (OH stretching, 3534cm^{-1}), silicates (Si-O stretching, 1100-1000 cm^{-1}) and oxalates (O-C-O stretching, 1324 cm^{-1}) has been individuated, as shown in figure 77d, 77e and 77f respectively. In this case, one of the major drawbacks is the difficulties in recognizing after squeezing the thin mordant layer 1 and the dark one above the gold leaf, which are closed together. Regarding the organic substances, the distribution of a siccative oil is obtained in layers 0 and 4 plotting the esters C=O asymmetric band at 1734 cm^{-1} (figure 77g). For the same reasons as exposed before, the distribution plots of the 1652 and 1546 cm^{-1} bands correspond to both amide I and oxalates or amide II and carboxylates respectively and thus are not specific. Hence, the localisation of proteinaceous material has been elaborated using another specific region. In figure 77 h and 77i, we can observe how either a peak area map of amide I and amide II bands between 1700 and 1500 cm^{-1} and a correlation map with a reference spectrum of glue have positioned proteinaceous material in the central layers. Moreover, its presence in the only mordant layer 1, which has been ascertained with ATR mapping measurements, can not here be confirmed. On the other hand, the higher spatial resolution and brightness of SR sources available at ERSF have allowed us to perform the measurements with small apertures without losing any spectral quality. Hence, spectra have been obtained after 45 scans with a very high signal-to-noise ratio.

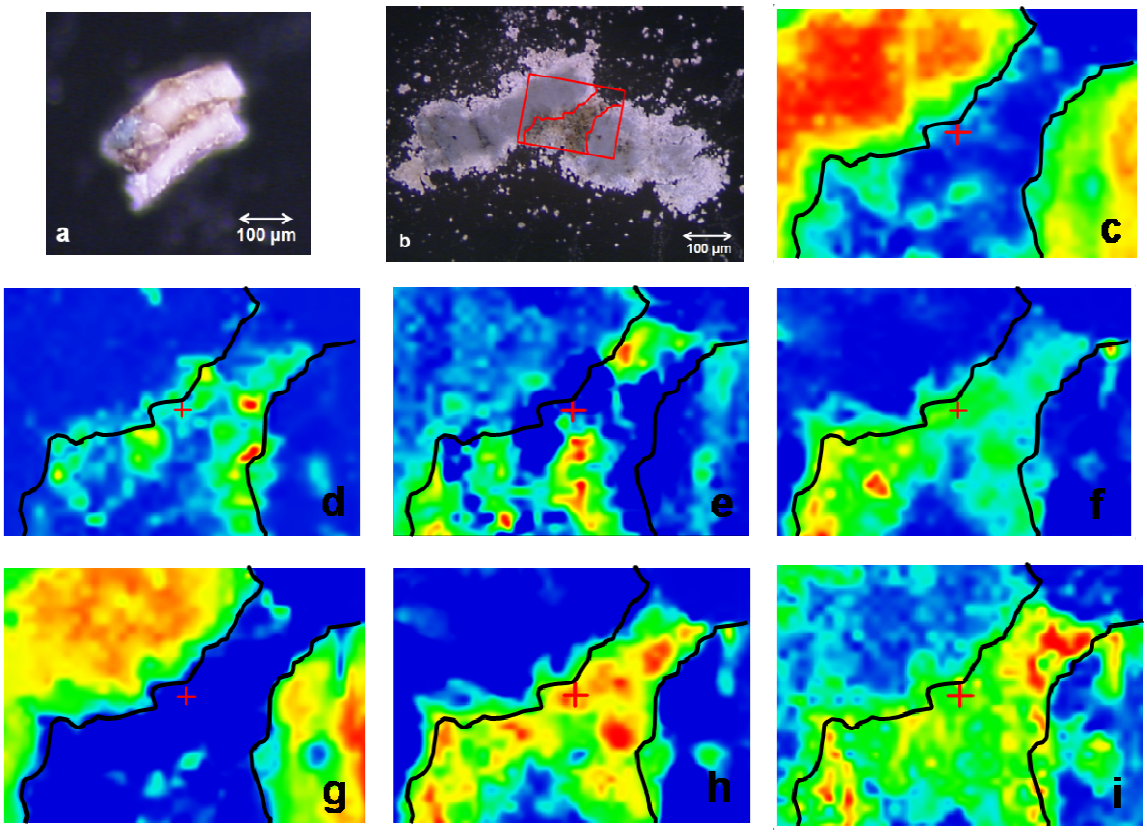

Figure 77 - a) visible light image of sample MCR13 before compression and b) after being pressed: the red box indicated the selected area for the ATR mapping; FTIR false colours plots representing c) lead white (peak area 1424 cm^{-1}), d) gypsum (peak area 3534 cm^{-1}), e) silicates (region of interest 1100 -1000 cm^{-1}), f) oxalates (peak area 1324 cm^{-1}), g) siccative oil (peak area 1734 cm^{-1}), h) amide I and II (region of interest 1700-1500 cm^{-1}), g) proteinaceous material (correlation map with areference spectrum of glue).

ROND13 KBr cross section

A second example (ROND13) with an external thin mordant layer (thickness of 10 µm) has been prepared in the same manner and a selected area (248 x 200 μm^2) analysed in transmission with a beam spot of 8 x 8 μm^2 and step size of 8 µm.

In order to better understand the stratigraphy under investigation, a similar fragment has previously been embedded in potassium bromide and observed in optical and SEM-EDX microscopy. When viewed under optical microscopy (figure 78a), a yellow mordant gilding (layer 3, 10-15 µm thick) has been applied to made adhering the gold leaf (2-3 µm thick). The mordant lies over two green paint layers: a light green paint layer (layer 2, ~30 µm thick) and a thin dark green layer (layer 1) with a thickness of about 15 µm, under which a grey

preparation layer (layer 0, ~30 µm thick) is visible. Under UV illumination (not shown), the mordant shows poor fluorescence whereas no fluorescence is visible for the green layer, suggesting the use of copper resinate (green glaze containing copper salts of resin acids) as further confirmed by EDX analyses which have highlighted the presence of copper.

For the FTIR measurements on the pressed fragment, the red box in figure 78b indicates the area where synchrotron transmission measurements have been carried out. Regarding the mordant layer, figure 78d shows the distribution of bole (aluminium silicate coloured by iron oxide) obtained integrating the OH stretching band at 3691 cm^{-1}. In the back scattered image, different grey scale areas can be distinguished (figure 78c). In fact, EDX analysis in the lighter particles show the presence of lead and tin in a relative content which suggest the use of lead and tin yellow while the darker areas contain Ca and Si, Al, K, Fe, which are ascribed to the bole added to give bulk. The presence of calcium oxalates (1318 cm^{-1}) has been individuated in the mordant layer as well as in the outermost layer over the gold leaf, signifying an ongoing degradation process (figure 78e). In particular, the FTIR map of the integrated ester carbonyl stretching absorbance bands at 1734 cm^{-1} suggested the presence of an aged oily binding medium (figure 78f). Ageing phenomenon resulting from the triglycerides hydrolysis is also more pronounced in the external part as shown by the splitting of the carbonyl band in the light green layer, which progressively changes into a unique acid carbonyl band at 1713 cm^{-1} in the outermost mordant layer (figure 78g). Regarding the green paint layers, copper resinate has been found in both layers, integrating the acetate asymmetric stretching band at 1554 cm^{-1} (figure 78h). Moreover, the light green layer has resulted containing also a mixture with calcite and lead-tin yellow (identified by EDX analysis). In fact, the distribution plot of calcite out-of-plane bending band at 875 cm^{-1} confirms its presence both in the light green layer and in the mordant (figure 78i). In the thin dark green layer below, the high spatial resolution of synchrotron source make possible the identification of a small blue particle as azurite integrating its characteristic out-of-plane bending at 950 cm^{-1} (figure 78j). In the preparation layer, lead white has been characterised using the OH stretching at 3530 cm^{-1} (figure 78k).

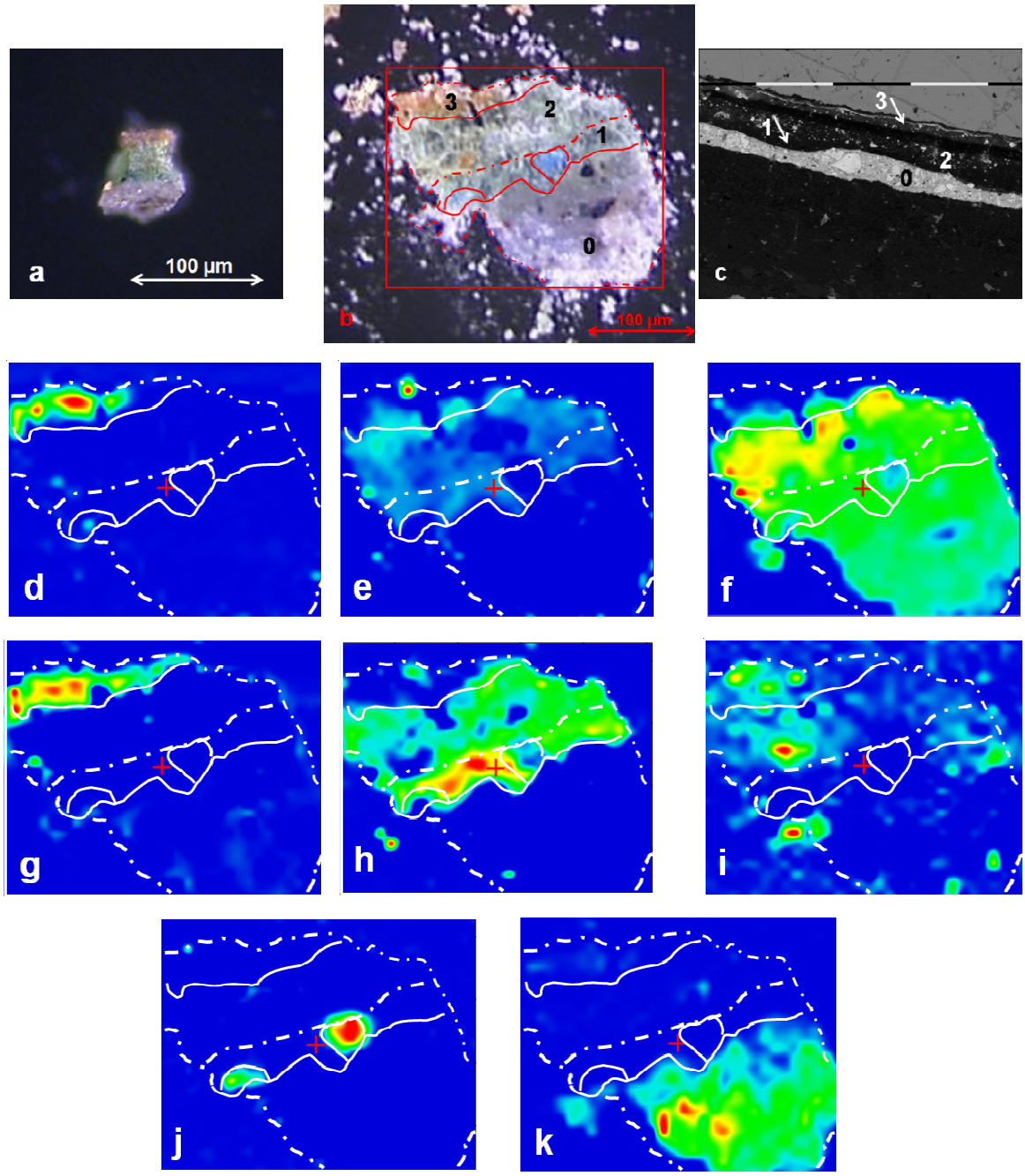

Figure 78 - a) visible light image of sample ROND13 before compression and b) after being pressed: the red box indicated the selected area for the ATR mapping; c) BSE image (original magnification 1300x) of another fragment of sample RON13 embedded in KBr with a similar structure: the different layers are numbered from 1 to 3: grey preparation layer (0), thin dark green layer (1), light green layer (2) and thin mordant layer 3. FTIR false colours plots representing d) bole (peak area 3691 cm^{-1}), e) oxalates (peak area 1318 cm^{-1}), f) siccative oil (1734 cm^{-1}), g) fatty acids (peak area 1713 cm^{-1}), h) copper resinate (peak area 1554 cm^{-1}), i) calcite (peak area 875 cm^{-1}), j) azurite (peak area 950 cm^{-1}) and k) lead white (peak area 3530 cm^{-1}).

A critical point in performing SR FTIR mapping is the sample preparation method, as the beam can only be used in transmission or reflection mode. In

fact, samples thin enough (less than 15 µm) are necessary to perform transmission measurements. An option is polishing a sample embedded in KBr on both sides until a thin slide remains, resulting rather destructive for the fragment (van der Weerd, Heeren et al. 2004), or a thin section can also be obtained after embedding in a polymer resin and microtoming, which is a tricky method (Derrick, Stulik et al. 1999). For reflection measurements on conventional cross sections, the surface quality should be improved using adequate and strenuous mechanical polishing methods (van Loon, Keune et al. 2005) or costly advanced techniques such as ion milling system or focused ion beam (Lins, Giannuzzi et al. 2002; Boon and Asahina 2006). However, in the perspective of the development of ATR accessories adapted for the synchrotron beam, the studies of brittle samples, which require to be embedded and analysed in cross-sections, will be greatly enhanced using SR sources.

III.3.3.c *ATR imaging on a embedded cross section*

In order to spatially characterise each identified painting material, ATR-FTIR imaging has been performed directly on the MCR13 cross-section on a representative area (63 x 63 μm^2) marked with a red box in figure 79.

The resulting image obtained plotting the intensity of the C=O fatty ester asymmetric stretching band at 1734 cm^{-1} has allowed localising the siccative oil used as binding medium in layers 0 and 3 (Figure 80a). Respect to the other analyses presented above, the distribution plot of the 1643 cm^{-1} band seems here to be contained in the mordant layer 1 and should only be related to the presence of proteinaceous material (Figure 80b), even if oxalates absorb also in this region. In fact, integrating the O-C-O stretching band at 1319 cm^{-1}, oxalates are located in the mordant layer 1 but also over the gold leaf 2 (Figure 80c). On the other hand, the integration of the 1550 cm^{-1} (amide II) band alone was not so accurate since carboxylates occurring in the same infrared region have been also individuated (Figure 80d). However, the different FTIR spectra extracted from the data cube have suggested that the presence of carboxylates is limited to layer 3 while the mordant layer 1 contains proteinaceous material due to the contemporary presence of the bands at 1643 cm^{-1} and 1550 cm^{-1} with a relative

intensity typical of proteins (Figure 80e). In fact, plotting both amide I (1643 cm^{-1}) and amide II (1550 cm^{-1}) bands, the chemical image obtained is similar to the one of the 1643 cm^{-1} band (Figure 80f). Concerning the stratigraphic identification of the pigments used, a carbonate has been detected as the main constituent of both layers 0 and 3 and its FTIR image has been obtained by selecting the integrated absorbance of the CO_3^{2-} asymmetric stretching at 1398 cm^{-1} (Figure 80g). Due to the cut-off of the focal plane array detector, the exact identification of lead white (basic lead carbonate), which has been achieved elsewhere with ATR and SR transmission mapping, has not been possible since the asymmetric stretching principal bands of the different carbonates are broad bands closed together and the bending ones (for example, 875 and 835 cm^{-1} respectively for calcite and lead white) are absent from the spectral region investigated (4000-900 cm^{-1}). Moreover, the pixel dimension of this type of detector allows to reach a high spatial resolution of approximately 5 µm but, unfortunately, this means also a poor signal-to-noise ratio and therefore the spectral quality should be enhanced using a greater acquisition time (128 scans). In fact, a small particle of gypsum (1108 cm^{-1}) has been individuated in the detachment between the mordant layer 1 and the below white layer 0 as well as in lower quantity in the layer 2 (Figure 80h). On the other hand, it has been possible to identify silicates (1070-970 cm^{-1}), even though a significative distribution plot has not been obtained.

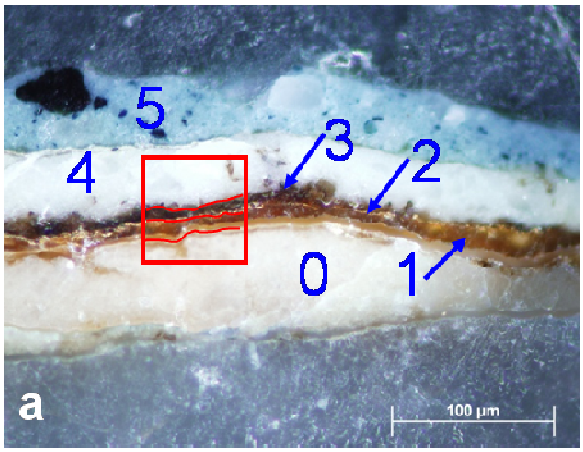

Figure 79 - visible light microscopic image of sample MCR13 embedded in KBr: the red box indicated the selected area for the ATR mapping.

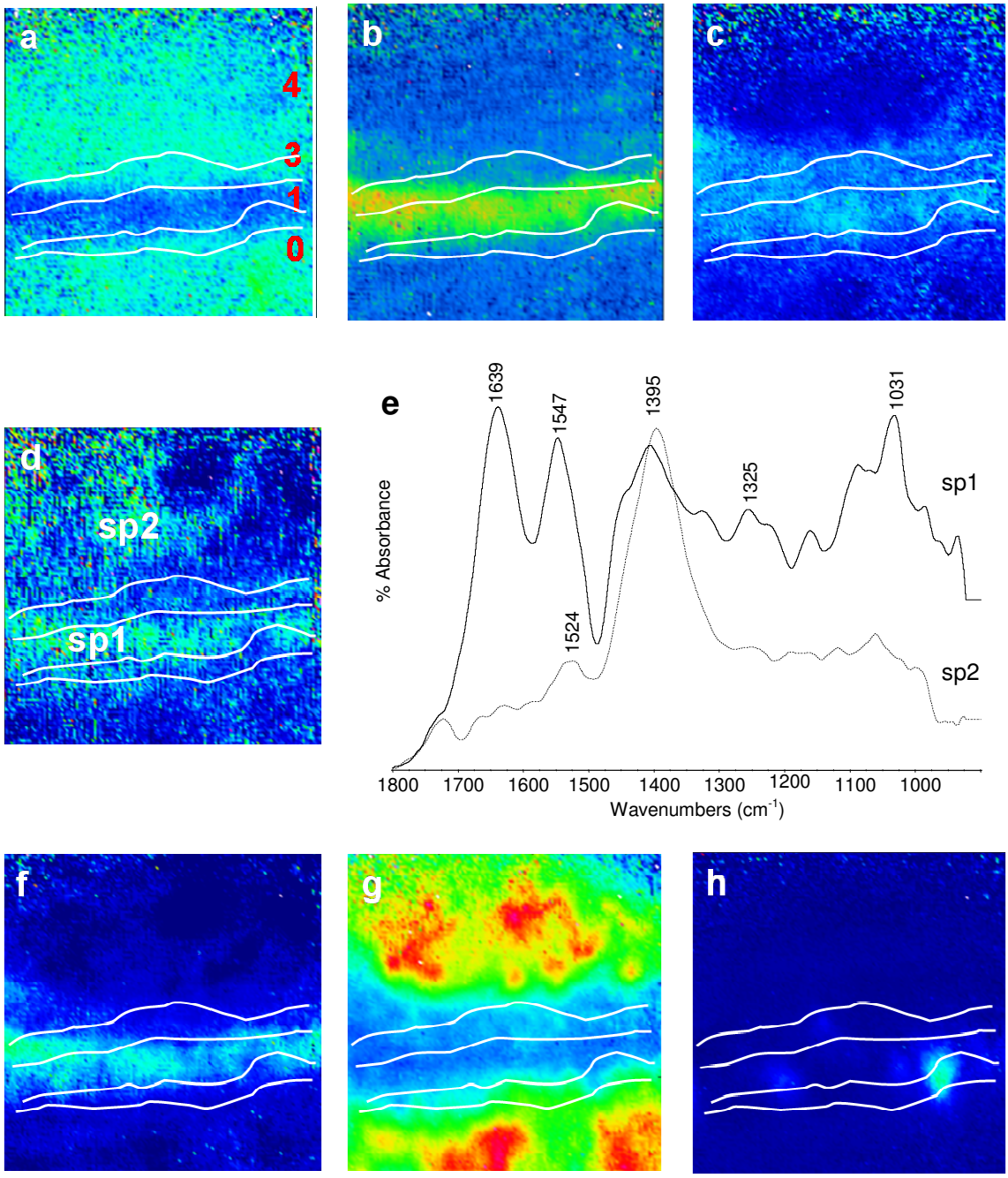

Figure 80 - FTIR false colours plots representing a) siccative oil (peak area 1734 cm^{-1}), b) proteinaceous material (peak area 1643 cm^{-1}), c) oxalates (peak area 1319 cm^{-1}), d) carboxylates (peak area 1550 cm^{-1}), f) amide I and II bands (region of interest 1700-1500 cm^{-1}), g) carbonates (peak area 1395 cm^{-1}) and h) gypsum (peak area 1108 cm^{-1}); e) FTIR spectra (1800-900 cm^{-1}) extracted from the top central area of d, marked sp1 and from the central area of d, marked sp2.

III.3.3.d *Raster scanning on a embedded cross section*

A selected area (225 x 130 μm^2) of the KBr cross-section of sample MCR13 has then been submitted to ATR raster scanning (Figure 81a). Lead white represents the main pigment used for the white layers (layers 0 and 3), as showed by the chemical map obtained using the CO_3^{-2} asymmetric stretching (1393 cm^{-1}) band (Figure 81b). In the same way as for ATR mapping measurements, cerusite has been localised in the white ground layer 0 (Figure 81c). Gypsum has been principally identified in the thin dark layer over the gold leaf (layer 2) using the SO_4^{-2} asymmetric stretching at 1117 cm^{-1} (Figure 81d). Since this system permits to investigate larger areas, it has been also possible to observe particular details, which would not appear performing measurements on small areas. In fact, in correspondence of discontinuities in the gold layer, gypsum has also been observed in the below mordant layer. This compound is often associated to deposition material and confirms therefore the existence of repaint for the area where the sample MCR13 has been collected. As demonstrated before, the 1636 cm^{-1} band is not specific for one compound and its presence in the mordant layer 1, over the gold leaf as well as in layers 4-5 indicates either proteinaceous material (amide I) than oxalates. Hence, the O-C-O stretching absorbance at 1320 cm^{-1} has been used for the oxalates as characteristic band (Figure 81e). On the other hand, the binding medium used for the gilding has been identified and exactly localised in the mordant layer 1 using a correlation map on the amide functional group (Figure 81f). Silicates are also present in this layer and in the upper dark deposit layer 2, as shown by the peak height map with the Si-O stretching band at 1043 cm^{-1} in figure 81g. Regarding the binding medium used in the paint layers, the presence of the ester C=O asymmetric stretching band at 1736 cm^{-1} that can be assigned either to the triglycerides is here confirmed (Figure 81h). It's interesting to observe how the distribution plots of proteinaceous material and lipids are specular images. Moreover, the thickness measured (8 µm) in the infrared image for proteins is of the same order than the thickness (5-15 µm) of the mordant layer in the visible light image, indicating the elevated spatial resolution thus achieved with raster scanning. In this case, the spectra of a large area have been obtained with only 8 scans with a high signal-to-noise ratio.

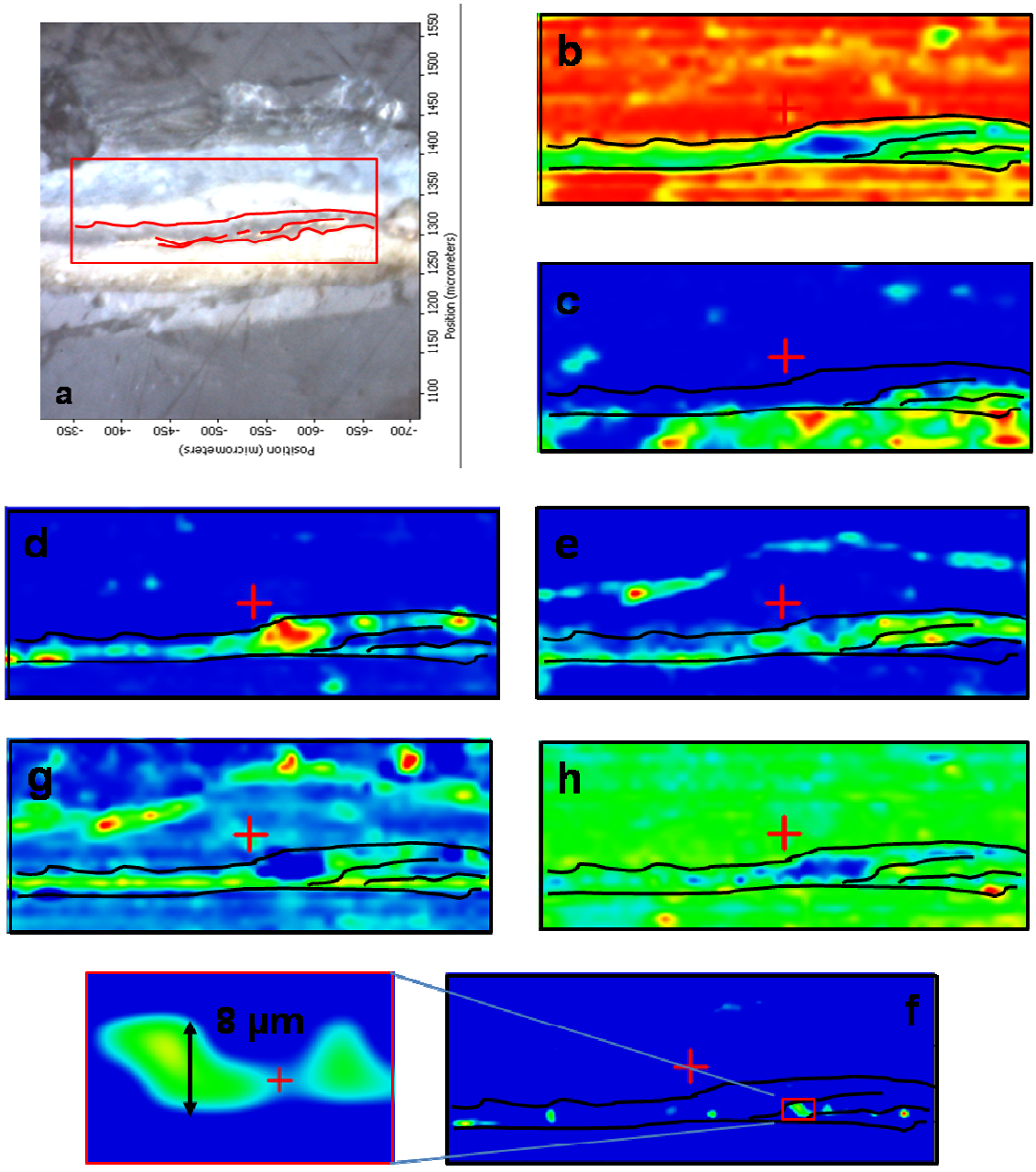

Figure 81 - a) visible light FTIR microscopic image of sample MCR13 embedded in KBr: the red box indicated the selected area for the ATR raster scanning. FTIR false colours plots representing b) lead white (peak area 1393 cm^{-1}), c) cerusite (peak area 839 cm^{-1}), d) gypsum (peak area 1117 cm^{-1}), e) oxalates (peak area 1319 cm^{-1}), f) amide correlation map with details of the layer thickness about 8 µm, g) silicate (peak area 1043 cm^{-1}), h) siccative oil (peak area 1736 cm^{-1}).

III.3.4 Conclusions

In this chapter, differences in terms of chemical information, data quality and accurate spatial localization obtained with various FTIR microspectroscopic techniques have been outlined for the characterisation of paint cross sections. In particular, an optimal spectral quality is achieved in transmission with a synchrotron source. However, this method sometimes does not permit to correlate the identified chemical compounds to specific thin layers. In fact, the required sample preparation is the critical point and may result in the mixing of the different materials, chiefly when presented in thin and close layers. With improvements, such as the development of ATR objectives adapted to the focused synchrotron beam, SR-FTIR microscopy will certainly become more popular. The combination of an ATR crystal with a FPA detector leads to a high spatial resolution but associated with a poor spectral quality and a cut-off at 900 cm^{-1}. Even if the signal-to-noise ratio can be improved upon accumulation of more scans, the spectral region investigated does not allow distinguishing between compounds having common functional groups, for example carbonates, as the few absorbance bands present may not be specific for one particular substance. With raster scanning measurements, the minimum analysed area is of 12 x 100 μm^2 and offers a fast and convenient method for the analysis of large areas of sample with a high spatial resolution and a good data quality. Given the larger spectral region (4000-720 cm^{-1}) investigated, this technique presents straightforward advantages on imaging for the characterisation of paint cross sections. ATR microspectroscopic mapping performed with a recently developed instrumentation shows here the best results with high spectral quality and spatial resolution. Moreover, thin organic layers (5 µm) have been not only identified but also accurately positioned. The different technical characteristics of each method are reported below in table 8. In particular, the S/N ratios have been estimated using band height of the carbonate asymmetric stretching divided by peak–peak noise on the baseline. The better spectral quality has been obtained with a synchrotron source. However, ATR mapping and raster scanning with iN™10MX provide S/N ratios comparable with shorter acquisition time. Hence, the operator will choose one

or another technique according to which parameter is more important between S/N ratio, spatial resolution or acquisition time.

	FPA imaging	**Raster scanning** iN™10MX	**Mapping** iN™10MX	**Mapping** continµum	**Mapping** continµum **ESRF**
Spectral region investigated (cm^{-1})	3800-900	4000-720	4000-675	4000-650	4000-800 (down to 650 with 12 x 12 μm^2 aperture)
Lower pratical limit of aperture (μm^2)	-	-	20 x 20	50 x 50	5x5
step size (µm)			3	5	3
Pixel dimension (µm)	~ 10	25	-	-	-
S/N ratio	rather high	very high	very high	high	excellent
Spatial resolution (µm)	5	6,25	5	10	5
Investigated area (μm^2)	Multiple of 63 x 63	multiple of 12 x 100	variable	variable	variable
detector lifetime	Low	high	high	high	high
Acquistion time	2-10 min	2-30 min	min-hours	hours	hours

Table 8 – Technical characteristics of the FTIR microscopic techniques present in this chapter.

III.3.5 Acknowledgements

This research has been partially carried out with the support of the European Union, within the VI Framework Programme (Contract: EU-ARTECH, RII3-CT-2004-506171). The ATR imaging results have been obtained during a short research period in the laboratory of Prof. S. Kazarian (Imperial College of London, UK). Dr. C. Ricci is thanked for assistance with FTIR imaging microscope. The authors also acknowledge the European Synchrotron Radiation Facility for providing synchrotron radiation facilities and would like to thank Dr. M. Cotte for assistance in using beamline ID21.

References

Aldrovandi, A., M. L. Altamura, et al. (1996). "I materiali pittorici: tavolette campione per la caratterizzazione mediante analisi multispettrale." OPD restauro **8**: 101-103,191-210.

Baker, M., D. Van Der Reyden, et al. (1989). "FTIR analysis of coated papers." The Book & Paper Group annual **8**: 1-12.

Baker, M., D. W. Von Endt, et al. (1988). FTIR microspectrometry: a powerful conservation analysis tool 16th AIC annual meeting. New Orleans, Louisiana, United States, American Institute for Conservation of Historic and Artistic Works**:** 1-13.

Baker, M. T. and D. W. Von Endt (1988). Use of FTIR-microspectrometry in examinations of artistic and historic works Materials issues in art and archaeology. E. V. Sayre, P. Vandiver, J. Druzik and C. Stevenson. Reno, Nevada, USA, Materials Research Society. **123:** 71-76.

Balas, K. and D. Pelecoudas (2000). An imaging method and apparatus for the non-destructive analysis of paintings and monuments, Foundation of Research and Technology-Hellas. **PCT/GR00/00039**.

Belali, R., J.-M. Vigoureux, et al. (1995). "Dispersion effects on infrared spectra in attenuated total reflection." Optical Society of America B **12**(12): 2377-2381.

Bell, S. H. (1970). "Controlling zinc oxide hazing in gloss paints." Paint and varnishes production **60**(4): 55-60.

Bhargava, R. and I. W. Levin (2007). Fourier Transform Mid-infrared Spectroscopic Imaging: Microspectroscopy with Multichannel Detectors. Spectrochemical Analysis Using Infrared Multichannel Detectors. I. W. L. Rohit Bhargava**:** 1-24.

Bhargava, R., B. G. Wall, et al. (2000). "Comparison of the FT-IR Mapping and Imaging Techniques Applied to Polymeric Systems." Applied Spectroscopy **54**(4): 470-479.

Bitossi, G., R. Giorgi, et al. (2005). "Spectroscopic Techniques in Cultural Heritage Conservation: A Survey." Applied Spectroscopy Reviews **40**(3): 187 - 228.

Bonizzoni, L., A. Galli, et al. (2008). "In situ EDXRF analyses on Renaissance plaquettes and indoor bronzes patina problems and provenance clues." X-Ray Spectrometry **37**(4): 388-394.

Boon, J. J. and S. Asahina (2006). "Surface Preparation of Cross Sections of Traditional and Modern Paint Using the Argon Ion Milling Polishing CP System." Microscopy and Microanalysis **12**(SupplementS02): 1322-1323.

Boon, J. J., J. van der Weerd, et al. (2002). Mechanical and chemical changes in old master paintings: dissolution, metal soap formation and remineralization processes in lead pigmented ground/intermediate paint layers of 17th century paintings. 13th Triennial Meeting of ICOM Committee for Conservation. R. Vontobel. Rio de Janeiro, James and James, London**:** 401- 406.

Braga, D. and F. Grepioni (2004). "Reactions Between or Within Molecular Crystals." Angewandte Chemie International Edition **43**(31): 4002-4011.

Brostoff, L. B. (2003). Coating strategies for the protection of outdoor bronze art and ornamentation. . National Gallery of Art, Washington, DC., Universiteit van Amsterdam. **PhD**.

Bruni, S., F. Cariati, et al. (1999). "Spectrochemical characterization by micro-FTIR spectroscopy of blue pigments in different polychrome works of art." Vibrational Spectroscopy **20**: 15-25.

Budevska, B. O., S. T. Sum, et al. (2003). "Application of Multivariate Curve Resolution for Analysis of FT-IR Microspectroscopic Images of in Situ Plant Tissue." Appl. Spectrosc. **57**(2): 124.

Burka, E. M. and R. Curbelo (2000). Imaging ATR spectrometer. Unites States, Bio-Rad Laboratories, Inc. **6141100**.

Cardamone, J. M. (1989). Reflectance absorption fourier transform infrared spectroscopy for nondestructive chemical analysis. 14th Annual IIC-CG conference. J. G. Wellheiser. Toronto, Ontario, Canada, IIC-Canadian Group**:** 53-63.

Casadio, F. and L. Toniolo (2001). "The analysis of polychrome works of art: 40 years of infrared spectroscopic investigations." Journal of Cultural Heritage **2**(1): 71-78.

Casellato, U., P. A. Vigato, et al. (2000). "A Mössbauer approach to the physico-chemical characterization of iron-containing pigments for historical wall paintings." Journal of Cultural Heritage **1**(3): 217-232.

Cesareo, R., A. Castellano, et al. (2002). Portable equipments for Energy Dispersive X-ray Fluorescence analysis of works of art. 7th International Conference on Non-Destructive Testings and Microanalysis for the Diagnostics and Conservation of the Cultural and Enviromental Heritage, Antwerp

Cesareo, R., A. Castellano, et al. (2004). "Giotto Nella Cappella degli Scrovegni: Analisi di Fluorescenza X Dispersiva in Energia con Apparecchiature Portatili." Il Giornale delle Prove non distruttive Monitoraggio Diagnostica **3**: 66-72.

Cesareo, R., A. Castellano, et al. (2005). From Giotto to De Chirico: analysis of paintings with EDXRFS equipment. Cultural Heritage Conservation and Environmental Impact Assessment by Non-Destructive Testing and Micro-

Analysis. R. van Grieken and K. Janssens. London, UK, A.A. Balkema**:** 183-196.

Cesareo, R., S. Ridolfi, et al. (2006). "From Giotto to De Chirico to Verrocchio: analyses of paintings and historical bronze alloys availing of portable EDXRF equipment." Journal of Neutron Research **14**(1): 17 - 27.

Chan, K. L. A., S. V. Hammond, et al. (2003). "Applications of Attenuated Total Reflection Infrared Spectroscopic Imaging to Pharmaceutical Formulations." Anal. Chem. **75**(9): 2140-2146.

Chan, K. L. A. and S. G. Kazarian (2003). "New Opportunities in Micro- and Macro-Attenuated Total Reflection Infrared Spectroscopic Imaging: Spatial Resolution and Sampling Versatility." Appl. Spectrosc. **57**(4): 381-389.

Chan, K. L. A. and S. G. Kazarian (2007). "Attenuated Total Reflection Fourier Transform Infrared Imaging with Variable Angles of Incidence: A Three-Dimensional Profiling of Heterogeneous Materials." Applied Spectroscopy **61**: 48.

Chan, K. L. A. and S. G. Kazarian (2007). "Chemical imaging of the stratum corneum under controlled humidity with the attenuated total reflection Fourier transform infrared spectroscopy method." Journal of Biomedical Optics **12**(4): 044010.

Chan, K. L. A., S. G. Kazarian, et al. (2005). "Fourier Transform Infrared Imaging of Human Hair with a High Spatial Resolution Without the Use of a Synchrotron." Appl. Spectrosc. **59**(2): 149-155.

Chen, Q., T. Sinkai, et al. (1997). "An analysis of pigments from Sung and Yuan Dynasty tomb wall paintings of Fujian Province in China." Bunkazai Hozon Shufuku Gakkai shi:kobunkazai no kagaku **41**: 78-87.

Chiavari, G., D. Fabbri, et al. (2005). "Effect of pigments on the analysis of fatty acids in siccative oils by pyrolysis methylation and silylation." Journal of Analytical and Applied Pyrolysis **74**(1-2): 39-44.

Colley, C. S., S. G. Kazarian, et al. (2004). "Spectroscopic imaging of arteries and atherosclerotic plaques." Biopolymers **74**(4): 328-335.

Colombini, M. P., A. Carmignani, et al. (2004). "Integrated analytical techniques for the study of ancient Greek polychromy." Talanta **63**(4): 839-848.

Colombini, M. P., F. Modugno, et al. (1999). "Two procedures for suppressing interference from inorganic pigments in the analysis by gas chromatography-mass spectrometry of proteinaceous binders in paintings." Journal of Chromatography A **846**(1-2): 101-111.

Cotte, M., E. Checroun, et al. (2007). "Micro-analytical study of interactions between oil and lead compounds in paintings." Applied Physics A: Materials Science & Processing **89**(4): 841-848.

Cotte, M., J. Susini, et al. (2008). "Applications of synchrotron-based micro-imaging techniques to the chemical analysis of ancient paintings." Journal of Analytical Atomic Spectrometry **23**: 820 - 828.

Crupi, V., R. Ficarra, et al. (2007). "UV-vis and FTIR-ATR spectroscopic techniques to study the inclusion complexes of genistein with [beta]-cyclodextrins." Journal of Pharmaceutical and Biomedical Analysis **44**(1): 110-117.

Dannenberg, H., J. W. Forbes, et al. (1960). "Infrared Spectroscopy of Surface Coatings in Reflected Light." Analytical Chemistry **32**(3): 365-370.

Derrick, M. (1989). "Fourier transform infrared spectral analysis of natural resins used in furniture finishes." The journal of the American Institute for conservation **28**(1): 43-56.

Derrick, M. R. (1991). "Evaluation of the State of Degradation of Dead Sea Scroll Samples Using FT-IR Spectroscopy." Book and Paper Group Annual **10**: 49-65.

Derrick, M. R. (1995). Infrared microspectroscopy in the analysis of cultural artifacts. Practical Guide to Infrared Microspectroscopy. H. J. Humecki. New York, Marcel Dekker**:** 287-322.

Derrick, M. R., D. C. Stulik, et al. (1999). Infrared spectroscopy in conservation science. Los Angeles, The Getty Conservation Institute

Derrick, M. R., D. C. Stulik, et al. (1992). "Furniture Finish Layer Identification by Infrared Linear Mapping Microspectroscopy." Journal of the American Institute for Conservation **30**(2): 163-177.

Desnica, V. and M. Schreiner (2006). "A LabVIEW-controlled portable x-ray fluorescence spectrometer for the analysis of art objects." X-Ray Spectrometry **35**(5): 280-286.

Dumas, P. and L. Miller (2003). "The use of synchrotron infrared microspectroscopy in biological and biomedical investigations." Vibrational Spectroscopy **32**(1): 3-21.

Ebizuka, N., M. Wakaki, et al. (1995). "Development of a multichannel Fourier transform spectrometer." Appl. Opt. **34**(34): 7899-7906.

Fernández-Bertrán, J. and E. Reguera (1996). "Mechanochemical reactions in alkali halide pressed disks." Solid State Ionics **93**(1-2): 139-146.

Ferrero, J. L., C. Roldán, et al. (2002). "Analysis of pigments from Spanish works of art using a portable EDXRF spectrometer." X-Ray Spectrometry **31**(6): 441-447.

Fischer, C. and I. Kakoulli (2006). "Multispectral and hyperspectral imaging technologies in conservation: current research and potential applications." Reviews in conservation **7**: 3-16.

G.Bottiroli, A.Gallone, et al. (2005). "Analisi microspettrofluorimetriche di leganti organici." Bollettino d'arte **volume speciale**(Giotto nella Cappella degli Scrovegni): 83-105.

Gettens, R. J. (1952). "Science in the art museum." Scientific American **187**(1): 22-27.

Gettens, R. J. and G. L. Stout (1966). Painting Materials. New York, Dover Publications, Inc.

Gettens, R. J. and E. West Fitzhung (1997). Azurite and Blueverditer. Artists' pigments. A. Roy. New York, Oxford University Press **2**.

Gharieb, M. I., M. I. Ali, et al. (2004). "Transformation of Copper Oxychloride Fungicide into Copper Oxalate by Tolerant Fungi and the Effect of Nitrogen Source on Tolerance." Biodegradation **15**(1): 49.

Gillard, R. D., S. M. Hardman, et al. (1994). "The detection of dyes by FTIR microscopy." Studies in conservation **39**(3): 187-192.

Gimeno-Adelantado, J. V., R. Mateo-Castro, et al. (2001). "Identification of lipid binders in paintings by gas chromatography: Influence of the pigments." Journal of Chromatography A **922**(1-2): 385-390.

Godlewska-Żyłkiewicz, B. (2006). "Microorganisms in inorganic chemical analysis." Analytical and Bioanalytical Chemistry **384**(1): 114-123.

Goodall, R. A., J. Hall, et al. (2008). "Micro-Attenuated Total Reflection Spectral Imaging in Archaeology: Application to Maya Paint and Plaster Wall Decorations." Applied Spectroscopy **62**: 10-16.

Graedel, T. E. (1987). "Copper patinas formed in the atmosphere--II. A qualitative assessment of mechanisms." Corrosion Science **27**(7): 721.

Graham, D. and T. Eddie (1985). X-ray techniques in art galleries and museums.

Griffiths, P. R. and J. A. De Haseth (1986). Fourier Transform Infrared Spectroscopy. New York, John Wiley & Sons.

Günzler, H. and H.-U. Gremlich (2002). IR Spectroscopy: An Introduction, Wiley-VCH.

Harthcock, M. A. and S. C. Atkin (1988). "Imaging with Functional Group Maps Using Infrared Microspectroscopy." Appl. Spectrosc. **42**(3): 449-455.

Harthcock, M. A. and S. C. Atkin (1988). Infrared microspectroscopy: development and applications of imaging capabilities. Infrared microspectroscopy. Theory and applications. R. G. Messerschmidt. United States, Marcel Dekker,New York, NY**:** 21-39.

Higgitt, C., M. Spring, et al. (2003). "Pigment-medium interactions in oil paint films containing red lead or lead-tin yellow." National Gallery Technical Bulletin **24**: 75-91.

Huffman, S. W. and C. W. Brown (2007). Multivariate Analysis of Infrared Spectroscopic Image Data. Spectrochemical Analysis Using Infrared Multichannel Detectors. I. W. L. Rohit Bhargava**:** 85-114.

Humecki, H. J. (1995). Practical Guide to Infrared Microspectroscopy, CRC Press.

Ishioka, T., M. Shimizu, et al. (2000). "Infrared and XAFS Study on Internal Structural Change of Ion Aggregate in a Zinc Salt of Poly(ethylene-co-methacrylic acid) Ionomer on Water Absorption." Macromolecules **33**(7): 2722-2727.

Johnson, R. (1984). The removal of microcrystalline wax from archaeological ironwork. Adhesives and consolidants. e. a. N. S. Brommelle. London, International Intstitute for Conservation of Historical and Artistic Works (IIC)**:** 107-109.

Joseph, E., P. Letardi, et al. (2007). Innovative Treatments for the Protection of Outdoor Bronze Monuments. Metal 07, triennialmeeting of ICOM-CC Metal Working Group, Amsterdam, September 17-21. B.Ankersmit, C. Degrigny, I. Joosten and R. van Langh. Amsterdam, Netherlands Institute of Conservation**:** 71-77.

Kambe, H. (1961). "Physicochemical Studies on Cobalt Salts of Higher Fatty Acids. II Compositions of Cobalt Soaps." Bulletin of the Chemical Society of Japan **34**(12): 1790-1793.

Kang, H., Y. Yi, et al. (2001). "The investigation and conservation of Central Asia wall painting." Conservation science in museum **3**: 43-50.

Karydas, A. G. (2007). "Application of a Portable XRF Spectrometer for the Non-Invasive analysis of Museum Metal Artefacts." Annali di Chimica **97**(7): 419-432.

Katon, J. E. (1996). "Infrared microspectroscopy. A review of fundamentals and applications." Micron **27**(5): 303-314.

Kazarian, S. G., K. L. Andrew Chan, et al. (2004). "Characterisation of bioactive and resorbable polylactide/Bioglass® composites by FTIR spectroscopic imaging." Biomaterials **25**(18): 3931-3938.

Keune, K. (2005). Binding medium, pigments and metal soaps characterised and localised in paint cross-sections. AMOLF (FOM Institute for Atomic and Molecular Physics), Universiteit von Amsterdam. **PhD**.

Keune, K. and J. J. Boon (2004). "Imaging Secondary Ion Mass Spectrometry of a Paint Cross Section Taken from an Early Netherlandish Painting by Rogier van der Weyden." Analytical Chemistry **76**(5): 1374-1385.

Keune, K., P. Noble, et al. (2002). Chemical changes in lead-pigmented oil paints: on the early stage of formation of protrusions. ART 2002, 7th international conference on non-destructive testing and microanalysis for the diagnostics and conservation of the cultural and environmental heritage. R. van Grieken, K. Janssens, L. Van' t dack and G. Meersman. Antwerp, Belgium.

Khanjian, H. P. and D. C. Stulik (2003). Infrared spectroscopic studies of photographic material. Conservation science 2002. J. H. Townsend, K. Eremin and A. Adriaens. Edinburgh, United Kingdom, Archetype Publications**:** 195-200.

Kharbade, B. V. and N. I. Saxena (1991). Infrared identification of inorganic artists' pigments using specular reflectance technique. Conservation of cultural property in India, Silver jubilee**:** 34-40.

Kratschmer, A., I. Odnevall Wallinder, et al. (2002). "The evolution of outdoor copper patina." Corrosion Science **44**(3): 425.

Krishnan, K., J. R. Powell, et al. (1995). Infrared microimaging. Practical Guide to Infrared Microspectroscopy. H. J. Humecki. New York, Marcel Dekker**:** 85-110.

Langley, A. and A. Burnstock (1999). The Analysis of Layered Paint Samples from Modern Paintings using FTIR Microscopy. 12th Triennial Meeting of ICOM Committee for Conservation. Lyon, James & James. **1:** 234-241.

Lena, K., Ed. (2004). Koguryo tomb murals. Seoul, Korea, ICOMOS Korea.

Letardi, P. (2004). Laboratory and field test on patinas and protective coating systems for outdoor bronze monuments. Metal2004. J. Ashton and D. Hallam. Canberra, National Museum of Australia**:** 379-387.

Levin, I. W. and R. Bhargava (2005). "Fourier Transform Infrared vibrational spectroscopic imaging: Integrating Microscopy and Molecular Recognition." Annual Review of Physical Chemistry **56**(1): 429-474.

Levitsky, M. M., A. I. Kokorin, et al. (2000). "Investigation of structures of mono- and diorgano-substituted oligosiloxanes containing transition metal atoms." Russian Chemical Bulletin **V49**(10): 1789.

Lewis, E. N., P. J. Treado, et al. (1995). "Fourier Transform Spectroscopic Imaging Using an Infrared Focal-Plane Array Detector." Analytical Chemistry **67**(19): 3377-3381.

Lewis, L. and A. J. Sommer (1999). "Attenuated Total Internal Reflection Microspectroscopy of Isolated Particles: An Alternative Approach to Current Methods." Applied Spectroscopy **53**: 375-380.

Lewis, L. L. and A. J. Sommer (2000). "Attenuated Total Internal Reflection Infrared Mapping Microspectroscopy of Soft Materials." Applied Spectroscopy **Volume 54**(Number 2): 324-330.

Leygraf, C. and T. E. Graedel (2000). Atmospheric corrosion. New York Wiley.

Lins, A., L. A. Giannuzzi, et al. (2002). FIB/TEM analysis of paint layers from Thomas Eakins' The Crucifixion, 1880. Symposium on materials issues in art and archaeology VI P. B. Vandiver, M. Goodway and J. L. Mass. Boston, Massachusetts, USA, Materials Research Society prooceedings. **712:** 113-118.

Low, M. J. D. and N. S. Baer (1977). "Application of infrared fourier transform spectroscopy to problems in conservation." Studies in Conservation **22**: 116-128.

Luján Lunsford, R. (2004). Two Similar Tombs with Divergent Conservation Problems – Assessment of the State of Preservation and Documentation of the Mural Paintings. UNESCO Symposium on the Conservation of Koguryo Tombs "Scientific and Methodological Approach". Seoul, Republic of Korea**:** 100-108.

Majolino, D., P. Migliardo, et al. (1996). "Ars Illuminandi and FTIR Microspectroscopy: an Advanced Way to Disclose Ancient Secrets." Science and Technology for Cultural Heritage **5**(2): 57-74.

Marabelli, M. and R. Mazzeo (1993). "La corrosione dei bronzi esposti all'aperto: problemi di caratterizzazione." La metallurgia italiana **85**(4): 247-254.

Marabelli, M. and G. Napolitano (1991). "Nuovi sistemi protettivi applicabili su opere o manufatti in bronzo esposti all'aperto." Materiali e strutture **1**(2): 51-58.

Marabelli, M., P. Santopadre, et al. (2005). "Giotto in the Scrovegni Chapel: materials used in the painting technique. Studies and researches by Istituto Centrale per il Restauro." Bollettino d'arte **Volume speciale**: 121-144.

Marengo, E., M. C. Liparota, et al. (2005). "Multivariate calibration applied to the field of cultural heritage: Analysis of the pigments on the surface of a painting." Analytica Chimica Acta **553**(1-2): 111.

Martoglio, P. A., S. P. Bouffard, et al. (1990). "Unlocking the secrets of the past: the analysis of archaeological textiles and dyes." Analytical Chemistry **62**(21): 1123A-1128A.

Matteini, M. and A. moles (2003). Scienza e restauro. Metodi di indagine. Florence, Italy.

Mazzeo, R. (2005). Patine su manufatti metallici. Le patine:genesi significato e conservazione. Firenze, Nardini editore. **Kermes quaderni:** 29-43.

Mazzeo, R., Ed. (2006). Far East Asian mural paintings: diagnosis, conservation and restoration. When east and west encounter and exchange. Ravenna, italy, Longo editore.

Mazzeo, R., P. Baraldi, et al. (2004). "Characterisation of mural painting pigments from the Thubchen Lakhang temple in Lo Manthang, Nepal." Journal of Raman spectroscopy **35**: 678-685.

Mazzeo, R., D. Cam, et al. (2004). "Analytical study of traditional decorative materials and techniques used in Ming Dynasty wooden architecture. The case of the Drum Tower in Xi'an, P.R. of Cina." Journal of Cultural Heritage **5**(3): 273-283.

Mazzeo, R., G. Chiavari, et al. (1989). Identificazione ed origene di patine ad ossalato su monumenti bronzei: il caso del Portale Centrale del Duomo di Loreto (AN) Le Pellicole ad ossalati: origene e significato nella conservazione delle opere d'arte, Milano.

Mazzeo, R. and E. Joseph (2005). Applicazione di imaging multispettrale allo studio e conservazione di graffiti e dipinti murali siti nell'edificio delle ex-carceri, Palazzo Steri (Pa). III Congresso Nazionale IGIIC, Lo stato dell'Arte. Palermo**:** 18-23.

Mazzeo, R. and E. Joseph (2007). "Attenuated total reflectance microspectroscopy mapping for the characterisation of bronze corrosion products." European Journal of Mineralogy **19**(3): 363-371.

Mazzeo, R., E. Joseph, et al. (2007). "Attenuated Total Reflection-Fourier transform infrared microspectroscopic mapping for the characterisation of paint cross-sections." Analytica Chimica Acta **599**(1): 107-117.

Meana-Esteban, B., C. Lete, et al. (2006). "Raman and in Situ FTIR-ATR Characterization of Polyazulene Films and Its Derivate." The Journal of Physical Chemistry B **110**(46): 23343-23350.

Meilunas, R. J., J. G. Bentsen, et al. (1990). "Analysis of aged paint binders by FTIR spectroscopy." Studies in Conservation **35**: 33-51.

Messerschmidt, R. G. and M. A. Harthcock (1988). Infrared microspectroscopy. Theory and applications. United States, Marcel Dekker,New York, NY.

Mills, J. S. (1966). "The gas chromatographic examination of paint media. Part I. Fatty acid composition and identification of dried oil films." Studies in conservation **11**(2): 92-108.

Moffett, D. I. (1996). "Wax coatings on ethnographic metal objects: justifications for allowing a tradition to wane." Journal of American Institute of Conservation **35**(1): 1-8.

Mohamed, W. A., N. M. Rateb, et al. (2004). Performance of copper corrosion inhibitors in a museum environment: a comparative study using FTIR spectroscopy Metal 04, international conference on metals conservation. J. Ashton and D. Hallam. Canberra, Australia, National Museum of Australia**:** 369-378.

Moioli, P. and C. Seccaroni (2000). "Analysis of art objects using a portable x-ray fluorescence spectrometer." X-Ray Spectrometry **29**(1): 48-52.

Moon, W.-S., J.-O. Hong, et al. (2002). "Scientific analysis of ancient mural pigments with emphasis on pigments in the Daeungjeon Hall of the Bongjeongsa Temple and an ancient tomb in Goadong." Mun hwa jae = Annual review in cultural properties studies **35**: 160-184.

Nakai, I., S. Yamada, et al. (2005). "Development of a portable x-ray fluorescence spectrometer equipped with two monochromatic x-ray sources and silicon drift detector and field analysis of Islamic glasses at an excavation site in Egypt." X-Ray Spectrometry **34**(1): 46-51.

Nassau, K., P. K. Gallagher, et al. (1987). "The characterization of patina components by X-ray diffraction and evolved gas analysis." Corrosion Science **27**(7): 669-684.

Nevin, A. (2005). "The use of micro-FTIR with attenuated total reflectance for the analysis of wall painting cross-section." Zeitschrift für Kunsttechnologie und Konservierung **19**(2): 356-368.

O'Connor, S. and M. M. Brooks (2007). X-radiography of textiles, dress and related objects. Oxford, Elsevier.

O'Neil, L. A. (1963). "Application of Infrared Spectroscopy for the Examination of the Drying and Yellow Discoloration of Oil Films." Paint Technology **27**(1): 44-47.

O'Neill, L. A. and R. A. Brett (1969). "Chemical reactions in paint films." Journal of the Oil and Colours Chemists' Association **52**: 1054-1074.

Oddy, W. A. (1975). The corrosion of metals on display. Conservation in archaeology and the applied arts. N. S. Brommelle and P. Smith. Stockholm, International institute for conservation**:** 235-237.

Olin, J. S. (1966). "The use of infrared spectrophotometry in the examination of paintings and ancient artifacts." Instrument news **17**: 1.

Omecinsky, D. and G. W. Carriveau (1982). IR investigation of resinous and synthetic varnishes. 10th annual meeting of American Institute for Conservation of Historic and Artistic Works. Milwaukee, Wisconsin**:** 141-149.

Padfield, J., D. Saunders, et al. (2002). "Improvements in the acquisition and processing of x-ray images of paintings." National Gallery technical bulletin **23**: 62-75.

Paluszkiewicz, C. and J. Dominik (2002). Changes in the chemical composition of historical objects determined by FTIR microspectroscopy. Art 2002: 7th International Conference on Non-destructive Testing and Microanalysis for the Diagnostics and Conservation of the Cultural and Environmental Heritage. R. Van Grieken, K. Janssens, L. Van't dack and G. Meersman. Congress Centre Elzenveld, Antwerp, Belgium, University of Antwerp.

Pappalardo, G., E. Costa, et al. (2004). "Non-destructive characterization of Della Robbia sculptures at the Bargello museum in Florence by the combined use of PIXE and XRF portable systems." Journal of Cultural Heritage **5**(2): 183-188.

Patterson, B. M. and G. J. Havrilla (2006). "Attenuated Total Internal Reflection Infrared Microspectroscopic Imaging Using a Large-Radius Germanium Internal Reflection Element and a Linear Array Detector." Appl. Spectrosc. **60**(11): 1256.

Patterson, B. M., G. J. Havrilla, et al. (2007). "Infrared Microspectroscopic Imaging Using a Large Radius Germanium Internal Reflection Element and a Focal Plane Array Detector." Applied Spectroscopy **61**: 1147.

Pilc, J. and R. White (1995). "The Application of FTIR-Microscopy to the Analysis of Paint Binders in Easel Paintings." National Gallery Technical Bulletin **16**: 73-84.

Pilz, M. and H. Römich (1998). Protective coatings for outdoor bronze monuments: available materials and new developments. Monuments and the Millenium. J.-M. Teutonico and j. Fidler. The Victoria and Albert Museum, London, James & James (Science publishers) Ltd**:** 120-127.

Pilz, M. and D. Vogel (1999). Evaluation of current ORMOCER Pilot Applications on Outdoor Bronze Surfaces. Bronnbach, germany, Fraunhofer-Institut für Silicatforschumg (ISC).

Planinsek, O., D. Planinsek, et al. (2006). "Surface analysis of powder binary mixtures with ATR FTIR spectroscopy." International Journal of Pharmaceutics **319**(1-2): 13-19.

Plater, M. J., B. De Silva, et al. (2003). "The characterisation of lead fatty acid soaps in `protrusions' in aged traditional oil paint." Polyhedron **22**(24): 3171-3179.

Popelka, S., L. k. Machová, et al. (2007). "Adsorption of poly(ethylene oxide)-block-polylactide copolymers on polylactide as studied by ATR-FTIR spectroscopy." Journal of Colloid and Interface Science **308**(2): 291-299.

Reffner, J. A. and P. A. Martoglio (1995). Uniting Microscopy and Spectroscopy. Practical Guide to Infrared Microspectroscopy. H. J. Humecki. New York, Marcel Dekker**:** 41-84.

Reffner, J. A., P. A. Martoglio, et al. (1995). Fourier transform infrared microscopical analysis with synchrotron radiation: The microscope optics and system performance (invited). Proceedings of the 5th international conference on synchrotron radiation instrumentation. Stony Brook, New York (USA), AIP. **66:** 1298-1302.

Ricci, C., S. Bloxham, et al. (2007). "ATR-FTIR imaging of albumen photographic prints." Journal of Cultural Heritage **8**(4): 387-395.

Ricci, C., K. L. A. Chan, et al. (2006). "Combining the Tape-Lift Method and Fourier Transform Infrared Spectroscopic Imaging for Forensic Applications." Appl. Spectrosc. **60**(9): 1013-1021.

Ricci, C., L. Nyadong, et al. (2007). "Combined Fourier-transform infrared imaging and desorption electrospray-ionization linear ion-trap mass spectrometry for analysis of counterfeit antimalarial tablets." Analytical and Bioanalytical Chemistry **387**(2): 551-559.

Ricci, C., P. Phiriyavityopas, et al. (2007). "Chemical Imaging of Latent Fingerprint Residues." Appl. Spectrosc. **61**(5): 514.

Robinet, L. and M.-C. Corbeil (2003). "The characterization of metal soaps." Studies in conservation **48**(1): 23-40.

Röhrs, S. and H. Stege (2004). "Analysis of Limoges painted enamels from the 16th to 19th centuries by using a portable micro x-ray fluorescence spectrometer." X-Ray Spectrometry **33**(6): 396-401.

Rokuro, U. and H. Mitsuharu (1931). Studies of ancient pigments in Japan. Eastern art. **3:** 47-60.

Ryhl-Svendsen, M. (2007). "Ozone detection using natural rubber dosimeters: quantitative measurements using light microscopy and attenuated total reflectance spectroscopy." Zeitschrift für Kunsttechnologie und Konservierung **21**(2): 240-249.

Sato, M. and Y. Sasaki (2005). Studies on ancient Japanese silk fibres using FTIR microscopy first annual conference on Scientific analysis of ancient and historic textiles: informing preservation, display and interpretation. . P. Wyeth and R. Janaway. AHRC research centre for textile conservation and textile studies, Southampton, United Kingdom, Archetype Publications**:** 44-47.

Sayer, J. A., M. Kierans, et al. (1997). "Solubilisation of some naturally occurring metal-bearing minerals, limescale and lead phosphate by Aspergillus niger." FEMS Microbiology Letters **154**(1): 29.

Scott, D. A. (2002). Copper and bronze in art: corrosion, colorants, conservation. Los Angeles, The Getty Conservation Institute

Shaeffer, J. A. (1933). "Some comments on lead pigments." Official Digest of the Federation of Paint and Varnish Production Clubs **126**: 180-189.

Shashoua, Y. and K. Bonde Johansen (2005). Investigation of ATR-FTIR spectroscopy as an alternative to the Water-Leach free acidity test for cellulose acetate-based film. 14th triennial meeting of ICOM Committee for conservation. The Hague, James & James**:** 548-555.

Shuye, D. (1987). Pigments used in Mogao caves of Dunhuang. Ars Buddhica. **175:** 90-100.

Smith, A. L. (1974). Analysis of Silicones. New York John Wiley.

Sommer, A. J., L. G. Tisinger, et al. (2001). "Attenuated Total Internal Reflection Infrared Mapping Microspectroscopy Using an Imaging Microscope." Applied spectroscopy **Volume 55**(Number 3): 252-256.

Spring, M., C. Ricci, et al. (2008). "ATR-FTIR imaging for the analysis of organic materials in paint cross sections: case studies on paint samples from the National Gallery, London." Analytical and Bioanalytical Chemistry **392**: 37-45.

Tabak, H., P. Lens, et al. (2005). "Developments in Bioremediation of Soils and Sediments Polluted with Metals and Radionuclides – 1. Microbial Processes and Mechanisms Affecting Bioremediation of Metal Contamination and Influencing Metal Toxicity and Transport." Reviews in Environmental Science and Biotechnology **4**(3): 115-156.

Tennent, N. H. and K. M. Antonio (1981). Bronze disease: synthesis and characterisation of botallackite, paratacamite and atacamite by infra-red spectroscopy 6th triennial meeting of Icom committee for conservation. . Ottawa, ICOM (Paris)**:** 921-925.

Teule, J. M. (1999). The Use of the MUSIS 2007 (Multispectral Imaging System) for the Analysis of Easel Paintings and Miniatures. 6th international conference on "Non destructive Testing and Microanalysis for the Diagnostics and Conservation of the Cultural Heritage and Environmental Heritage". Rome.

Thompson Jr, D. V. (1954). Il libro dell'arte, the craftsman's handbook of Cennino d'Andrea Cennini. New York, Dover Publications, Inc.

Tintori, L. (1982). "Golden tin in Sienese murals of the early trecento." The Burlington Magazine **124**: 94-95.

Treado, P. J. and M. D. Morris (1993). Infrared and Raman spectroscopic imaging. Microscopic and spectroscopic imaging of the chemical state. M. D. Morris. New York, Marcel Dekker**:** 71-108.

Turner, N. J. E. and D. E. Watkinson (1993). Use of FTIR microscopy to assess the relative efficiency of various storage environments for waterlogged archaeological glass. Conservation science in the U.K. N. H. Tennent. Glasgow, United Kingdom, James & James**:** 77-84.

Uhlir, K., M. Griesser, et al. (2008). "Applications of a new portable (micro) XRF instrument having low-Z elements determination capability in the field of works of art." X-Ray Spectrometry **37**(4): 450-457.

Vahur, S., K. Virro, et al. (2005). "Web-based infrared spectral databases relevant to conservation." Journal of the Canadian Association for Conservation: 10-17.

van der Weerd, J., J. J. Boon, et al. (2002). "Chemical changes in old master paintings: dissolution, metal soap formation and remineralization processes in lead pigmented paint layers of 17th century paintings." Zeitschrift für Kunsttechnologie und Konservierung **16**(1): 36-51.

van der Weerd, J., H. Brammer, et al. (2002). "Fourier Transform Infrared Microscopic Imaging of an Embedded Paint Cross-Section." Applied Spectroscopy **56**(3): 276-283.

van der Weerd, J., R. M. A. Heeren, et al. (2004). "Preparation methods and accessories for the infrared spectroscopic analysis of multi-layer paint films." Studies in conservation **49**(3): 193-210.

van der Weerd, J., A. van Loon, et al. (2005). "FTIR studies of the effects of pigments on the aging of oil." Studies in conservation **50**(1): 3-22.

van Loon, A., K. Keune, et al. (2005). Improving the surface quality of paint cross-sections for imaging analytical studies art'05 - 8th International Conference on "Non Destructive Investigations and Micronalysis for the Diagnostics and Conservation of the Cultural and Environmental Heritage". Lecce (Italy)**:** unpaginated.

van Zelst, L., D. W. Von Endt, et al. (1988). Non-destructive and micro-sample FTIR spectrometric analysis of organic materials in art objects. 2nd international conference on non-destructive testing, microanalytical methods and environment evaluation for study and conservation of works of art. Perugia, Istituto Centrale Per Il Restauro--Associazione Italiana Prove Non Distruttive**:** 30.1-30.17.

Van't Hul-Ehrnreich, E. H. (1970). "Infrared Microspectroscopy for the analysis of old painting materials." Studies in Conservation **15**(3): 175-182.

Ward, K. J., J. A. Reffner, et al. (1994). Applications of principal components analyses to multidimensional FTIR microscopy data. 9th International Conference on Fourier Transform Spectroscopy. Calgary, Canada, SPIE. **2089:** 252-253.

Winter, J. (1983). "The characterization of pigments based on carbon." Studies in conservation **28**(2): 49-66.

Yi, Y., H. Yu, et al. (2003). "The conservation treatment of the Central Asian mural painting (II): an investigation on the pigments for the mural paintings and of the plants used for making the original wall." Conservation science in museum **4**(12): 1-6.

Zhang, P., D. B. Otts, et al. (2002). "Recent advances in imaging of polymers; toward nano-level 3D spatial resolution using infrared spectroscopy." PMSE Preprints **87**: 170-171.

Zieba-Palus, J. (1999). "Micro-Fourier transform infrared spectroscopy in examination of easel paintings." Journal of Trace and Microprobe Techniques **17**(3): 299-308.

Zucchi, F., V. Grassi, et al. (2004). "Inhibition of copper corrosion by silane coatings." Corrosion Science **46**(11): 2853-2865.

Summary

Research in art conservation has been developed from the early 1950s, giving a significant contribution to the conservation-restoration of cultural heritage artefacts. In fact, only through a profound knowledge about the nature and conditions of constituent materials, suitable decisions on the conservation and restoration measures can thus be adopted and preservation practices enhanced. The study of ancient artworks is particularly challenging as they can be considered as heterogeneous and multilayered systems where numerous interactions between the different components as well as degradation and ageing phenomena take place. However, difficulties to physically separate the different layers due to their thickness (1-200 µm) can result in the inaccurate attribution of the identified compounds to a specific layer. Therefore, details can only be analysed when the sample preparation method leaves the layer structure intact, as for example the preparation of embedding cross sections in synthetic resins. Hence, spatially resolved analytical techniques are required not only to exactly characterize the nature of the compounds but also to obtain precise chemical and physical information about ongoing changes. This thesis focuses on the application of FTIR microspectroscopic techniques for cultural heritage materials. The first section is aimed at introducing the use of FTIR microscopy in conservation science with a particular attention to the sampling criteria and sample preparation methods. The second section is aimed at evaluating and validating the use of different FTIR microscopic analytical methods applied to the study of different art conservation issues which may be encountered dealing with cultural heritage artefacts: the characterisation of the artistic execution technique (chapter II-1), the studies on degradation phenomena (chapter II-2) and finally the evaluation of protective treatments (chapter II-3). The third and last section is divided into three chapters which underline recent developments in FTIR spectroscopy for the characterisation of paint cross sections and in particular thin organic layers: a newly developed preparation method with embedding systems in infrared transparent salts (chapter III-1), the new opportunities offered by macro-ATR imaging

spectroscopy (chapter III-2) and the possibilities achieved with the different FTIR microspectroscopic techniques nowadays available (chapter III-3).
In chapter II-1, FTIR microspectroscopy as molecular analysis, is presented in an integrated approach with other analytical techniques. The proposed sequence is optimized in function of the limited quantity of sample available and this methodology permits to identify the painting materials and characterise the adopted execution technique and state of conservation. Chapter II-2 describes the characterisation of the degradation products with FTIR microscopy since the investigation on the ageing processes encountered in old artefacts represents one of the most important issues in conservation research. Metal carboxylates resulting from the interaction between pigments and binding media are characterized using synthesised metal palmitates and their production is detected on copper-, zinc-, manganese- and lead- (associated with lead carbonate) based pigments dispersed either in oil or egg tempera. Moreover, significant effects seem to be obtained with iron and cobalt (acceleration of the triglycerides hydrolysis). For the first time on sienna and umber paints, manganese carboxylates are also observed. Finally in chapter II-3, FTIR microscopy is combined with further elemental analyses to characterise and estimate the performances and stability of newly developed treatments, which should better fit conservation-restoration problems.

In the second part, in chapter III-1, an innovative embedding system in potassium bromide is reported focusing on the characterisation and localisation of organic substances in cross sections. Not only the identification but also the distribution of proteinaceous, lipidic or resinaceous materials, are evidenced directly on different paint cross sections, especially in thin layers of the order of 10 µm. Chapter III-2 describes the use of a conventional diamond ATR accessory coupled with a focal plane array to obtain chemical images of multi-layered paint cross sections. A rapid and simple identification of the different compounds is achieved without the use of any infrared microscope objectives. Finally, the latest FTIR techniques available are highlighted in chapter III-3 in a comparative study for the characterisation of paint cross sections. Results in terms of spatial resolution, data quality and chemical information obtained are presented and in particular, a new FTIR microscope equipped with a linear

array detector, which permits reducing the spatial resolution limit to approximately 5 µm, provides very promising results and may represent a good alternative to either mapping or imaging systems.

Acknowledgements

In primo luogo, ringrazio il Prof. Mazzeo per essersi fidato di me 5 anni fa, sulla base del solo mio entusiasmo. Durante questi anni è stato per me un punto di riferimento a cui contatto ho imparato tanto, come la tecnica della *gocca chinese*...

E bello vedere come il laboratorio diagnostico di microchimica e microscopia dei beni culturali sia cresciuto con il passare degli anni e vorrei ringraziare le persone vicine come Silvia, Daria ed Elsebeth. In particolar modo, ho un pensiero per Cristina, Francesco e Marta ma anche per tutti gli studenti che si sono alternati come Angela, Vanessa, Enrico...

Sono felice di aver incontrato sulla mia strada persone entusiaste nella loro propria ricerca. Paola Letardi per la sua grande serietà nel lavoro e il suo sorriso. Marie Wörle, pour m'avoir dit un jour de novembre 2003 "Inch' Allah" et m'avoir toujours encouragée et soutenue à poursuivre ma voie. Daniel Job, pour avoir répondu oui sans hésitation à une idée un peu folle sur des champignons. Daniela Pinna e Susanna Bracci per la loro simpatia durante un escursione in Macedonia...All eu-artech partners for the activities accomplished together in a challenging environment.

Cosa dire alle due persone piu care, Anna e Giorgia, se non un enorme grazie per la nostra complicità e per essere state vicine in ogni momento di bisogno. Ricordo un "sarà perchè ti amo" immortalizzato con la video e dei deliri fotografici color seppia...e poi le risate con conquilline temporanee ed altri amici come Mariaelena, Enrica, Natascia, Carlotta e Alessio...

Merci aussi à ceux plus ou moins loin en France ou en Suisse qui ont du mal à me suivre dans mes pérénigrations: Marlène, Eric, Myriam, Didier, Elise, Guillaume, Elodie, Anca, Julien, Madelyne, Christophe, Myriam, Josep, Sabine, Florent, Mickaël, Agathe, Julia, Rob, Marc, Nicolas, Kaspar, Silvia, Andrea, Anne, Julieta, Andreas, Edy, Natasha, Nicoletta, Luca, Ilaria...

Finalment, un très grand merci à ma famille pour me soutenir à distance dans mes choix de vie et à Olivier pour avoir, avec moi, pris la route et surtout les trains...